Ramesh Gupta, LBL

School at CAT, Indore, India

January 27-28, 1998

Field Calculations and Computations

This presentation will be broken in two sections. The first section will deal with the development of basic formalism used in designing and analysing superconducting magnets. The second section will deal with magnetic design and analysis of the actual magnets which depart from the ideal geometry. The magnets for the Superconducting Super collider (SSC) and the Relativistic Heavy Ion Collider (RHIC) will be used as examples.

1. Superconducting Magnets

A description of the cosine theta superconducting magnets is given here. A similar description can be found elsewhere [86,128,144,175,177,179]. Type II superconductors, which allow penetration of magnetic field lines, are used in all superconducting magnets. They can retain their superconducting state up to a field of $\sim$20 tesla and are being currently used in designing magnets in the range of 3 to 15 tesla. Type I superconductors, which were discovered first and which completely exclude field lines, lose superconductivity at a much lower field of 0.18 tesla or below and therefore are not suitable for such applications. Despite the promising prospects of high temperature superconductors [93] they are not yet suitable for accelerator magnets.

In superconducting magnets which are mostly intended for operation above 3 tesla maximum field, the field shape is primarily determined by the superconducting coils. Superferric magnets are a hybrid version of superconducting and iron dominated room temperature magnets. In superferric magnets though, superconducting coils are used but the iron plays an important role in shaping the field. The presentation here will be mostly limited to the superconducting magnets.

The two main design goals for superconducting magnets are to obtain (a) a good quench performance (a quench implies the loss of superconductivity in the cable) and (b) a good field quality. After an overall introduction to the magnet geometry, the superconducting cable, the cryogenic system, the magnetic design, the mechanical design, the magnet construction and the magnet measurements will be briefly described.

1.1. Introduction to the Magnet Geometry

Superconducting accelerator magnets are basically long cylindrical magnets whose cross section is mostly uniform along the length except at the two ends. The cross section of the 80 mm aperture RHIC arc dipole magnet inside the cryostat is shown in Fig. 1.1. The overall size of superconducting magnets is usually much larger then the aperture required for the particle beam. As compared to the 80 mm coil inner diameter and 69 mm beam tube inner diameter, the outside diameter of the RHIC cryostat is 610 mm. Similarly, in the SSC main dipole magnet design, for a coil aperture of 50 mm, the cryostat outside diameter was 660 mm.

The superconducting coils are made of Nb-Ti superconductor configured in a *"Rutherford Type"* [154,176] cable. The coils are kept below a temperature of 4.65 kelvin. The cryogenic system is designed to minimize the heat leak to room temperature outside the cryostat. The coils are kept under compression to minimize conductor motion under Lorentz forces when the magnet is energized. In RHIC magnets the space between the superconducting coils and the yoke is filled with RX630 phenolic spacers and in SSC magnets with stainless steel collars. The purpose of the yoke is to provide magnetic shielding and additional field in the magnet aperture. The yoke has several features (see Fig. 1.1) to serve a variety of purposes. These features include (a) loading flats to provide compression on the coil through a heavy

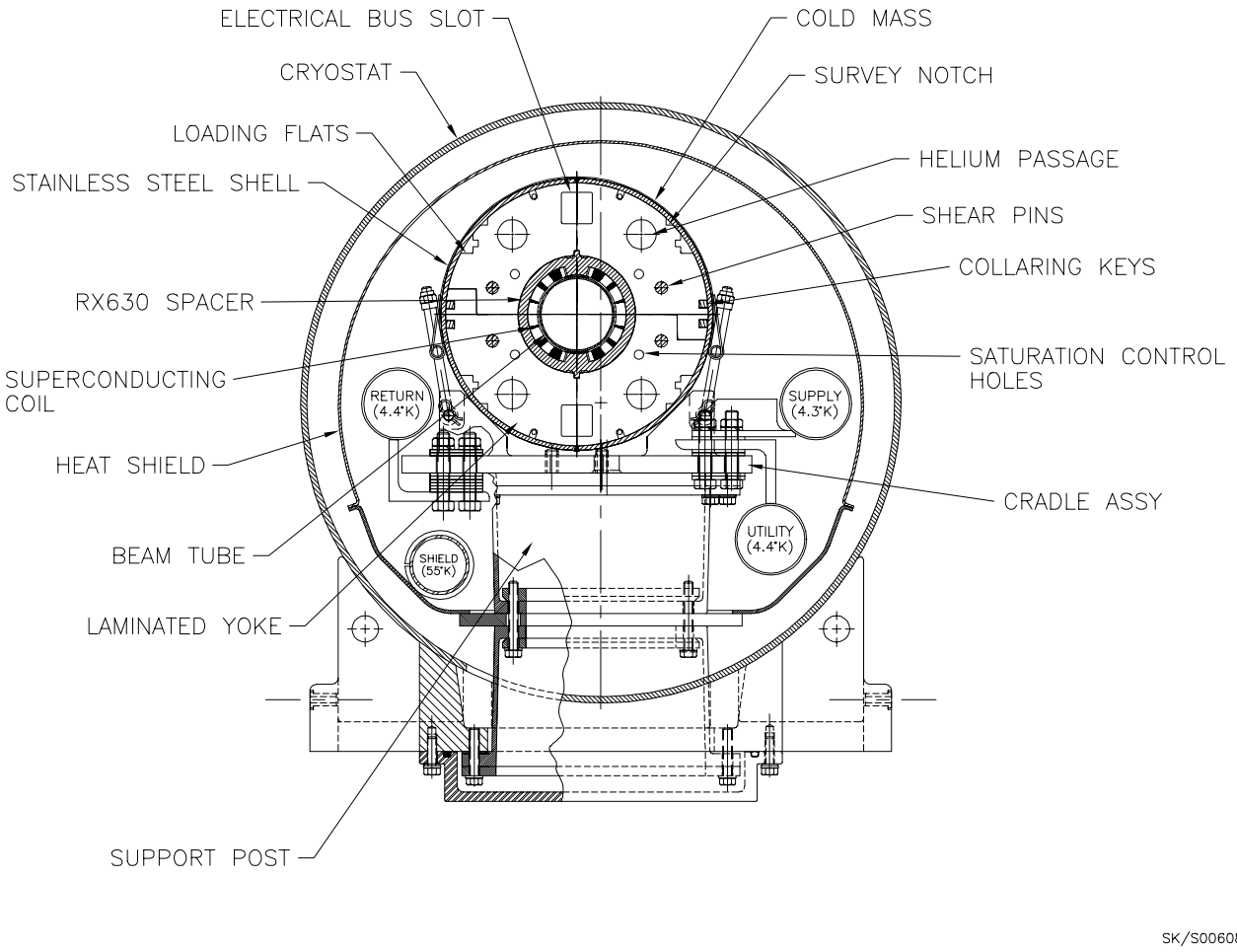

Figure 1.1: A cross section of the 80 mm aperture RHIC arc dipole magnet with the important magnetic, mechanical and cryogenic system components marked. The cold mass is asymmetrically located inside the cryostat. The cross section shown here is at the axial center.

press (b) holes for helium flow, saturation control and yoke pins (c) cutouts for electrical bus work, collaring keys, tabs which align the RX630 spacers to define the coil pole location and survey notches for aligning the magnet in the cryostat. A stainless steel shell, which also provides radial pressure, is put outside the yoke for helium containment.

The part of the magnet assembly described above (superconducting coils, iron yoke and stainless steel) is called the "coldmass" which remains below 4.65 degree kelvin in RHIC and SSC designs. The coldmass is put inside the cryostat which is a vacuum vessel. A number of components between the coldmass and the cryostat are required for structural and thermal purposes.

1.2. Superconducting Cable

In most magnet designs the superconducting wire is made of NbTi filaments embedded in a copper matrix. NbTi has good mechanical properties (ductility) but is generally limited to producing ~7.5 tesla at 4.5 kelvin and ~10.5 tesla at 1.8 kelvin. A higher field can be reached with the more expensive Nb_3Sn superconductor. However, Nb_3Sn does not have similarly good mechanical properties and therefore coil manufacturing becomes much more complicated. The titanium in NbTi alloy is generally about 46% by weight. The measured critical current density (the current density at which the wire looses its superconducting properties) as a function of applied field at 4.2 K is shown in Fig. 1.2 (courtesy A. Ghosh) for the NbTI wire used in RHIC corrector magnets. A similar $B - J$ performance is obtained in the superconducting cable used in the other types of RHIC magnets. In addition to the superconductor, the cable contains copper to provide stability against quench and for heat conduction. The amount of copper in the cable is usually more than the amount of superconductor. The superconducting cable, used in RHIC magnets, has a copper to superconductor ratio (by volume) of 3.0 in corrector magnets, of 2.5 in trim quadrupole and sextupole magnets, of 2.2 in the 80 mm and 100 mm aperture magnets and 1.8 in the 130 mm aperture and 180 mm aperture insertion magnets. The cable used in the inner layer of the SSC dipole had a copper to superconductor ratio of 1.3 and the one used in the outer layer had a copper to superconductor ratio of 1.8. The filament size in the superconducting wire used in the RHIC and SSC dipole magnet design is 6 μm except for the wire used in

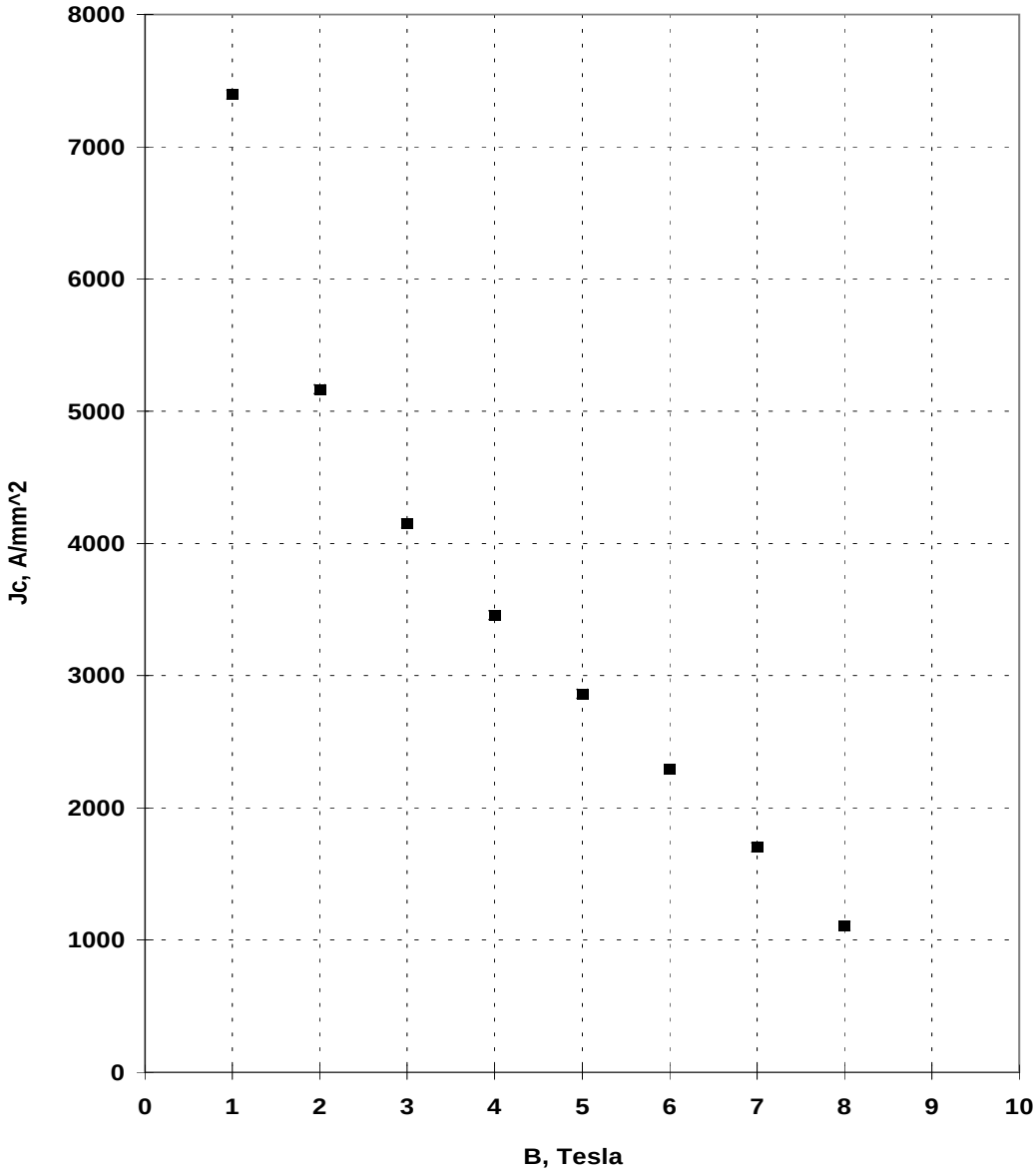

Figure 1.2: The measured (courtesy A. Ghosh) critical current density (J_c) at 4.2 K in the superconductor of the wire used in the RHIC corrector magnets as a function of applied field (B).

the RHIC corrector, sextupole and trim quadrupole magnets where it is 10 μm. There are about 3500 filaments in each wire of the RHIC dipole cable. The wire (strand) diameter is about 0.65 mm. The parameter list of the cable used in RHIC dipole magnet is given in Table 1.1.

Table 1.1: Design specifications of the superconducting cable for the 80 mm aperture RHIC arc dipole and quadrupole magnets.

Cable parameters	Value
Filament diameter	6.0 μm
Filament spacing	$>$1.0 μm
Number of filaments per wire	3510 $\pm$ 20
Copper to Superconductor Ratio	(2.25$\pm$0.1):1
Strand (wire) diameter	0.648$\pm$0.003 mm
No. of strands in cable	30
Critical current in wire at 5 T, 4.2 K	264 A
Critical current in cable at 5 T, 4.2 K	7524 A
Cable width	9.73 $\pm$ 0.03 mm
Cable mid-thickness	1.166$\pm$0.006 mm
Cable keystone angle	1.2$\pm$0.1 degree
Cable lay pitch	74 $\pm$5 mm

"Rutherford" cable is used in most large scale production of accelerator magnets. This type of cable is wide and flat and is made of a number of wires (strands) twisted together in a spiral shape. The cable is asymmetrically compressed across the flat side with one edge being thinner than the other. This provides a "keystone" angle in the cable which helps the coils to conform to a circular geometry with each turn lying approximately on a radius. In a fully keystoned cable, the ratio of thickness of the two edges of the cable is the same as that between the coil inner radius and outer radius. The cable is electrically

insulated to deal with the high voltage (over 1 kV) that is created during a quench when one turn is in the superconducting phase and the other in the normal. The RHIC design uses all-Kapton (Kapton is a registered trademark of Dupont Corporation) insulation which has good electrical break down, cryogenic and stability in ionizing radiation properties and has good dimensional tolerance. Another type of insulation used on superconducting cables is fiberglass tape impregnated with B-stage epoxy.

The superconducting cable produced for the RHIC magnet program is the result of significant R&D and a close collaboration with industry. The standard deviation in the variation in the cable thickness and other mechanical dimensions has been generally kept to about the 5 μm level. This has been crucial to providing good field quality and proper compression on the coils in the magnet. Moreover, the variation in the critical current density is also kept to about 2% to minimize the variation in the field harmonics associated with superconductor effects.

1.3. Cryogenic System

Cooling is provided by supercritical helium. A small radial gap between the beam tube and the superconducting coil provides a space for helium flow which partly cools the coil and removes the heat deposited during machine operation or instability in the magnet. The major portion of the heat removal and helium flow takes place in the four helium holes in the yoke. In order to reduce the heat load on the cryogenic system, the design of the coldmass and cryostat is optimized to minimize heat leak. To deal with a large thermal gradient between the low temperature in the superconducting coils and room temperature outside the cryostat, either one or two staged thermal shields are used where the heat is intercepted and removed. In the SSC dipole design two stage heat removal was planned (a) at 20 kelvin by gaseous helium and (b) at 80 kelvin by liquid nitrogen. In the RHIC dipole design, heat leakage is removed at 55 kelvin. Since the radiation heat leak loss goes as the difference between the fourth power of the two temperatures, only a small difference is expected between the two and one shield cases. A blanket of thermal insulation is placed just inside the vacuum vessel wall and between and interior to the shields.

The coldmass is put inside the vessel on a few support posts. The location of the support posts is chosen to reduce sagging of the coldmass. To minimize the heat leak through them, they are made as long as possible and to accommodate that larger length without increasing the cryostat outer diameter, the coldmass is positioned above the center of the cryostat (see Fig. 1.1). In both RHIC and SSC magnets the cryostat is made of low carbon magnetic steel which reduces the exterior field. However, a systematic offset between the vertical center of the cryostat and the center of the coldmass creates a skew quadrupole harmonic in the dipole at high field.

1.4. Mechanical Design

Good quench performance of the superconducting magnets is closely related to a good mechanical design which minimizes the motion of the superconducting wires. The design must be structurally sound to deal with the Lorentz forces when the magnet is energized, the thermal forces during cool-down and the mechanical forces during transportation of the magnet.

A large magnetic field in superconducting magnets generates a large Lorentz forces on the superconducting coils which may cause a small amount of conductor motion. This conductor motion generates heat which may start a quench in the magnet. The direction of the Lorentz forces in the cross section of the magnet is such that compression of the coil from the coil pole to the coil midplane is by the azimuthal component and compression outward is by the radial component. To deal with this situation, the coils are pre-compressed with a large mechanical compressive force which counters the Lorentz forces and thus minimizes conductor movement. In the SSC magnets, this compression on the coil is provided by stainless steel collars and in RHIC magnets by the yoke itself. In these designs, a significant part of the compression applied at room temperature is lost when the magnet is brought to a lower temperature. This is because of a difference in the coefficients of thermal expansion of superconducting coils, stainless steel and the yoke iron. Therefore, in order to assure an adequate compression when the magnet is cold, a much higher (a factor of two to three) compression is applied at room temperature. There are some alternate design concepts which have been tested in some magnets, where this loss of compression is avoided [41,127].

Finally a stainless steel shell is welded on the yoke outer diameter to contain the helium. This also provides a radial pressure on the coil-yoke assembly and in the RHIC-type design the radial component of the Lorentz forces are finally transmitted to it. To deal with the outward axial component of the Lorentz forces, the ends are restrained and sometimes even compressed (loaded) axially. A detailed description of the mechanical design and analysis of the SSC magnets can be found elsewhere [44].

1.5. Magnetic Design

The main goal of the magnetic design is to optimize the geometry of the coil and iron shape to produce a highly uniform field. In addition, it is beneficial to minimize the maximum field on the conductor (peak field) and to maximize the transfer function (tesla per ampere) to obtain a high quench field (computed from cable short sample measurements). The design must also fulfill all mechanical and cryogenic requirements and a magnet based on this design should be as simple as possible to manufacture.

The coils are made of a number of turns of superconducting cable which are grouped in several current blocks. A cosine theta current distribution produces an ideal dipole field. Copper wedges are placed between the blocks of turns to approximate the cosine theta current distribution. In designs which use partially keystoned cables, the wedges also serve an important mechanical purpose in providing a proper arc shape to the current blocks in the circular coil geometry. The size of the current blocks and the copper wedges are parameters used to minimize the field harmonics and to maximize the quench field.

The iron yoke provides magnetic shielding. In addition, the magnetized yoke gives an extra contribution to the central field which in most RHIC magnets is $\sim$50% of the coil field. However, at high field, the magnetization in the iron yoke is not proportional to the current in the coils, so the yoke geometry must be carefully designed to maintain a good field quality at all fields.

The coil end design is complicated. The cable must be bent carefully to bring it from one side of the coil to the other side. Spacers are inserted between the blocks of turns in the end not only to minimize the peak field and field harmonics but also for the mechanical purpose of reducing the strain on the cable. In most RHIC magnet designs the ends are

enclosed by the iron yoke laminations but in SSC and in most other magnet designs the iron laminations are replaced by stainless steel laminations to minimize the peak field in the ends.

The field errors in magnets are described in terms of field harmonics (see next section Eq. (2.17)) which are also referred to as multipoles. The are generally divided in the following three categories based on their sources :

1. Geometric multipoles
2. Persistent current multipoles
3. Saturation multipoles

The geometric multipoles are related to the magnet geometry. An error (or a departure) from the ideal geometry would create harmonics other than those desired. The persistent current multipoles are related to the persistent current in the superconductors. As the field in magnet is changed, the persistent (shielding) currents are induced in a direction to oppose the changing field [144]. Unlike in normal conductors, these currents persist for a long time in superconductors and contribute significantly to the field errors at low fields where their relative contribution is high. The saturation multipoles are related to the saturation magnetization of iron at high field. A non-uniform field and hence a non-uniform (as a function of azimuth) relative contribution of the iron distorts the field shape and field errors are thereby introduced.

1.6. Magnet Construction

The construction of the superconducting magnets is a long and complex process which requires a high level of engineering and quality control to assure consistently good quality in large scale magnet production [6]. The magnet manufacturing tooling must itself be carefully designed to realize the computed field quality and quench performance. Some of the major steps of the manufacturing process are briefly described here in the case of RHIC arc dipole magnets.

The superconducting cable and the copper wedges are insulated with Kapton layers. The magnet coils are wound on a precision convex surface with a winding machine feeding

the cable continuously. The copper wedges in the coil cross section and the wedge tips in the coil ends are periodically inserted as required by the optimized design. The Kapton tape, wound around the cable, is coated on one side with a dry adhesive which is activated (cured) by heat at a temperature of about 130 C while under compression. The coils are cured in a curing fixture (mold) and the temperature and curing pressure described above may contain several curing cycles with different combinations of curing temperature and curing pressure. Once cooled, the coil is firmly fixed in the shape determined by the dimensions of the curing mold.

The coils are installed in the iron yoke together with the RX630 phenolic spacers and other parts. The following is the sequence of the steps required in this operation: (a) the laminations for the lower yoke half are stacked (b) the RX630 spacers are put in place (c) the lower coil is installed (d) the beam tube is inserted (e) the upper coil, pre-assembled with the RX630 insulator, is put in place and (f) the laminations for the upper yoke half are stacked on this assembly. The coil is compressed with a press applying pressure on the yoke collar at the loading flats. The keys are inserted to retain this compression. The stainless steel shell is welded with the required sagitta (axial curvature of the magnet) in the coldmass. The stainless steel end plates are welded and coil end force is applied before the electrical installation is completed. Then the coldmass is placed inside the cryostat on the support posts. All cryogenic piping and heat shields are also installed.

1.7. Magnet Measurements

Apart from a variety of mechanical and electrical measurements at the various stages of magnet construction, the two measurements which define the final quality of magnets for machine operation are (a) the quench performance and (b) the field harmonics. For these measurements the magnets must be tested at cryogenic temperatures. It is, however, expensive and time consuming to test each and every magnet cold (in the superconducting phase). Therefore, in the RHIC magnet program only a part of the magnets are tested cold before they are installed in the tunnel [170]. The selection of the magnets chosen for cold testing is carefully made to minimize the risk of not testing all magnets cold. The required maximum operating current for RHIC is about 5 kA and the design margin over

the machine requirements for most magnets for the computed quench current is over 30%. The measured performance of the magnets tested cold show that most magnets require only a few (2-5) quenches to reach the computed quench current [170].

Warm magnetic measurements are performed on all magnets. At room temperature, the current in the cable is carried by the copper intermixed with the superconductor. There is an expected systematic difference between warm and cold harmonics because of (a) a change in the magnet geometry due to thermal contraction during cool-down (b) the persistent current effects in the superconductor and (c) the saturation effects due to the non-linear properties of the iron yoke. Based on those magnets that are tested both warm and cold, a good warm-to-cold correlation in the field harmonics has been obtained [170]. This correlation is used to estimate the field quality in those magnets that are not tested cold.

The magnetic measurements are carried out with an array of windings having a certain radius [175], mounted on a rotating cylinder which intercept the field in the magnet aperture. The geometry of these coils is chosen so that the Fourier analysis of the voltage induced in the various windings determine the field harmonics. The accuracy of the measurements depends on the accuracy of the measuring coil geometry, the electronic signal measurement and the analysis of the measured signal.

In the long curved RHIC magnets, the complete measurements are made in 10 steps with a meter long measuring coil system which is referred to as a mole [49]. In addition, the integral of the field along the axis is also measured with a long stationary coil. For a more accurate measurement of the field strength at a point an NMR (Nuclear Magnetic Resonance) probe is also used.

The measured field quality in 80 mm aperture RHIC arc dipoles is shown in Table 1.2 and Table 1.3. Measuring the field harmonics accurately and managing it in a large number of magnets (1740 are required for RHIC) is a quite complex task.

The "Mean" of the distribution for the harmonic b_n (which is also sometimes referred to as the systematic value of b_n) in N magnets is defined as follows :

$$< b_n >= \frac{1}{N}\sum_{k=1}^{N}(b_n)_k, \tag{1.1}$$

where $(b_n)_k$ is the value of harmonic b_n in the k^{th} magnet. The "SIGMA" (σ), also the RMS (Root Mean Square) deviation from the "Mean" b_n, is defined as follows :

$$\sigma\left(b_n\right) = \sqrt{\frac{1}{N}\sum_{k=1}^{N}\left[\left(b_n\right)_k - < b_n >\right]^2}. \tag{1.2}$$

The primary purpose of the harmonic measurements is to verify that the machine requirements needed for beam stability and design beam life time in RHIC are satisfied. In addition, the field harmonics are also used as a tool to detect possible manufacturing defects in the magnets or a drift in the mechanical dimensions of the components used in the manufacturing process. Since the harmonics are the analysis of the field created by the geometry of the coil and yoke, they are a reflection of magnet geometry. The accuracy of the magnetic measurements is sufficient to find a 100μm or less error in most of the critical components used in manufacturing the magnets.

Table 1.2: The measured integral transfer function (ITF) in tesla·m/kA, body transfer function (SSTF) in tesla/kA and normal field harmonics (b_n, defined elsewhere) at 25 mm reference radius in the 9.45 m long 80 mm aperture RHIC arc dipole magnets (data courtesy Jain and Wanderer). The current at which measurements are made and the number of magnets (shown in parenthesis) used in arriving at the statistics are shown here. The 30 A measurements are made when the magnet is warm (room temperature), in the non-superconducting state and the current is carried by the copper in the cable. $< b_n >$ is the mean and $\sigma(b_n)$ is the standard deviation of harmonic b_n in the number of magnets measured.

	$< b_n > \pm\sigma(b_n)$	$< b_n > \pm\sigma(b_n)$	$< b_n > \pm\sigma(b_n)$	$< b_n > \pm\sigma(b_n)$
	30A(296)	660A(63)	1450A(61)	5000A(62)
ITF	6.6545± 0.0021	6.6698± 0.0027	6.6769± 0.0021	6.4180± 0.0024
SSTF	0.7042± 0.00021	0.7078± 0.0003	0.7080± 0.00028	0.6798± 0.00034
b_1	0.25±0.37	0.08±0.28	0.04±0.27	0.10±0.28
b_2	3.54±1.74	-0.17±2.22	2.18±1.77	0.83±1.76
b_3	-0.03±0.10	0.00±0.08	0.00±0.08	0.01±0.08
b_4	0.22±0.44	-0.33±0.57	-0.15±0.58	0.15±0.59
b_5	0.01±0.03	0.00±0.03	0.00±0.03	-0.03±0.04
b_6	0.12±0.11	-0.13±0.13	-0.02±0.14	1.19±0.14
b_7	0.00±0.01	-0.01±0.01	-0.01±0.01	-0.01±0.01
b_8	0.09±0.11	0.14±0.12	0.13±0.12	0.12±0.12
b_9	0.00±0.01	0.02±0.02	0.02±0.02	0.02±0.02
b_{10}	-0.53±0.02	-0.58±0.02	-0.56±0.02	-0.58±0.02

Table 1.3: The measured a_n (skew harmonics) at 25 mm reference radius in the 9.45 m long 80 mm aperture RHIC arc dipole magnets (data courtesy Jain and Wanderer). The current at which the measurements are made and the number of magnets (shown in parenthesis) used in arriving at the statistics are shown here. The 30 A measurements are made when the magnet is warm (room temperature), non-superconducting and the current is carried by the copper in the cable. $< a_n >$ is the mean and $\sigma(a_n)$ is the standard deviation a_n in the number of magnets measured.

	$< a_n > \pm\sigma(a_n)$	$< a_n > \pm\sigma(a_n)$	$< a_n > \pm\sigma(a_n)$	$< a_n > \pm\sigma(a_n)$
	30A(296)	660A(63)	1450A(61)	5000A(62)
a_1	-0.20±1.62	0.28±1.53	0.21±1.52	-1.51±1.51
a_2	-1.11±0.20	-1.03±0.17	-1.03±0.17	-1.07±0.18
a_3	-0.01±0.49	-0.03±0.42	-0.02±0.42	-0.36±0.41
a_4	0.18±0.07	0.21±0.06	0.21±0.06	0.20±0.06
a_5	-0.01±0.17	0.02±0.15	0.01±0.15	-0.06±0.16
a_6	-0.11±0.03	-0.10±0.02	-0.10±0.02	-0.10±0.02
a_7	0.00±0.05	-0.01±0.05	-0.01±0.05	-0.01±0.05
a_8	0.02±0.01	0.02±0.01	0.02±0.01	0.02±0.01
a_9	0.00±0.01	0.04±0.02	0.04±0.02	0.04±0.02
a_{10}	-0.01±0.00	-0.01±0.01	-0.01±0.01	-0.01±0.01

2. Magnetic Field Analysis in Accelerator Magnets

In this section an outline of the formalism and theory used in carrying out the field calculations in the superconducting magnets is given. Starting from first principles, basic expressions are developed which are used in designing and describing the magnetic fields in the accelerator magnets.

The uniformity of the magnetic field is very important since it determines the performance of the machine. A typical requirement for the field quality in the accelerator magnets is that the deviation from the ideal shape should be within a few parts in 10^4. The uniformity of the field is expressed in terms of the Fourier harmonic components.

2.1. Basic Electromagnetic Field Equations

The calculation of the magnetic field in accelerator magnets is too complex to be done directly by solving Maxwell's equations. However, the most complicated formulae describing the field shape in the magnets are derived primarily from them. In this section, Maxwell's equations and other commonly used expressions of electro-magnetic theory [95,129,150] are briefly described. Although the magnetic field in the accelerator magnets is not static in time, the effects of time variation are by and large negligible in the problems to be addressed during the course of this work. Therefore, most of the detailed analysis is limited to the magneto-static case only.

The four Maxwell's equations are :

$$\nabla \cdot \vec{D} = \rho, \tag{2.1a}$$

$$\nabla \cdot \vec{B} = 0, \tag{2.1b}$$

$$\nabla \times \vec{E} + \frac{\partial \vec{B}}{\partial t} = 0, \tag{2.1c}$$

$$\nabla \times \vec{H} = \vec{J} + \frac{\partial \vec{D}}{\partial t}. \tag{2.1d}$$

Here $\vec{H}$ is the magnetic field, $\vec{E}$ is the electric field, $\vec{B}$ is the magnetic induction and $\vec{D}$ is the displacement vector. ρ denotes the charge density and $\vec{J}$ the current density, and these two are related by the following continuity equation,

$$\nabla \cdot \vec{J} + \frac{\partial \rho}{\partial t} = 0. \tag{2.2}$$

Furthermore, $\vec{B}$ and $\vec{H}$ are related by the following equations:

$$\frac{\vec{B}}{\mu_o} = \vec{H} + \vec{M}, \tag{2.3a}$$

$$\frac{\vec{B}}{\mu\mu_o} = \vec{H}, \tag{2.3b}$$

where μ_o is the permeability of the vacuum ($\mu_o = 4\pi \times 10^{-7}$ henry/meter) and μ is the relative permeability of the medium (relative with respect to that of vacuum). Often, μ is simply referred to as the permeability (which is in fact the case in CGS units) and the same convention is followed here unless otherwise explicitly mentioned. $\vec{M}$ denotes the magnetization (or magnetic polarization) of the medium. In free space (vacuum) $\vec{M}$ is 0. In an isotropic medium $\vec{H}$, $\vec{B}$ and $\vec{M}$ are parallel to each other.

Furthermore, $\vec{D}$ and $\vec{E}$ are related by the following equations:

$$\vec{D} = \epsilon_o \vec{E} + \vec{P}, \tag{2.4a}$$

$$\vec{D} = \epsilon\epsilon_o \vec{E}, \tag{2.4b}$$

where $\vec{P}$ is the electric polarization and ϵ_o is the permittivity in vacuum ($\epsilon_o = 8.854 \times 10^{-12}$ farad/meter). ϵ is the relative permittivity of the medium. In free space (vacuum), the electric polarization is 0.

The constants ϵ_o and μ_o are related through the relation

$$\epsilon_o \mu_o = \frac{1}{c^2},$$

where c is the velocity of light (c=2.998 $\times$ 10^8 m/s). Since $\vec{B}$ has a zero divergence, it may be expressed in term of a magnetic vector potential $\vec{A}$ as

$$\vec{B} = \nabla \times \vec{A}. \tag{2.5}$$

The vector potential $\vec{A}$ can be obtained at any point ($\vec{r}$) due to a current density $\vec{J}(\vec{r'})$ with the help of the following integral equation :

$$\vec{A}(\vec{r}) = \frac{\mu\mu_o}{4\pi}\int_V \frac{\vec{J}\left(\vec{r'}\right)}{|\vec{r}-\vec{r'}|}dv, \tag{2.6}$$

where $\vec{r}$ and $\vec{r'}$ are three dimensional coordinates and dv is the three dimensional volume element.

The components of the field in Eqs. (2.5) in Cartesian coordinates are given by

$$B_x = \frac{\partial A_z}{\partial y} - \frac{\partial A_y}{\partial z}, \tag{2.7a}$$

$$B_y = \frac{\partial A_x}{\partial z} - \frac{\partial A_z}{\partial x}, \tag{2.7b}$$

$$B_z = \frac{\partial A_y}{\partial x} - \frac{\partial A_z}{\partial y}, \tag{2.7c}$$

and in cylindrical coordinates by

$$B_r = \frac{1}{r}\left(\frac{\partial A_z}{\partial \theta}\right) - \frac{\partial A_\theta}{\partial z}, \tag{2.7d}$$

$$B_\theta = \frac{\partial A_r}{\partial z} - \frac{\partial A_z}{\partial r}, \tag{2.7e}$$

$$B_z = \frac{1}{r}\left(\frac{\partial\left(rA_\theta\right)}{\partial r} - \frac{\partial A_r}{\partial \theta}\right). \tag{2.7f}$$

The research work to be described is restricted to static magnetic fields only and electric fields are not considered. During the accelerating cycle of the machine, the magnetic field does change with time in the superconducting magnets. However, for the problems to be discussed during the course of this work, the change in magnetic field has negligible effect on field quality. Therefore the following two Maxwell's equations for the magnetostatic case are used in developing various formulae

$$\nabla \cdot \vec{B} = 0, \tag{2.8a}$$

$$\nabla \times \vec{H} = \vec{J}. \tag{2.8b}$$

Ampère's law

$$\oint_S \vec{H} \cdot d\vec{s} = I, \tag{2.9}$$

can be obtained from Eqs. (2.8b) by integrating and using Stoke's theorem :

$$\oint_C \vec{V} \cdot d\vec{l} = \int_S \left(\nabla \times \vec{V}\right) \cdot \vec{n} da$$

where $\vec{V}$ is a well behaved vector field, S is an open arbitrary surface, C is the closed curve bounding S, $d\vec{l}$ is a line element of C, and $\vec{n}$ is a vector element normal to S. The right hand side of the equation simply states that $I = \int \vec{J} \cdot \vec{n} da$ is the total current flowing through the area.

Poisson's equation for the vector potential is derived here under the assumptions that $\vec{B} = \mu_0 \mu \vec{H}$, the medium is homogeneous (i.e. μ is constant over a finite space) and isotropic. Using $\vec{B} = \mu_0 \mu \vec{H}$ and $\vec{B} = \nabla \times \vec{A}$ in Eqs. (2.8), one obtains :

$$\nabla \times \nabla \times \vec{A} = \mu_0 \mu \vec{J}. \tag{2.10}$$

The following identity is used to simplify the above equation :

$$\nabla^2 \vec{A} = \nabla \left(\nabla \cdot \vec{A} \right) - \nabla \times \nabla \times \vec{A}. \tag{2.11}$$

In Cartesian coordinates the above Laplacian operator (∇^2) can be applied to a vector $\vec{A}$ whose i^{th} component is $\nabla^2 A_i$. In other coordinate systems Eq. (2.11) must be used to determine the expression for $\nabla^2 \vec{A}$. In the cylindrical coordinate system :

$$\nabla^2 \vec{A}_z = \frac{1}{r} \frac{\partial}{\partial r} \left(r \frac{\partial A_z}{\partial r} \right) + \frac{1}{r^2} \frac{\partial^2 A_z}{\partial \theta^2}, \tag{2.12}$$

when $A_r = A_\theta = 0$ by symmetry (axial symmetric case).

The choice of $\nabla \cdot \vec{A}$ has thus far has been arbitrary and it is made zero in the Coulomb gauge (in the magnetostatic case). In that case Eq. (2.10) leads to Poisson's Equation as

$$\nabla^2 \vec{A} = -\mu_0 \mu \vec{J}. \tag{2.13}$$

In the 2-dimensional case, when the direction of current flow is parallel to the z-axis, $J_x = J_y = 0$. This implies that $A_x = A_y = 0$ and $\frac{\partial A_z}{\partial z} = 0$. Therefore, the above expression becomes,

$$\nabla^2 A_z = -\mu_0 \mu J_z, \tag{2.14}$$

which in the Cartesian coordinate system gives :

$$\frac{\partial^2 A_z}{\partial x^2} + \frac{\partial^2 A_z}{\partial y^2} = -\mu_0 \mu J_z. \tag{2.15}$$

In the case of axial symmetry, the Eq. (2.14) in cylindrical coordinates becomes :

$$\frac{1}{r} \frac{\partial}{\partial r} \left(r \frac{\partial A_z}{\partial r} \right) + \frac{1}{r^2} \frac{\partial^2 A_z}{\partial \theta^2} = -\mu_0 \mu J_z, \tag{2.16}$$

on using Eq. (2.12).

2.2. Field Harmonic Definitions

It is useful to describe the magnetic field inside the aperture of accelerator magnets in terms of harmonic coefficients [96,140,144,175]. The discussion will be limited to 2-dimensional analysis, which describes the field in the body (or straight section) of a long magnet. When the magnetic field is evaluated a few aperture diameters away from the two ends of the magnet, the axial component of the field is negligible. The accelerator magnets examined here are those in which the field is consists of one fundamental harmonic which is several orders of magnitude larger (usually 10^4) than any other harmonic present.

The skew (a_n) and the normal (b_n) field harmonics are defined through the following relation :

$$B_y + iB_x = 10^{-4} B_{R_0} \sum_{n=0}^{\infty} [b_n + i\ a_n]\,[cos\,(n\theta) + i\ sin\,(n\theta)] \left(\frac{r}{R_0}\right)^n, \qquad (2.17)$$

where B_x and B_y are the horizontal and vertical components of the magnetic field at (r,θ) and $i = \sqrt{-1}$. R_0 is the normalization radius. The magnets for the Relativistic Heavy Ion Collider (RHIC) have a coil radius ranging from 40 mm to 90 mm. In most of these magnets, the normalization radius is taken to be $\frac{5}{8}$ of the coil radius. The value of the normalization radius is 25 mm for the 80 mm aperture diameter of the RHIC arc dipoles and quadrupoles, 40 mm for the 130 mm aperture of the RHIC insertion quadrupoles, 31 mm for the 100 mm aperture of the RHIC insertion dipoles and 60 mm for the 180 mm aperture RHIC insertion dipoles [140]. B_{R_0} is the magnitude of the field due to the fundamental harmonic at the reference radius on the midplane. In the dipoles, $B_{R_0} = B_0$ (the field at the center of the magnet), in the quadrupoles, $B_{R_0} = G \times R_0$ (G being the field gradient at the center of the magnet), and in general for a $2(m+1)^{th}$ pole magnet,

$$B_{R_0} = \frac{R^m}{m!} \left[\frac{\partial^m B_y}{\partial x^m}\right]_{x=0,y=0}. \qquad (2.18)$$

Eq. (2.17) can be re-written in several other forms using complex variables. In this section z represents the complex coordinate and $B(z)$ represents the complex field as follows:

$$z = x + i\ y,$$
$$(x + i\ y)^n = r^n\,(cos\,[n\theta] + i\ sin\,[n\theta]),$$

$$B(z) = B_y \;+\; i\; B_x,$$
$$c_n = b_n + \;\; i\; a_n,$$

Thus :

$$B_y + iB_x = 10^{-4} B_{R_0} \sum_{n=0}^{\infty} [b_n + i\; a_n]\,[x \;+\; i\; y]^n \left(\frac{1}{R_0}\right)^n \tag{2.19}$$

$$B(z) = 10^{-4} B_{R_0} \sum_{n=0}^{\infty} c_n \left(\frac{z}{R_0}\right)^n \tag{2.20}$$

The harmonics used so far ($a_n,\ b_n,\ c_n$) are all dimensionless coefficients. However, in another representation, the field is expressed in terms of coefficients which carry the units of magnetic field. These are usually distinguished from the harmonics a_n and b_n given in Eq. (2.17) by the use of the uppercase alphabet. The two are related as follows:

$$A_{n+1} = 10^{-4} B_{R_0}\; a_n, \tag{2.21a}$$

$$B_{n+1} = 10^{-4} B_{R_0}\; b_n, \tag{2.21b}$$

$$C_{n+1} = 10^{-4} B_{R_0}\; c_n. \tag{2.21c}$$

Using these, Eq. (2.20) can be written as :

$$B(z) = \sum_{n=1}^{\infty} C_n \left(\frac{z}{R_0}\right)^{n-1}. \tag{2.22}$$

In this case the summation begins from $n = 1$ instead of $n = 0$. Sometimes C_n is also written as $C(n)$.

The definition for the field harmonics used so far is the one which is more common in U.S. laboratories. The European laboratories (such as CERN and HERA) use a slightly different definition [179]. The two are related as follows :

$$(a_{n+1})_{Europe} = \;\; -\,10^{-4}\;\; (a_n)_{US}$$
$$(b_{n+1})_{Europe} = \;\; 10^{-4}\;\; (b_n)_{US}$$

Yet another representation of field harmonic is used in beam dynamics calculations where the particle trajectory is studied in the machine [25]. For this purpose, the field is

expressed in the form of a Taylor series. The vertical component of the field on the median plane is expressed as

$$B_y(x,0) = \sum_{n=0}^{\infty} \frac{1}{n!} \left[\frac{d^n B_y}{dx^n}\right]_0 x^n, \tag{2.23}$$

where the subscript 0 implies that the derivatives are evaluated at the equilibrium orbit (which is generally at the center of the magnet). n=0 gives the vertical component of the field at the center of the magnet, which is represented as B_0 and the above equation becomes

$$B_y(x,0) = B_0 + \sum_{n=1}^{\infty} \frac{1}{n!} \left[\frac{d^n B_y}{dx^n}\right]_0 x^n, \tag{2.24}$$

Similarly, the horizontal component of the field (B_x) on the horizontal axis (X-axis) is expressed as :

$$B_x(x,0) = \sum_{n=0}^{\infty} \frac{1}{n!} \left[\frac{d^n B_x}{dx^n}\right]_0 x^n. \tag{2.25}$$

where, the subscript 0 implies that the derivatives are evaluated at the equilibrium orbit. n=0 gives the horizontal component of the field at the center of the magnet, which is ideally zero in the magnets considered here.

The following are defined :

$$k_n = \frac{1}{B_0\rho} \left[\frac{d^n B_y}{dx^n}\right]_0, \tag{2.26a}$$

$$h_n = \frac{1}{B_0\rho} \left[\frac{d^n B_x}{dx^n}\right]_0, \tag{2.26b}$$

with ρ as the bending radius of the particle in the magnet and ($B_0\rho$) as the magnetic rigidity. Therefore, the Eq. (2.24) and Eq. (2.25) become

$$B_y(x,0) = B_0\rho \left(\frac{1}{\rho} + \sum_{n=1}^{\infty} \frac{1}{n!} k_n \; x^n\right), \tag{2.27a}$$

$$B_x(x,0) = B_0\rho \left(\sum_{n=0}^{\infty} \frac{1}{n!} h_n \; x^n\right). \tag{2.27b}$$

k_n and h_n used in the above equations can be related to a_n and b_n given in Eq. (2.19) when the horizontal and vertical components of the field are evaluated on the horizontal axis, respectively. Therefore, with $b_0 = 10^4$ and $B_{R_0} = B_0$, one obtains

$$h_n = \frac{10^{-4}\; n!}{\rho\; R_0^n}\; a_n, \tag{2.28a}$$

$$k_n = \frac{10^{-4}\; n!}{\rho\; R_0^n}\; b_n. \tag{2.28b}$$

The expressions for the horizontal and vertical component of the field in Eq. (2.17) can be separated out as

$$B_x = 10^{-4} B_{R_0} \sum_{n=0}^{\infty} [b_n \ sin(n\theta) \ + \ a_n \ cos(n\theta)] \left(\frac{r}{R_0}\right)^n, \tag{2.29a}$$

$$B_y = 10^{-4} B_{R_0} \sum_{n=0}^{\infty} [b_n \ cos(n\theta) \ - \ a_n \ sin(n\theta)] \left(\frac{r}{R_0}\right)^n. \tag{2.29b}$$

The radial and azimuthal components of the field can be computed by using the following relations :

$$\begin{pmatrix} B_r \\ B_\theta \end{pmatrix} = \begin{pmatrix} cos(\theta) & sin(\theta) \\ -sin(\theta) & cos(\theta) \end{pmatrix} \begin{pmatrix} B_x \\ B_y \end{pmatrix} \tag{2.30}$$

Therefore, the radial and azimuthal components of the field can be written as :

$$B_r = 10^{-4} B_{R_0} \sum_{n=0}^{\infty} [b_n \ sin[(n+1)\theta] \ + \ a_n \ cos[(n+1)\theta]] \left(\frac{r}{R_0}\right)^n, \tag{2.31a}$$

$$B_\theta = 10^{-4} B_{R_0} \sum_{n=0}^{\infty} [b_n \ cos[(n+1)\theta] \ - \ a_n \ sin[(n+1)\theta]] \left(\frac{r}{R_0}\right)^n. \tag{2.31b}$$

In order to represent the vector potential in terms of harmonics, the following relations can be used :

$$B_r = \frac{1}{r}\frac{\partial A_z}{\partial \theta} \quad \text{and} \quad B_\theta = -\frac{\partial A_z}{\partial r},$$

since in the 2-dimensional case $A_x = A_y = 0$. Therefore, on integrating Eqs. (2.31) one obtains

$$A_z = -10^{-4} B_{R_0} \sum_{n=0}^{\infty} \left(\frac{R_0}{n+1}\right) [b_n cos[(n+1)\theta] - a_n sin[(n+1)\theta]] \left(\frac{r}{R_0}\right)^{n+1}. \tag{2.32}$$

The inverse transform can be used to obtain individual field harmonics at a reference radius R_0 in terms of field or vector potential. For this, first a component of the field or vector potential is evaluated at a radius r and then the integration is performed over the azimuth as follows :

$$a_n = -\frac{10^4}{\pi B_{R_0}} \left(\frac{R_0}{r}\right)^n \int_0^{2\pi} B_y(r,\theta) sin(n\theta) \ d\theta, \tag{2.33a}$$

$$= \frac{10^4}{\pi B_{R_0}} \left(\frac{R_0}{r}\right)^n \int_0^{2\pi} B_x(r,\theta) cos(n\theta) \quad d\theta, \tag{2.33b}$$

$$= \frac{10^4}{\pi B_{R_0}} \left(\frac{R_0}{r}\right)^n \int_0^{2\pi} B_r(r,\theta) cos((n+1)\theta) \quad d\theta, \tag{2.33c}$$

$$= -\frac{10^4}{\pi B_{R_0}} \left(\frac{R_0}{r}\right)^n \int_0^{2\pi} B_\theta(r,\theta) sin((n+1)\theta) \quad d\theta, \tag{2.33d}$$

$$= \frac{10^4(n+1)}{\pi R_0 B_{R_0}} \left(\frac{R_0}{r}\right)^{n+1} \int_0^{2\pi} A_z(r,\theta) sin((n+1)\theta) \quad d\theta, \tag{2.33e}$$

$$b_n = \frac{10^4}{\pi B_{R_0}} \left(\frac{R_0}{r}\right)^n \int_0^{2\pi} B_y(r,\theta) cos(n\theta) \quad d\theta, \tag{2.33f}$$

$$= \frac{10^4}{\pi B_{R_0}} \left(\frac{R_0}{r}\right)^n \int_0^{2\pi} B_x(r,\theta) sin(n\theta) \quad d\theta, \tag{2.33g}$$

$$= \frac{10^4}{\pi B_{R_0}} \left(\frac{R_0}{r}\right)^n \int_0^{2\pi} B_r(r,\theta) sin((n+1)\theta) \quad d\theta, \tag{2.33h}$$

$$= \frac{10^4}{\pi B_{R_0}} \left(\frac{R_0}{r}\right)^n \int_0^{2\pi} B_\theta(r,\theta) cos((n+1)\theta) \quad d\theta, \tag{2.33i}$$

$$= -\frac{10^4(n+1)}{\pi R_0 B_{R_0}} \left(\frac{R_0}{r}\right)^{n+1} \int_0^{2\pi} A_z(r,\theta) cos((n+1)\theta) \quad d\theta. \tag{2.33j}$$

For the primary harmonic component $n = m$, when the field is perpendicular to the horizontal plane, one obtains

$$b_m = 10^4 \quad \text{and} \quad a_m = 0.$$

2.3. Analytic Expressions for Accelerator Magnets

Analytic expressions for the basic cosine theta superconducting magnet design have been previously obtained and described by several authors [12-18,144,175,179]. Superconducting accelerator magnets are usually long cylindrical magnets with the current flowing parallel to the magnet axis (z-axis). The geometry of these magnets is such that one can compute the field in the body of the magnet by assuming that the current is carried by a large number of wires parallel to the z-axis. The total field is obtained by simply superimposing the field created by these wires. For this purpose, it is suitable to carry out a 2-dimensional analysis in the cylindrical coordinate system. A three dimensional analysis will be necessary for computing the field at the ends of the magnet.

Accelerator magnets are designed to produce a well defined field in the aperture of the magnets. The *field* in the aperture is constant for *dipoles*, the *first derivative* of the field is constant for *quadrupoles* and, in general, the nth *derivative* is constant for the n^{th}-order *multipole*. In the following sections, the current distributions needed to produce such multipole fields will be obtained.

2.3.1. Field and Vector Potential due to a Line Current

To compute the magnetic field and vector potential due to a single infinitely long wire, it is assumed to carry a current I in the z-direction which is perpendicular to the plane of paper. The field outside this wire at a perpendicular distance R from it will be computed. The cylindrical coordinate system is used to take advantage of the symmetry of the problem.

The magnetic field produced by this wire can be directly calculated by using the integral equation $\oint \vec{H} \cdot ds = I$ (Eqs. (2.9)) which gives:

$$H = \frac{I}{2\pi R}, \tag{2.34}$$

and in a medium having a relative permeability of μ

$$B = \frac{I\mu\mu_0}{2\pi R}. \tag{2.35}$$

The components of vector potential in cylindrical and Cartesian geometry can be written as

$$A_z = \frac{\mu\mu_0 I}{2\pi} ln\left(\frac{1}{R}\right), \tag{2.36a}$$

$$A_r = A_\theta = 0, \tag{2.36b}$$

$$A_x = A_y = 0. \tag{2.36c}$$

The validity of the above relation is verified when the curl of the vector potential is taken to obtain the magnetic field as per Eqs. (2.7). This gives $B_r = B_z = 0$ and $B_\theta = \frac{\mu\mu_0 I}{2\pi R}$; which is the same as in Eqs. (2.34) with only one component of the field present.

In accelerator magnets, the magnetic field and vector potential are usually expressed in terms of harmonic components. To develop this formalism a line current is assumed to be located at a point "Q" (at $\vec{a}$) and the magnetic field produced by it is computed at point "P" (at $\vec{r}$), as shown in Fig. 2.1. The distance between the two is $\vec{R} = \vec{r}$ - $\vec{a}$ with the magnitude $|R| = \sqrt{r^2 + a^2 - 2racos(\theta - \phi)}$.

In this section, the computations will be mostly done in a space free of magnetic material where the relative permeability μ is one. Moreover, to simplify the expressions to follow, Eq. $(2.36a)$ is re-written after adding a constant :

$$A_z\,(r, \theta) = -\frac{\mu_o I}{2\pi} ln\left(\frac{R}{a}\right); \tag{2.37}$$

the addition of such a constant does not change the magnetic field which is a derivative of A_z.

Now $A_z(r, \theta)$ will be given in terms of a series expansion containing, in general, summation of terms like $\left(\frac{r}{a}\right)^m$ and $\left(\frac{a}{r}\right)^m$, together with trigonometric functions like $cos(m\theta)$ and $sin(m\theta)$. The exact solution will depend on a particular problem. For example, in the solution of the case when r approaches the origin $(r \to 0)$, the $\left(\frac{a}{r}\right)^m$ terms can't be present. Similarly in the solution of the case when r approaches infinity $(r \to \infty)$, the $\left(\frac{a}{r}\right)^m$ terms can't be present.

In order to obtain an expansion of the ln in Eq. (2.37), the following manipulation is carried out :

$$R^2 = r^2 + a^2 - 2ra\ cos\,(\theta - \phi)\,,$$

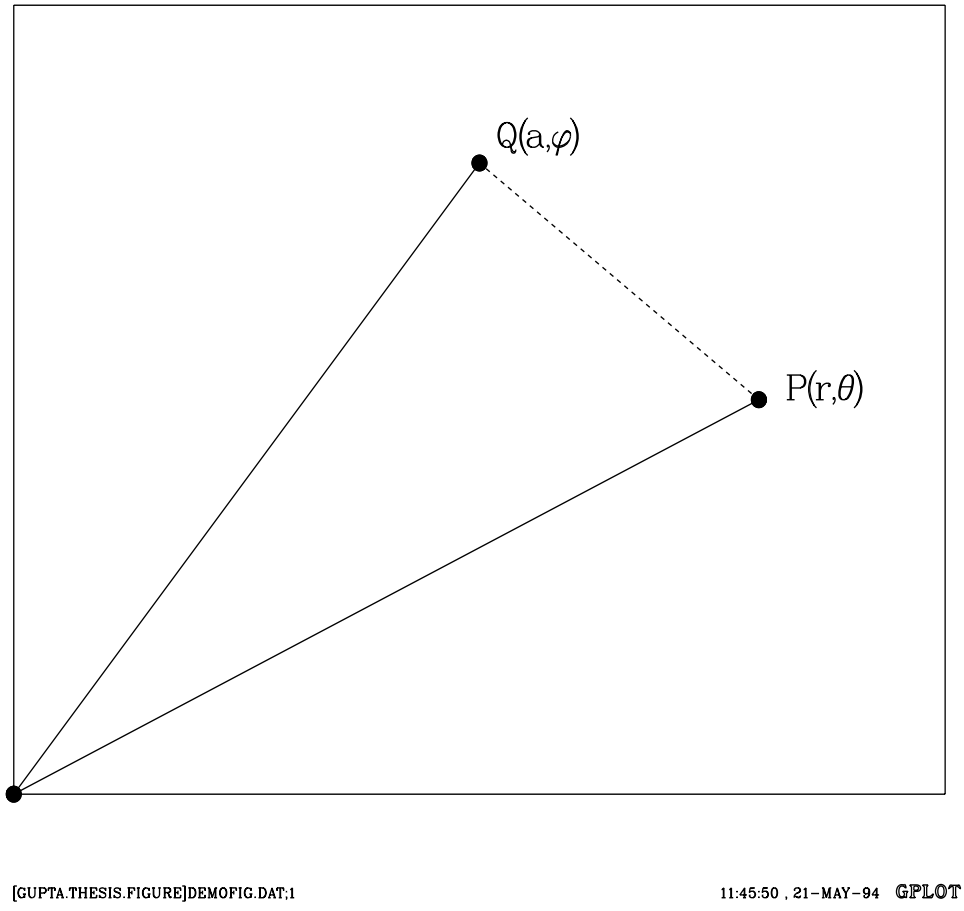

Figure 2.1: Computation of the field at a location "P" produced by the line current located at a position "Q".

$$\frac{R}{a} = \left(1 - \left(\frac{r}{a}\right)e^{i(\phi-\theta)}\right)^{\frac{1}{2}} \cdot \left(1 - \left(\frac{r}{a}\right)e^{-i(\phi-\theta)}\right)^{\frac{1}{2}},$$

$$ln\left(\frac{R}{a}\right) = \frac{1}{2}ln\left(1 - \left(\frac{r}{a}\right)e^{i(\phi-\theta)}\right) + \frac{1}{2}ln\left(1 - \left(\frac{r}{a}\right)e^{-i(\phi-\theta)}\right).$$

For $|z| < 1$, the logarithmic expansion is given by

$$ln(1-z) = -\left[z + \left(\frac{z^2}{2}\right) + \left(\frac{z^3}{3}\right) + ...\right] = -\sum_{n=1}^{\infty} \frac{z^n}{n}.$$

Therefore, for r < a

$$ln\left(\frac{R}{a}\right) = -\left[\frac{1}{2}\sum_{n=1}^{\infty}\left(\frac{1}{n}\right)\left(\frac{r}{a}\right)^n e^{i\ n(\phi-\theta)} + \frac{1}{2}\sum_{n=1}^{\infty}\left(\frac{1}{n}\right)\left(\frac{r}{a}\right)^n e^{-i\ n(\phi-\theta)}\right],$$

$$ln\left(\frac{R}{a}\right) = -\sum_{n=1}^{\infty}\left(\frac{1}{n}\right)\left(\frac{r}{a}\right)^n cos\left(n\left(\phi-\theta\right)\right). \tag{2.38}$$

Substituting Eqs. (2.38) in Eqs. (2.37) the desired expansion for the vector potential is obtained (for r < a) :

$$A_z\left(r,\theta\right) = \frac{\mu_o I}{2\pi}\sum_{n=1}^{\infty}\left(\frac{1}{n}\right)\left(\frac{r}{a}\right)^n cos\left(n\left(\phi-\theta\right)\right). \tag{2.39}$$

The magnetic field components are obtained by using Eqs. (2.7) and Eqs. (2.37) with $A_r = A_\theta = 0$:

$$B_r = \frac{1}{r}\left(\frac{\partial A_z}{\partial \theta}\right), \tag{2.40a}$$

$$B_\theta = -\frac{\partial A_z}{\partial r}, \tag{2.40b}$$

$$B_z = 0. \tag{2.40c}$$

Therefore, for r < a, one would obtain :

$$B_r = \frac{\mu_o I}{2\pi a}\sum_{n=1}^{\infty}\left(\frac{r}{a}\right)^{n-1} sin\left[\left(n\right)\left(\phi-\theta\right)\right], \tag{2.41a}$$

$$B_\theta = -\frac{\mu_o I}{2\pi a}\sum_{n=1}^{\infty}\left(\frac{r}{a}\right)^{n-1} cos\left[\left(n\right)\left(\phi-\theta\right)\right], \tag{2.41b}$$

$$B_z = 0. \tag{2.41c}$$

In order to compute the harmonics components, the above equations are compared with Eqs. (2.31). It should be noted that there the summation starts from $n = 0$ instead of $n = 1$ in Eq. (2.39). The following expressions for the normal and skew harmonics at a reference radius R_0 are obtained for a line current located at (a, ϕ) :

$$b_n = 10^4\left(\frac{R_0}{a}\right)^n cos\left[\left(n+1\right)\phi\right], \tag{2.42a}$$

$$a_n = -10^4\left(\frac{R_0}{a}\right)^n sin\left[\left(n+1\right)\phi\right], \tag{2.42b}$$

and $B_{R_o} = -\frac{\mu_o I}{2\pi a}$.

For r > a case, the following rearrangement is performed to obtain an appropriate expansion :

$$\frac{R}{a} = \left(\frac{r}{a}\right)\left(1 - \left(\frac{a}{r}\right)e^{i(\phi-\theta)}\right)^{\frac{1}{2}} \cdot \left(1 - \left(\frac{a}{r}\right)e^{-i(\phi-\theta)}\right)^{\frac{1}{2}},$$

$$ln\left(\frac{R}{a}\right) = ln\left(\frac{r}{a}\right) + \left[\frac{1}{2}ln\left(1 - \left(\frac{a}{r}\right)e^{i(\phi-\theta)}\right) + \frac{1}{2}ln\left(1 - \left(\frac{a}{r}\right)e^{-i(\phi-\theta)}\right)\right],$$

$$ln\left(\frac{R}{a}\right) = ln\left(\frac{r}{a}\right) - \left[\frac{1}{2}\sum_{n=1}^{\infty}\left(\frac{1}{n}\right)\left(\frac{a}{r}\right)^n e^{i\ n(\phi-\theta)} + \frac{1}{2}\sum_{n=1}^{\infty}\left(\frac{1}{n}\right)\left(\frac{a}{r}\right)^n e^{-i\ n(\phi-\theta)}\right],$$

$$ln\left(\frac{R}{a}\right) = ln\left(\frac{r}{a}\right) - \sum_{n=1}^{\infty}\left(\frac{1}{n}\right)\left(\frac{a}{r}\right)^n cos\left(n\left(\phi-\theta\right)\right). \tag{2.43}$$

Therefore, for r > a, one obtains the following expression for the vector potential :

$$A_z\left(r,\theta\right) = -\frac{\mu_o I}{2\pi}ln\left(\frac{r}{a}\right) + \frac{\mu_o I}{2\pi}\sum_{n=1}^{\infty}\left(\frac{1}{n}\right)\left(\frac{a}{r}\right)^n cos\left(n\left(\phi-\theta\right)\right). \tag{2.44}$$

The magnetic field components are obtained by using Eqs. (2.40) :

$$B_r = \frac{\mu_o I}{2\pi a}\sum_{n=0}^{\infty}\left(\frac{a}{r}\right)^{n+1} sin\left(n\left(\phi-\theta\right)\right), \tag{2.45a}$$

$$B_\theta = \frac{\mu_o I}{2\pi a}\sum_{n=0}^{\infty}\left(\frac{a}{r}\right)^{n+1} cos\left(n\left(\phi-\theta\right)\right), \tag{2.45b}$$

$$B_z = 0. \tag{2.45c}$$

It may be noted that in the expression for B_θ, the summation in n starts from $n = 0$ instead of $n = 1$. The (B_x, B_y) components of the field can be computed using the following relation:

$$\begin{pmatrix} B_x \\ B_y \end{pmatrix} = \begin{pmatrix} cos\left(\theta\right) & -sin\left(\theta\right) \\ sin\left(\theta\right) & cos\left(\theta\right) \end{pmatrix} \begin{pmatrix} B_r \\ B_\theta \end{pmatrix}. \tag{2.46}$$

2.3.2. Line Current in a Cylindrical Iron Cavity

Expressions are obtained here for the vector potential and magnetic field due to an infinitely long paraxial filament of current I at a radius a in a cylindrical cavity having a radius $R_f > a$. The iron is infinitely long and infinitely thick and has a constant relative permeability μ, which is referred to here simply as permeability following the convention explained earlier. The method of image currents can be applied to include the contribution from the iron [179]. The expressions are obtained here by matching the boundary conditions at the interface of the air and iron boundary [19]. General expressions for the vector potential and the components of the field in the region $a < r < R_f$, are given by :

$$A_z(r,\theta) = -\frac{\mu_o I}{2\pi} ln\left(\frac{r}{a}\right) + \frac{\mu_o I}{2\pi}\sum_{n=1}^{\infty}\left(\frac{1}{n}\right)\left(\frac{a}{r}\right)^n cos\left(n\left(\phi-\theta\right)\right) + \mu_o\sum_{n=1}^{\infty} E_n r^n cos\left(n\left(\phi-\theta\right)\right), \tag{2.47}$$

$$B_r = \frac{\mu_o I}{2\pi a}\sum_{n=1}^{\infty}\left(\frac{a}{r}\right)^{n+1} sin\left(n\left(\phi-\theta\right)\right) + \mu_o\sum_{n=1}^{\infty} nE_n r^{n-1} sin\left(n\left(\phi-\theta\right)\right), \tag{2.48a}$$

$$H_\theta = \frac{I}{2\pi a}\sum_{n=0}^{\infty}\left(\frac{a}{r}\right)^{n+1} cos\left(n\left(\phi-\theta\right)\right) - \sum_{n=1}^{\infty} nE_n r^{n-1} cos\left(n\left(\phi-\theta\right)\right), \tag{2.48b}$$

and in the region $r > R_f$:

$$A_z(r,\theta) = \mu\mu_o F_o ln\left(\frac{r}{a}\right) + \mu\mu_o\sum_{n=1}^{\infty} F_n\left(\frac{1}{r}\right)^n cos\left(n\left(\phi-\theta\right)\right), \tag{2.49}$$

$$B_r = \mu\mu_o\sum_{n=1}^{\infty} nF_n\left(\frac{1}{r}\right)^{n+1} sin\left(n\left(\phi-\theta\right)\right), \tag{2.50a}$$

$$H_\theta = -\frac{F_o}{r} + \sum_{n=1}^{\infty} nF_n\left(\frac{1}{r}\right)^{n+1} cos\left(n\left(\phi-\theta\right)\right), \tag{2.50b}$$

where E_n and F_n are coefficients which can be determined by the boundary conditions at $r = R_f$ that

$$(B_r)_{air} = (B_r)_{iron}\,,$$
$$(H_\theta)_{air} = (H_\theta)_{iron}\,,$$

i.e. the normal component of B and the azimuthal component of H are continuous. Therefore, the required boundary conditions at $r = R_f$ for $n \neq 0$ gives :

$$\frac{\mu_o I}{2\pi a}\left(\frac{a}{R_f}\right)^{n+1} + n\ \mu_o\ E_n {R_f}^{n-1} = n\ \mu_0\ \mu\ F_n\left(\frac{1}{R_f}\right)^{n+1},$$
$$\frac{I}{2\pi a}\left(\frac{a}{R_f}\right)^{n+1} - \ n\ E_n {R_f}^{n-1} = n\ F_n\left(\frac{1}{R_f}\right)^{n+1},$$

which gives

$$E_n = \frac{1}{n}\frac{\mu-1}{\mu+1}\ \frac{I}{2\pi}\ \left(\frac{a}{R_f^2}\right)^n, \tag{2.51a}$$

$$F_n = \frac{1}{n}\frac{2}{\mu+1}\ \frac{I}{2\pi a}\ a^{n+1}. \tag{2.51b}$$

The $n = 0$ term appears only in the expression for H_θ and on matching the boundary condition, one obtains :

$$\frac{I}{2\pi R_f} = -\frac{F_o}{R_f},$$

which gives

$$F_o = -\frac{I}{2\pi}. \tag{2.52}$$

The expressions for vector potential and field components for $a < r < R_f$ case are obtained when E_n from Eq. (2.51a) is substituted in Eq. (2.47) and Eqs. (2.48) :

$$A_z\,(r,\theta) = -\frac{\mu_o I}{2\pi} ln\left(\frac{r}{a}\right) + \frac{\mu_o I}{2\pi}\sum_{n=1}^{\infty}\frac{1}{n}\left(\frac{a}{r}\right)^n cos\,(n\,(\phi-\theta))\left[1+\frac{\mu-1}{\mu+1}\left(\frac{r}{R_f}\right)^{2n}\right], \tag{2.53}$$

$$B_r = \frac{\mu_o I}{2\pi a}\sum_{n=1}^{\infty}\left(\frac{a}{r}\right)^{n+1} sin\,(n\,(\phi-\theta))\left[1+\frac{\mu-1}{\mu+1}\left(\frac{r}{R_f}\right)^{2n}\right], \tag{2.54a}$$

$$B_\theta = \frac{\mu_o I}{2\pi r} + \frac{\mu_o I}{2\pi a}\sum_{n=1}^{\infty}\left(\frac{a}{r}\right)^{n+1} cos\,(n\,(\phi-\theta))\left[1-\frac{\mu-1}{\mu+1}\left(\frac{r}{R_f}\right)^{2n}\right]. \tag{2.54b}$$

In the above equations, the second term in the square brackets is the additional contribution of the iron to the field produced by the coil.

To obtain the expressions for the vector potential and field for $r < a$ it must be noted that a current filament is present at $r = a$. However, the radial component of the field B_r must still be continuous, i.e. at $r = a$

$$B_r\,(in) = B_r\,(out)\,,$$

where $B_r(in)$ and $B_r(out)$ are the magnetic induction for $r < a$ and $a < r < R_f$ respectively. The presence of the source (current), however, gives a discontinuity in the azimuthal component of the field H_θ with $H_\theta(in)$ - $H_\theta(out)$ determined by the current density at $r = a$. A general expression for the vector potential for $r < a$ is given by (see Eq. (2.39)) :

$$A_z\,(r,\theta) = \mu_o \sum_{n=1}^{\infty} I_n \;\; r^n cos\,(n\,(\phi - \theta))\,, \tag{2.55}$$

where the I_n are unknown coefficients. Using Eqs. (2.40) :

$$B_r = \mu_o \sum_{n=1}^{\infty} I_n \;\; n \;\; r^{n-1} sin\,(n\,(\phi - \theta))\,, \tag{2.56a}$$

$$B_\theta = -\mu_o \sum_{n=1}^{\infty} I_n \;\; n \;\; r^{n-1} cos\,(n\,(\phi - \theta))\,, \tag{2.56b}$$

$$B_z = 0. \tag{2.56c}$$

In order for B_r to be continuous at $r = a$ one obtains from Eq. (2.56a) and Eq. (2.54a) :

$$I_n = \frac{I}{2\pi}\left(\frac{1}{n}\right)\left(\frac{1}{a}\right)^n \left[1 + \frac{\mu - 1}{\mu + 1}\left(\frac{a}{R_f}\right)^{2n}\right]. \tag{2.57}$$

Using this in Eqs. (2.56) gives the expressions for the field and vector potential for $r < a$ as :

$$A_z\,(r,\theta) = \frac{\mu_o I}{2\pi} \sum_{n=1}^{\infty} \left(\frac{1}{n}\right)\left(\frac{r}{a}\right)^n cos\,(n\,(\phi - \theta)) \left[1 + \frac{\mu - 1}{\mu + 1}\left(\frac{a}{R_f}\right)^{2n}\right]. \tag{2.58}$$

$$B_r = \frac{\mu_o I}{2\pi a} \sum_{n=1}^{\infty} \left(\frac{r}{a}\right)^{n-1} sin\,(n\,(\phi - \theta)) \left[1 + \frac{\mu - 1}{\mu + 1}\left(\frac{a}{R_f}\right)^{2n}\right], \tag{2.59a}$$

$$B_\theta = -\frac{\mu_o I}{2\pi a} \sum_{n=1}^{\infty} \left(\frac{r}{a}\right)^{n-1} cos\,(n\,(\phi - \theta)) \left[1 + \frac{\mu - 1}{\mu + 1}\left(\frac{a}{R_f}\right)^{2n}\right], \tag{2.59b}$$

$$B_z = 0. \tag{2.59c}$$

To compute the field harmonics the procedure of Eqs. (2.42) is repeated. As before, the summation over n in the above is now changed so that it starts from n=0 instead of n=1.

$$b_n = 10^4 \left(\frac{R_0}{a}\right)^n \cos\left((n+1)\phi\right)\left[1 + \frac{\mu-1}{\mu+1}\left(\frac{a}{R_f}\right)^{2(n+1)}\right], \tag{2.60a}$$

$$a_n = -10^4 \left(\frac{R_0}{a}\right)^n \sin\left((n+1)\phi\right)\left[1 + \frac{\mu-1}{\mu+1}\left(\frac{a}{R_f}\right)^{2(n+1)}\right]. \tag{2.60b}$$

All expressions derived so far reproduce the results obtained from the method of images [179] which says that the effect of iron can be replaced by an additional line current I' located at (a', ϕ) with

$$I' = \left(\frac{\mu-1}{\mu+1}\right) I,$$
$$a' = \frac{R_f^2}{a}.$$

The expressions for vector potential and field components for $r > R_f$ case are obtained when F_n from Eq. (2.51b) and Eq. (2.52) are substituted in Eqs. (2.49) and Eqs. (2.50) :

$$A_z(r,\theta) = -\frac{\mu\mu_o I}{2\pi} ln\left(\frac{r}{a}\right) + \frac{2\mu}{\mu+1}\frac{\mu_o I}{2\pi}\sum_{n=1}^{\infty}\left(\frac{1}{n}\right)\left(\frac{a}{r}\right)^n \cos\left(n\left(\phi-\theta\right)\right) \tag{2.61}$$

$$B_r = \frac{2\mu}{\mu+1}\frac{\mu_o I}{2\pi a}\sum_{n=1}^{\infty}\left(\frac{a}{r}\right)^{n+1} \sin\left(n\left(\phi-\theta\right)\right), \tag{2.62a}$$

$$B_\theta = \frac{\mu\mu_o I}{2\pi r} + \frac{2\mu}{\mu+1}\frac{\mu_o I}{2\pi a}\sum_{n=1}^{\infty}\left(\frac{a}{r}\right)^{n+1} \cos\left(n\left(\phi-\theta\right)\right). \tag{2.62b}$$

2.3.3. Line Current in a Cylindrical Iron Shell

In deriving the expressions for the vector potential and field due to a line current inside an cylindrical iron it was assumed in the last section that the iron outer boundary extends to infinity. This is, however, not the case in practice. If the outer diameter of the cylindrical iron shell is R_a, then the general expressions for the vector potential in the various regions are given by :

$$A_z(r,\theta) = \mu_o \sum_{n=1}^{\infty} I_n^{'}\ r^n cos\left(n\left(\phi-\theta\right)\right), \qquad [for \quad \mathrm{r} < \mathrm{a}] \tag{2.63a}$$

$$A_z(r,\theta) = -\frac{\mu_o I}{2\pi} ln\left(\frac{r}{a}\right) + \frac{\mu_o I}{2\pi}\sum_{n=1}^{\infty}\left(\frac{1}{n}\right)\left(\frac{a}{r}\right)^n cos\left(n\left(\phi-\theta\right)\right) + \mu_o \sum_{n=1}^{\infty} E_n^{'} r^n cos\left(n\left(\phi-\theta\right)\right), \qquad [for \quad \mathrm{a} < \mathrm{r} < \mathrm{R_f}] \tag{2.63b}$$

$$A_z(r,\theta) = \mu\mu_o F_o^{'} ln\left(\frac{r}{a}\right) + \mu\mu_o \sum_{n=1}^{\infty} F_n^{'}\left(\frac{1}{r}\right)^n cos\left(n\left(\phi-\theta\right)\right) + \mu\mu_o \sum_{n=1}^{\infty} G_n^{'} r^n cos\left(n\left(\phi-\theta\right)\right), \qquad [for \quad \mathrm{R_f} < \mathrm{r} < \mathrm{R_a}] \tag{2.63c}$$

$$A_z(r,\theta) = \mu_o H_o^{'} ln\left(\frac{r}{a}\right) + \mu_o \sum_{n=1}^{\infty} H_n^{'}\left(\frac{1}{r}\right)^n cos\left(n\left(\phi-\theta\right)\right), \qquad [for \quad \mathrm{r} > \mathrm{R_a}] \tag{2.63d}$$

Following an approach similar to one used in previous section, the five coefficients ($E_n^{'},\ F_n^{'},\ G_n^{'},\ H_n^{'},\ I_n^{'}$) are obtained by matching the five boundary conditions (B_r is continuous at $r = a$, $r = R_f$ and $r = R_a$ and B_θ is continuous at $r = R_f$ and $r = R_a$). The results of that exercise for $n > 0$ are given here :

$$I_n^{'} = \frac{I}{2\pi}\left(\frac{1}{n}\right)\left(\frac{1}{a}\right)^n \left[1 + \frac{\mu-1}{\mu+1}\left(\frac{a}{R_f}\right)^{2n} \frac{\left[1-\left(\frac{R_f}{R_a}\right)^{2n}\right]}{\left[1-\left(\frac{\mu-1}{\mu+1}\right)^2\left(\frac{R_f}{R_a}\right)^{2n}\right]}\right] \quad , \tag{2.64a}$$

$$E_n^{'} = \frac{1}{n}\frac{\mu-1}{\mu+1}\ \frac{I}{2\pi}\ \left(\frac{a}{R_f^2}\right)^n \frac{\left[1-\left(\frac{R_f}{R_a}\right)^{2n}\right]}{\left[1-\left(\frac{\mu-1}{\mu+1}\right)^2\left(\frac{R_f}{R_a}\right)^{2n}\right]} \quad , \tag{2.64b}$$

$$F_n^{'} = \frac{1}{\mu+1}\ \frac{I}{n\pi}\ \frac{a^n}{\left[1-\left(\frac{\mu-1}{\mu+1}\right)^2\left(\frac{R_f}{R_a}\right)^{2n}\right]}\quad , \tag{2.64c}$$

$$G_n^{'} = -\frac{(\mu-1)}{(\mu+1)^2}\ \frac{I}{n\pi}\frac{\left(\frac{a}{R_a^2}\right)^n}{\left[1-\left(\frac{\mu-1}{\mu+1}\right)^2\left(\frac{R_f}{R_a}\right)^{2n}\right]}\quad , \tag{2.64d}$$

$$H_n^{'} = \frac{2\mu}{(\mu+1)^2}\ \frac{I}{n\pi}\ \frac{a^n}{\left[1-\left(\frac{\mu-1}{\mu+1}\right)^2\left(\frac{R_f}{R_a}\right)^{2n}\right]}\quad , \tag{2.64e}$$

and for $n = 0$, the terms are:

$$F_o^{'} \ = \ H_o^{'} = -\frac{I}{2\pi}. \tag{2.65}$$

Therefore, the expressions for the vector potential and field components in various regions due to a line current I at (a,θ) inside a cylindrical iron shell having inner radius R_f and outer radius R_a are given as follows (in each case $B_z(r,\theta)=0$) :

Inside Coil($\mathbf{r < a}$)

$$A_z(r,\theta) = \frac{\mu_o I}{2\pi}\sum_{n=1}^{\infty}\left(\frac{1}{n}\right)\left[1+\frac{\mu-1}{\mu+1}\left(\frac{a}{R_f}\right)^{2n}\frac{\left[1-\left(\frac{R_f}{R_a}\right)^{2n}\right]}{\left[1-\left(\frac{\mu-1}{\mu+1}\right)^2\left(\frac{R_f}{R_a}\right)^{2n}\right]}\right]\times \left(\frac{r}{a}\right)^n cos\left(n\left(\phi-\theta\right)\right)\quad . \tag{2.66}$$

$$B_r = \frac{\mu_o I}{2\pi a}\sum_{n=1}^{\infty}\left[1+\frac{\mu-1}{\mu+1}\left(\frac{a}{R_f}\right)^{2n}\frac{\left[1-\left(\frac{R_f}{R_a}\right)^{2n}\right]}{\left[1-\left(\frac{\mu-1}{\mu+1}\right)^2\left(\frac{R_f}{R_a}\right)^{2n}\right]}\right]\times \left(\frac{r}{a}\right)^{n-1} sin\left(n\left(\phi-\theta\right)\right)\quad , \tag{2.67a}$$

$$B_\theta = -\frac{\mu_o I}{2\pi a}\sum_{n=1}^{\infty}\left[1+\frac{\mu-1}{\mu+1}\left(\frac{a}{R_f}\right)^{2n}\frac{\left[1-\left(\frac{R_f}{R_a}\right)^{2n}\right]}{\left[1-\left(\frac{\mu-1}{\mu+1}\right)^2\left(\frac{R_f}{R_a}\right)^{2n}\right]}\right]\times \left(\frac{r}{a}\right)^{n-1} cos\left(n\left(\phi-\theta\right)\right)\quad , \tag{2.67b}$$

Between Coil and Iron ($\mathbf{a < r < R_f}$)

$$A_z(r,\theta) = -\frac{\mu_o I}{2\pi} ln\left(\frac{r}{a}\right) + \frac{\mu_o I}{2\pi}\sum_{n=1}^{\infty}\left(\frac{1}{n}\right)\left(1+\frac{\frac{\mu-1}{\mu+1}\left(\frac{r}{R_f}\right)^{2n}\left[1-\left(\frac{R_f}{R_a}\right)^{2m}\right]}{1-\left(\frac{\mu-1}{\mu+1}\right)^2\left(\frac{R_f}{R_a}\right)^{2n}}\right)\times$$

$$\left(\frac{a}{r}\right)^{n} cos\left(n\left(\phi-\theta\right)\right) \quad , \tag{2.68}$$

$$B_r = \frac{\mu_o I}{2\pi a}\sum_{n=1}^{\infty}\left(1+\frac{\frac{\mu-1}{\mu+1}\left(\frac{r}{R_f}\right)^{2n}\left[1-\left(\frac{R_f}{R_a}\right)^{2m}\right]}{1-\left(\frac{\mu-1}{\mu+1}\right)^{2}\left(\frac{R_f}{R_a}\right)^{2n}}\right)\times$$

$$\left(\frac{a}{r}\right)^{n+1} sin\left(n\left(\phi-\theta\right)\right) \quad , \tag{2.69a}$$

$$B_\theta = \frac{\mu_o I}{2\pi r}+\frac{\mu_o I}{2\pi a}\sum_{n=1}^{\infty}\left(1-\frac{\frac{\mu-1}{\mu+1}\left(\frac{r}{R_f}\right)^{2n}\left[1-\left(\frac{R_f}{R_a}\right)^{2m}\right]}{1-\left(\frac{\mu-1}{\mu+1}\right)^{2}\left(\frac{R_f}{R_a}\right)^{2n}}\right)\times$$

$$\left(\frac{a}{r}\right)^{n+1} cos\left(n\left(\phi-\theta\right)\right) \quad . \tag{2.69b}$$

Inside Iron ($\mathbf{R_f < r < R_a}$)

$$A_z\left(r,\theta\right) = -\frac{\mu\mu_o I}{2\pi} ln\left(\frac{r}{a}\right) + \frac{\mu\mu_o I}{\pi\left(\mu+1\right)}\sum_{n=1}^{\infty}\left(\frac{1}{n}\right)\frac{1-\frac{\mu-1}{\mu+1}\left(\frac{r}{R_a}\right)^{2n}}{1-\left(\frac{\mu-1}{\mu+1}\right)^{2}\left(\frac{R_f}{R_a}\right)^{2n}}\times \left(\frac{a}{r}\right)^{n} cos\left(n\left(\phi-\theta\right)\right) \quad , \tag{2.70}$$

$$B_r = \frac{\mu\mu_o I}{\pi a\left(\mu+1\right)}\sum_{n=1}^{\infty}\frac{1-\frac{\mu-1}{\mu+1}\left(\frac{r}{R_a}\right)^{2n}}{1-\left(\frac{\mu-1}{\mu+1}\right)^{2}\left(\frac{R_f}{R_a}\right)^{2n}}\times \left(\frac{a}{r}\right)^{n+1} sin\left(n\left(\phi-\theta\right)\right) \quad , \tag{2.71a}$$

$$B_\theta = \frac{\mu\mu_o I}{2\pi r}+\frac{\mu\mu_o I}{\pi a\left(\mu+1\right)}\sum_{n=1}^{\infty}\frac{1+\frac{\mu-1}{\mu+1}\left(\frac{r}{R_a}\right)^{2n}}{1-\left(\frac{\mu-1}{\mu+1}\right)^{2}\left(\frac{R_f}{R_a}\right)^{2n}}\times \left(\frac{a}{r}\right)^{n+1} cos\left(n\left(\phi-\theta\right)\right) \quad . \tag{2.71b}$$

Outside Iron ($\mathbf{r > R_a}$)

$$A_z\left(r,\theta\right) = -\frac{\mu_o I}{2\pi} ln\left(\frac{r}{a}\right)+\frac{2\mu\mu_o I}{\pi\left(\mu+1\right)^{2}}\sum_{n=1}^{\infty}\frac{1}{1-\left(\frac{\mu-1}{\mu+1}\right)^{2}\left(\frac{R_f}{R_a}\right)^{2n}}\times \left(\frac{1}{n}\right)\left(\frac{a}{r}\right)^{n} cos\left(n\left(\phi-\theta\right)\right) \tag{2.72}$$

$$B_r = \frac{2\mu}{(\mu+1)^2}\frac{\mu_o I}{\pi a}\sum_{n=1}^{\infty}\frac{1}{1-\left(\frac{\mu-1}{\mu+1}\right)^2\left(\frac{R_f}{R_a}\right)^{2n}} \times \left(\frac{a}{r}\right)^{n+1} sin\left(n\left(\phi-\theta\right)\right), \tag{2.73a}$$

$$B_\theta = \frac{\mu_o I}{2\pi r} + \frac{2\mu}{(\mu+1)^2}\frac{\mu_o I}{\pi a}\sum_{n=0}^{\infty}\frac{1}{1-\left(\frac{\mu-1}{\mu+1}\right)^2\left(\frac{R_f}{R_a}\right)^{2n}} \times \left(\frac{a}{r}\right)^{n+1} cos\left(n\left(\phi-\theta\right)\right). \tag{2.73b}$$

Field Harmonics

The field harmonics are given by :

$$b_n = 10^4\left(\frac{R_0}{a}\right)^n cos\left(\left(n+1\right)\phi\right) \left[1+\frac{\mu-1}{\mu+1}\left(\frac{a}{R_f}\right)^{2(n+1)}\frac{1-\left(\frac{R_f}{R_a}\right)^{2(n+1)}}{1-\left(\frac{\mu-1}{\mu+1}\right)^2\left(\frac{R_f}{R_a}\right)^{2(n+1)}}\right], \tag{2.74a}$$

$$a_n = -10^4\left(\frac{R_0}{a}\right)^n sin\left(\left(n+1\right)\phi\right) \left[1+\frac{\mu-1}{\mu+1}\left(\frac{a}{R_f}\right)^{2(n+1)}\frac{1-\left(\frac{R_f}{R_a}\right)^{2(n+1)}}{1-\left(\frac{\mu-1}{\mu+1}\right)^2\left(\frac{R_f}{R_a}\right)^{2(n+1)}}\right]. \tag{2.74b}$$

2.3.4. Field and Harmonics due to Current Blocks in Air

The expressions derived for the line current in the section 1.5.3.1 are extended here for one or more blocks of current. The geometry of the problem is such that a wire is replaced by a radial block between radii ρ_1 and ρ_2 and angle ϕ_1 and ϕ_2. The block has a constant current density J such that the total current is still I with $I = \frac{1}{2}J(\rho_2^2 - \rho_1^2)(\phi_2 - \phi_1)$. To compute the vector potential and component of field at (r, θ) Eq. (2.36) and Eqs. (2.41) should be integrated [179] as (for $r < \rho_1$) :

$$A_z(r,\theta) = \sum_{n=1}^{\infty} \int_{\rho_1}^{\rho_2} \frac{\mu_o J}{2\pi}\left(\frac{1}{n}\right)\left(\frac{r}{a}\right)^n a \; da \int_{\phi_1}^{\phi_2} cos\left[n\left(\phi - \theta\right)\right] \; d\phi, \tag{2.75}$$

$$B_r(r,\theta) = \sum_{n=1}^{\infty} \int_{\rho_1}^{\rho_2} \frac{\mu_o J}{2\pi a}\left(\frac{r}{a}\right)^{n-1} a \; da \int_{\phi_1}^{\phi_2} sin\left[n\left(\phi - \theta\right)\right] d\phi, \tag{2.76a}$$

$$B_\theta(r,\theta) = -\sum_{n=1}^{\infty} \int_{\rho_1}^{\rho_2} \frac{\mu_o J}{2\pi a}\left(\frac{r}{a}\right)^{n-1} a \; da \int_{\phi_1}^{\phi_2} cos\left[n\left(\phi - \theta\right)\right] \; d\phi. \tag{2.76b}$$

The integration of the above equations for the vector potential and the field components gives :

$$\begin{aligned} A_z(r,\theta) = {} & \frac{\mu_o J r}{2\pi}(\rho_2 - \rho_1)\left[sin\left(\phi_2 - \theta\right) - sin\left(\phi_1 - \theta\right)\right] \\ & + \frac{\mu_o J r^2}{8\pi} ln\left(\frac{\rho_2}{\rho_1}\right)\left[sin\left(2\left(\phi_2 - \theta\right)\right) - sin\left(2\left(\phi_1 - \theta\right)\right)\right] \\ & - \frac{\mu_o J}{2\pi}\sum_{n=3}^{\infty} \frac{r^n}{n^2\left(n-2\right)}\left(\frac{1}{\rho_2^{n-2}} - \frac{1}{\rho_1^{n-2}}\right) \quad \times \\ & \qquad \left[sin\left(n\left(\phi_2 - \theta\right)\right) - sin\left(n\left(\phi_1 - \theta\right)\right)\right], \end{aligned} \tag{2.77}$$

$$\begin{aligned} B_r(r,\theta) = {} & -\frac{\mu_o J}{2\pi}(\rho_2 - \rho_1)\left[cos\left(\phi_2 - \theta\right) - cos\left(\phi_1 - \theta\right)\right] \\ & - \frac{\mu_o J r}{4\pi} ln\left(\frac{\rho_2}{\rho_1}\right)\left[cos\left(2\left(\phi_2 - \theta\right)\right) - cos\left(2\left(\phi_1 - \theta\right)\right)\right] \\ & + \frac{\mu_o J}{2\pi}\sum_{n=3}^{\infty} \frac{r^{n-1}}{n\left(n-2\right)}\left(\frac{1}{\rho_2^{n-2}} - \frac{1}{\rho_1^{n-2}}\right) \quad \times \\ & \qquad \left[cos\left(n\left(\phi_2 - \theta\right)\right) - cos\left(n\left(\phi_1 - \theta\right)\right)\right], \end{aligned} \tag{2.78a}$$

$$\begin{aligned} B_\theta(r,\theta) = {} & -\frac{\mu_o J}{2\pi}(\rho_2 - \rho_1)\left[sin\left(\phi_2 - \theta\right) - sin\left(\phi_1 - \theta\right)\right] \\ & - \frac{\mu_o J r}{4\pi} ln\left(\frac{\rho_2}{\rho_1}\right)\left[sin\left(2\left(\phi_2 - \theta\right)\right) - sin\left(2\left(\phi_1 - \theta\right)\right)\right] \\ & + \frac{\mu_o J}{2\pi}\sum_{n=3}^{\infty} \frac{r^{n-1}}{n\left(n-2\right)}\left(\frac{1}{\rho_2^{n-2}} - \frac{1}{\rho_1^{n-2}}\right) \quad \times \\ & \qquad \left[sin\left(n\left(\phi_2 - \theta\right)\right) - sin\left(n\left(\phi_1 - \theta\right)\right)\right]. \end{aligned} \tag{2.78b}$$

Now the harmonics components a_n and b_n (the dimensionless coefficients as defined in Eqs. (2.31)) are computed due to the field from a single current block. It should be noted that the summation of a_n and b_n starts from $n = 0$ instead of $n = 1$ in Eq. (2.78). For $n > 1$ and harmonics normalized to the dipole field, the following expressions for the normal and skew harmonics at a reference radius R_o are obtained using the procedure of Eqs. (2.42) :

$$b_n = \frac{-10^4 R_0^n}{(n^2-1)} \left[\left(\frac{1}{\rho_2^{n-1}} - \frac{1}{\rho_1^{n-1}} \right) / (\rho_2 - \rho_1) \right] \frac{sin\left((n+1)\phi_2\right) - sin\left((n+1)\phi_1\right)}{sin\left(\phi_2\right) - sin\left(\phi_1\right)}, \tag{2.79a}$$

$$a_n = \frac{-10^4 R_0^n}{(n^2-1)} \left[\left(\frac{1}{\rho_2^{n-1}} - \frac{1}{\rho_1^{n-1}} \right) / (\rho_2 - \rho_1) \right] \frac{cos\left((n+1)\phi_2\right) - cos\left((n+1)\phi_1\right)}{sin\left(\phi_2\right) - sin\left(\phi_1\right)}, \tag{2.79b}$$

and the harmonic expressions for $n = 1$ are

$$b_n = \frac{10^4 R_0 ln\left(\frac{\rho_2}{\rho_1}\right)}{\rho_2 - \rho_1} \frac{sin\left(2\phi_2\right) - sin\left(2\phi_1\right)}{sin\left(\phi_2\right) - sin\left(\phi_1\right)}, \tag{2.80a}$$

$$a_n = \frac{10^4 R_0 ln\left(\frac{\rho_2}{\rho_1}\right)}{\rho_2 - \rho_1} \frac{cos\left(2\phi_2\right) - cos\left(2\phi_1\right)}{sin\left(\phi_2\right) - sin\left(\phi_1\right)}. \tag{2.80b}$$

To compute A_n and B_n (having the dimensions of field and defined in Eqs. (2.21)) one derives the expressions for field components from Eqs. (2.78) at a reference radius R_o in the form of :

$$B_r = \sum_{n=1}^{\infty} \left(\frac{r}{R_o} \right)^{n-1} \left[B_n \ sin\left(n\theta\right) \ + \ A_n \ cos\left(n\theta\right) \right], \tag{2.81a}$$

$$B_\theta = \sum_{n=1}^{\infty} \left(\frac{r}{R_o} \right)^{n-1} \left[B_n \ cos\left(n\theta\right) \ - \ A_n \ sin\left(n\theta\right) \right], \tag{2.81b}$$

to obtain

$$A_1 = -\frac{\mu_o J}{2\pi} (\rho_2 - \rho_1) \left[cos\left(\phi_2\right) - cos\left(\phi_1\right) \right], \tag{2.82a}$$

$$A_2 = -\frac{\mu_o J R_o}{2\pi} ln\left(\frac{\rho_2}{\rho_1}\right) \left[cos\left(2\phi_2\right) - cos\left(2\phi_1\right) \right], \tag{2.82b}$$

for n $\geq$ 3

$$A_n = \frac{\mu_o J}{2\pi} \frac{R_o^{n-1}}{n\left(n-2\right)} \left(\frac{1}{\rho_2^{n-2}} - \frac{1}{\rho_1^{n-2}} \right) \left[cos\left(n\phi_2\right) - cos\left(n\phi_1\right) \right], \tag{2.82c}$$

and

$$B_1 = -\frac{\mu_o J}{2\pi}(\rho_2 - \rho_1)\left[sin\left(\phi_2\right) - sin\left(\phi_1\right)\right], \tag{2.83a}$$

$$B_2 = -\frac{\mu_o J R_o}{2\pi} ln\left(\frac{\rho_2}{\rho_1}\right)\left[sin\left(2\phi_2\right) - sin\left(2\phi_1\right)\right], \tag{2.83b}$$

for n ≥ 3

$$B_n = \frac{\mu_o J}{2\pi}\sum_{n=3}^{\infty}\frac{R_o^{n-1}}{n\left(n-2\right)}\left(\frac{1}{\rho_2^{n-2}} - \frac{1}{\rho_1^{n-2}}\right)\left[sin\left(n\phi_2\right) - sin\left(n\phi_1\right)\right]. \tag{2.83c}$$

In a typical superconducting magnet several current blocks are used to generate the desired multipolar field. In order to compute the harmonics due to several current blocks, the field and field harmonics A_n and B_n (coefficients having the dimension of field) can be directly superimposed. However, a_n and b_n (dimensionless coefficients) can not be directly added and they must be obtained from A_n and B_n as follows :

$$b_n = 10^4 \frac{\sum_k \left(B_{n+1}\right)_k}{\sum_k \left(B_{m+1}\right)_k}, \tag{2.84a}$$

$$a_n = 10^4 \frac{\sum_k \left(A_{n+1}\right)_k}{\sum_k \left(B_{m+1}\right)_k}, \tag{2.84b}$$

where the summation k is carried over all k blocks with the k^{th} block carrying a current density of J_k and located between radii ρ_{1k} and ρ_{2k} and angles ϕ_{1k} and ϕ_{2k}. The A_n and B_n for each current blocks are computed using the expressions given above. The harmonics are defined such that the fundamental harmonic b_m is normalized to 10^4.

The field components outside a current block ($r > \rho_2$) are obtained similarly by integrating Eqs. (2.78) and the results are given below

$$B_r\left(r,\theta\right) = -\frac{\mu_o J}{2\pi}\sum_{n=1}^{\infty}\frac{\rho_2^{n+1} - \rho_1^{n+1}}{n\left(n+2\right)r^{n+1}}\left[cos\left(n\left(\phi_2 - \theta\right)\right) - cos\left(n\left(\phi_1 - \theta\right)\right)\right], \tag{2.85a}$$

$$B_\theta\left(r,\theta\right) = \frac{\mu_o J}{2\pi}\sum_{n=1}^{\infty}\frac{\rho_2^{n+1} - \rho_1^{n+1}}{n\left(n+2\right)r^{n+1}}\left[sin\left(n\left(\phi_2 - \theta\right)\right) - sin\left(n\left(\phi_1 - \theta\right)\right)\right]. \tag{2.85b}$$

The field inside a current block ($\rho_1 < r < \rho_2$) can be obtained by dividing the current block in two parts (a) from radius ρ_1 to radius r and (b) from radius r to radius ρ_2. Then the superimposition principle can be used to determine the field components with the (a) part evaluated from Eqs. (2.78) with ρ_2 replaced by r and the (b) part from Eqs. (2.85) with ρ_1 replaced by r.

2.3.5. Field Harmonics due to Current Blocks in a Cylindrical Iron Shell

As shown in a previous section (Eqs. (2.67) for $r < a$), the expressions for the field component due to current blocks get modified when they are placed inside an iron shell having an iron inner radius of R_f and outer radius of R_a. The harmonic coefficients A_n and B_n are enhanced by :

$$K_n = \left[1 + \frac{\mu - 1}{\mu + 1}\left(\frac{a}{R_f}\right)^{2n}\right] \frac{\left[1 - \left(\frac{R_f}{R_a}\right)^{2n}\right]}{\left[1 - \left(\frac{\mu-1}{\mu+1}\right)^2 \left(\frac{R_f}{R_a}\right)^{2n}\right]},$$

To give

$$A_n^{'} = K_n \times A_n,$$

and

$$B_n^{'} = K_n \times B_n.$$

The harmonics coefficients a_n and b_n given in Eqs. (2.84) are modified to :

$$b_n = 10^4 \frac{\sum_k \left(K_{n+1} \ B_{n+1}\right)_k}{\sum_k \left(K_{m+1} \ B_{m+1}\right)_k} \tag{2.86a}$$

$$a_n = 10^4 \frac{\sum_k \left(K_{n+1} \ A_{n+1}\right)_k}{\sum_k \left(K_{m+1} \ B_{m+1}\right)_k} \tag{2.86b}$$

2.3.6. COS($m\theta$) Current Distribution for Ideal Fields

In this section, it is demonstrated that an ideal $2m$ (m=1 for dipole) multipolar field shape in accelerator magnets can be produced by a COS($m\theta$) current distribution. In the last section the expressions for the field and vector potential produced by a line current were obtained. The field in the cross section of the magnet can be described by superimposing the field produced by a large number of such wires.

A cylindrical current sheet [12–18] at a radius of a is shown in Fig. 2.2, where the angular current density $I(\phi)$ in $Amperes/radian$ as a function of angle ϕ is given by the relation

$$I(\phi) \;=\; I_o \; cos\,(m\phi)\,. \tag{2.87}$$

[In the case of skew harmonics the current distribution is $I(\phi) \;=\; I_o \; sin(m\phi)$].

It will be demonstrated that a pure dipole field is created by m=*1*, quadrupole by m=*2*, sextupole by m=*3*, etc. The total current required (Ampere-turns) per pole for generating a $2m$-pole field is given by

$$I_{pole} \;=\; \int_o^{\pi/2m} I_o \; cos\,(m\phi)\; d\phi \;=\; \frac{I_o}{m}.$$

In Eqs. (2.39), the vector potential produced by a single wire at any position is computed. To obtain the vector potential at (r,θ) inside the sheet (i.e. r $<$ a), the expression is integrated over ϕ

$$A_z\,(r,\theta) = \frac{\mu_o I_o}{2\pi} \sum_{n=1}^{\infty} \left(\frac{1}{n}\right)\left(\frac{r}{a}\right)^n \int_o^{2\pi} cos\,(m\phi)\;\; cos\,(n\,(\phi-\theta))\;\; d\phi, \tag{2.88}$$

to obtain

$$A_z\,(r,\theta) = \frac{\mu_o I_o}{2m}\left(\frac{r}{a}\right)^m \; cos\,(m\theta)\,, \tag{2.89}$$

where the following trigonometric relations have been used

$$cos\,[n\,(\phi-\theta)] = cos\,(n\phi)\;\; cos\,(n\theta) + sin\,(n\phi)\;\; sin\,(n\theta)\,, \tag{2.90}$$

$$\int_o^{2\pi} cos\,(m\phi)\;\; cos\,(n\phi)\;\; d\phi = \pi\delta_{m,n}, \tag{2.91a}$$

$$\int_o^{2\pi} cos\,(m\phi)\;\; sin\,(n\phi)\;\; d\phi = 0. \tag{2.91b}$$

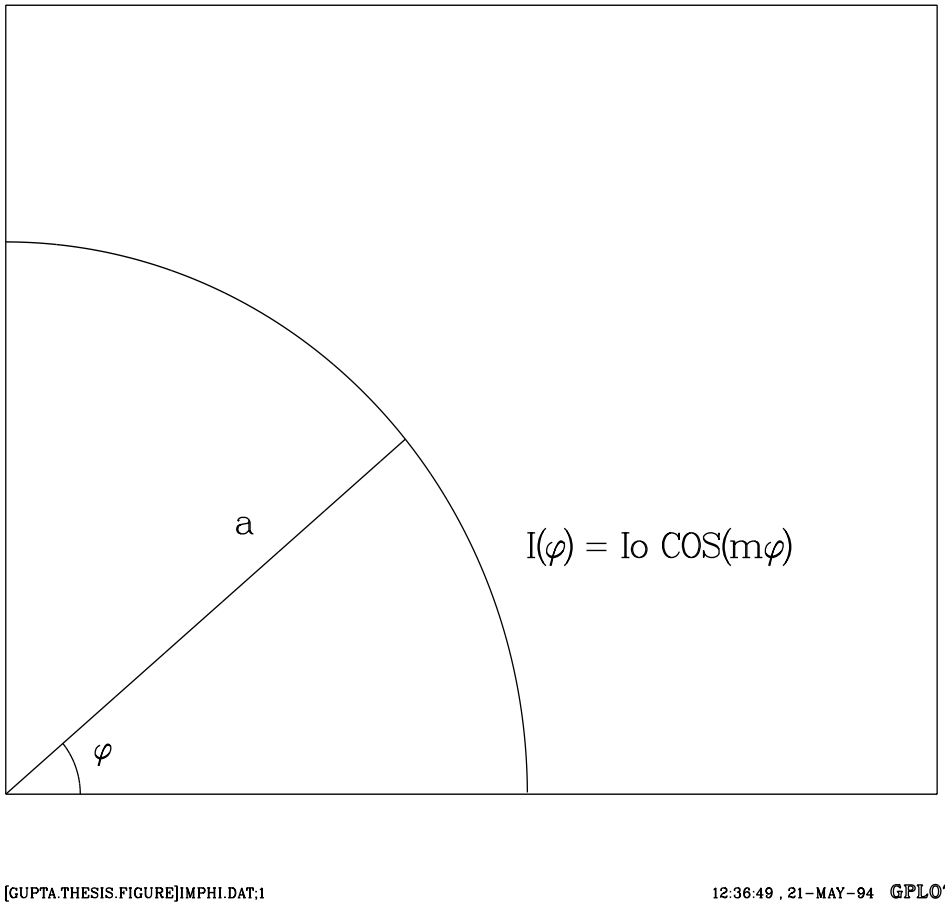

Figure 2.2: Computation of the field at (r, θ) produced by a current sheet at a radius a in which the current density varies as a function of angle given by $I(\phi) = I_o \cos(m\phi)$.

The field components inside the current sheet are obtained by using Eqs. (2.40)

$$B_\theta(r,\theta) = -\frac{\mu_o I_o}{2a}\left(\frac{r}{a}\right)^{m-1} \cos(m\theta), \tag{2.92a}$$

$$B_r(r,\theta) = -\frac{\mu_o I_o}{2a}\left(\frac{r}{a}\right)^{m-1} \sin(m\theta), \tag{2.92b}$$

$$B_z\,(r,\theta) = 0. \tag{2.92c}$$

It may be noted that the magnitude of the field $|B|$ is independent of θ. On using Eqs. (2.46)

$$B_x\,(r,\theta) = -\frac{\mu_o I_o}{2a}\left(\frac{r}{a}\right)^{m-1} sin\left((m-1)\,\theta\right), \tag{2.93a}$$

$$B_y\,(r,\theta) = -\frac{\mu_o I_o}{2a}\left(\frac{r}{a}\right)^{m-1} cos\left((m-1)\,\theta\right). \tag{2.93b}$$

For the m=1 case, this generates a pure dipole field, as the field components from Eqs. (2.92) reduce to

$$B_\theta\,(r,\theta) = -\frac{\mu_o I_o}{2a} cos\,(\theta),$$
$$B_r\,(r,\theta) = -\frac{\mu_o I_o}{2a} sin\,(\theta),$$

and, from Eqs. (2.93)

$$B_x = 0, \tag{2.94a}$$

$$B_y = -\frac{\mu_o I_o}{2a}. \tag{2.94b}$$

This implies that a cylindrical current sheet with a cosine θ current distribution would create a uniform vertical field inside it. This basic result is widely used in designing superconducting accelerator dipole magnets, although the actual current distribution is somewhat modified for practical reasons.

Likewise, for m=2, a pure quadrupole field is generated

$$B_\theta\,(r,\theta) = -\frac{\mu_o I_o r}{2a^2} cos\,(2\theta),$$
$$B_r\,(r,\theta) = -\frac{\mu_o I_o r}{2a^2} sin\,(2\theta),$$

and, from Eqs. (2.93)

$$B_x = g\ y, \tag{2.95a}$$

$$B_y = g\ x, \tag{2.95b}$$

with $g = -(\mu_o I_o)/(2a^2)$.

Similarly, for m=3, a pure sextupole field is generated

$$B_\theta(r,\theta) = -\frac{\mu_o I_o r^2}{2a^3} cos(3\theta),$$
$$B_r(r,\theta) = -\frac{\mu_o I_o r^2}{2a^3} sin(3\theta),$$

and, from Eqs. (2.93)

$$B_x = 2S\ x\ y, \tag{2.96a}$$
$$B_y = S(x^2 - y^2), \tag{2.96b}$$

with $S = -(\mu_o I_o)/(2a^3)$.

In general, a $cos(m\theta)$ current distribution gives a $2m$ order multipole with field components given by Eqs. (2.93).

On the x-axis (midplane), $\theta = 0$, these components become

$$B_x(x,0) = 0, \tag{2.97a}$$
$$B_y(x,0) = -\frac{\mu_o I_o}{2a}\left(\frac{x}{a}\right)^{m-1}, \tag{2.97b}$$

and on the y-axis

$$\begin{aligned} B_x(0,y) &= 0, && for \quad m = 1,3,5,... \\ &= \pm\frac{\mu_o I_o}{2a}\left(\frac{y}{a}\right)^{m-1}, && for \quad m = 2,4,6,... \end{aligned} \tag{2.98a}$$

$$\begin{aligned} B_y(0,y) &= \pm\frac{\mu_o I_o}{2a}\left(\frac{y}{a}\right)^{m-1}, && for \quad m = 1,3,5,... \\ &= 0. && for \quad m = 2,4,6,... \end{aligned} \tag{2.98b}$$

To obtain the field outside the current sheet (r > a), Eqs. (2.44) is integrated using the trigonometric relations given in Eq. (2.90)and Eqs. (2.91)

$$A_z(r,\theta) = -\frac{\mu_o I_o}{2\pi} ln\left(\frac{r}{a}\right)\int_o^{2\pi} cos(m\phi)\ d\phi$$
$$+\ \frac{\mu_o I_o}{2\pi}\sum_{n=1}^{\infty}\left(\frac{1}{n}\right)\left(\frac{a}{r}\right)^n \int_o^{2\pi} cos(m\phi)\ cos(n(\phi-\theta))\ d\phi,$$

therefore, $A_z(r,\theta) = \dfrac{\mu_o I_o}{2m}\left(\dfrac{a}{r}\right)^m cos(m\theta).$ (2.99)

The field components for r > a are obtained using Eqs. (2.40)

$$B_\theta(r,\theta) = \frac{\mu_o I_o}{2a}\left(\frac{a}{r}\right)^{m+1} cos(m\theta), \tag{2.100a}$$

$$B_r(r,\theta) = -\frac{\mu_o I_o}{2a}\left(\frac{a}{r}\right)^{m+1} sin(m\theta), \tag{2.100b}$$

$$B_z(r,\theta) = 0, \tag{2.100c}$$

and the (B_x, B_y) components of the field are obtained as :

$$B_x = B_r\ cos(\theta) - B_\theta\ sin(\theta),$$

and

$$B_y = B_r\ sin(\theta) + B_\theta\ cos(\theta),$$

therefore,

$$B_x = -\frac{\mu_o I_o}{2a}\left(\frac{a}{r}\right)^{m+1} sin[(m+1)\theta], \tag{2.101a}$$

$$B_y = \frac{\mu_o I_o}{2a}\left(\frac{a}{r}\right)^{m+1} cos[(m+1)\theta]. \tag{2.101b}$$

In the case of the dipole (m=1), the field components outside the current sheet, fall as $\frac{1}{r^2}$, and are given by :

$$B_\theta(r,\theta) = \frac{\mu_o I_o a}{2r^2} cos[\theta], \tag{2.102a}$$

$$B_r(r,\theta) = -\frac{\mu_o I_o a}{2r^2} sin[\theta], \tag{2.102b}$$

$$B_x(r,\theta) = -\frac{\mu_o I_o a}{2r^2} sin[2\theta], \tag{2.102c}$$

$$B_y(r,\theta) = \frac{\mu_o I_o a}{2r^2} cos[2\theta]. \tag{2.102d}$$

In deriving the above expressions, for simplicity it is assumed that the current is localized in a sheet. However, in accelerator magnets, the current is present between two radii a_1 and a_2. It is assumed that the current density in Amperes/m^2 is given by

$$J(\phi) = J_o\ cos(m\phi).$$

For a sheet of infitesimal thickness da, J_o is related to the angular current density (I_o) as

$$I_o = J_o\ a\ da,$$

In this case the expression for the vector potential and field components for r < a are by integrating Eqs. (2.39):

$$A_z(r,\theta) = \frac{\mu_o J_o}{2\pi} \sum_{n=1}^{\infty} \left(\frac{r^n}{n}\right) \int_{a_1}^{a_2} \frac{1}{a^n} a \; da \int_o^{2\pi} \cos(m\phi) \;\; \cos(n(\phi-\theta)) \;\; d\phi,$$

Therefore,

$$A_z(r,\theta) = \frac{\mu_o J_o r^m}{2m} \cos(m\theta) \int_{a_1}^{a_2} \frac{1}{a^{m-1}} \; da, \tag{2.103}$$

$$B_\theta(r,\theta) = -\frac{\mu_o J_o r^{m-1}}{2} \cos(m\theta) \int_{a_1}^{a_2} \frac{1}{a^{m-1}} \; da, \tag{2.104a}$$

$$B_r(r,\theta) = -\frac{\mu_o J_o r^{m-1}}{2} \sin(m\theta) \int_{a_1}^{a_2} \frac{1}{a^{m-1}} \; da, \tag{2.104b}$$

$$B_z(r,\theta) = 0. \tag{2.104c}$$

Except for $m = 2$ case (the quadrupole case, for which the expressions are given later), one obtains :

$$A_z(r,\theta) = \frac{\mu_o J_o {a_1}^2}{2m(m-2)} \cos(m\theta) \left(\frac{r}{a_1}\right)^m \left(1 - \left(\frac{a_1}{a_2}\right)^{m-2}\right), \tag{2.105}$$

$$B_\theta(r,\theta) = -\frac{\mu_o J_o a_1}{2(m-2)} \cos(m\theta) \left(\frac{r}{a_1}\right)^{m-1} \left(1 - \left(\frac{a_1}{a_2}\right)^{m-2}\right), \tag{2.106a}$$

$$B_r(r,\theta) = -\frac{\mu_o J_o a_1}{2(m-2)} \sin(m\theta) \left(\frac{r}{a_1}\right)^{m-1} \left(1 - \left(\frac{a_1}{a_2}\right)^{m-2}\right), \tag{2.106b}$$

$$B_y(r,\theta) = -\frac{\mu_o J_o a_1}{2(m-2)} \cos((m-1)\theta) \left(\frac{r}{a_1}\right)^{m-1} \left(1 - \left(\frac{a_1}{a_2}\right)^{m-2}\right), \tag{2.106c}$$

$$B_x(r,\theta) = -\frac{\mu_o J_o a_1}{2(m-2)} \sin((m-1)\theta) \left(\frac{r}{a_1}\right)^{m-1} \left(1 - \left(\frac{a_1}{a_2}\right)^{m-2}\right). \tag{2.106d}$$

In the case of the dipole (m=1), this gives a vertical field

$$B_y = -\mu_o J_o \left(\frac{a_2 - a_1}{2}\right) = -\mu_o J_o \left(\frac{\Delta a}{2}\right).$$

For $m = 2$ (quadrupole), the integration of Eqs. (2.104) gives :

$$A_z(r,\theta) = \frac{\mu_o J_o r^2}{4} \cos(2\theta) \;\; ln\left(\frac{a_2}{a_1}\right) \tag{2.107}$$

$$B_\theta(r,\theta) = -\frac{\mu_o J_o r}{2} \cos(2\theta) \;\; ln\left(\frac{a_2}{a_1}\right) \tag{2.108a}$$

$$B_r(r,\theta) = -\frac{\mu_o J_o r}{2} \sin(2\theta) \;\; ln\left(\frac{a_2}{a_1}\right) \tag{2.108b}$$

$$B_y(r,\theta) = -\frac{\mu_o J_o r}{2} \cos(\theta) \;\; ln\left(\frac{a_2}{a_1}\right) \tag{2.108c}$$

$$B_x(r,\theta) = -\frac{\mu_o J_o r}{2} \sin(\theta) \;\; ln\left(\frac{a_2}{a_1}\right) \tag{2.108d}$$

If the sheet thickness $\Delta a = a_2 - a_1$ is very small compared to the the average radius $\bar{a} = \frac{(a_2+a_1)}{2}$, then the expressions in Eqs. (2.106) for $r < a$ may be simplified to the following equations since the integral in Eq. (2.103) and Eqs. (2.104) can be approximated as $(\Delta a/\bar{a}^{m-1})$:

$$A_z(r,\theta) = \frac{\mu_o J_o r \Delta a}{2m}\left(\frac{r}{\bar{a}}\right)^{m-1} cos(m\theta), \tag{2.109}$$

$$B_\theta(r,\theta) = -\frac{\mu_o J_o \Delta a}{2}\left(\frac{r}{\bar{a}}\right)^{m-1} cos(m\theta), \tag{2.110a}$$

$$B_r(r,\theta) = -\frac{\mu_o J_o \Delta a}{2}\left(\frac{r}{\bar{a}}\right)^{m-1} sin(m\theta). \tag{2.110b}$$

2.3.7. COS($m\theta$) Current Distribution in a Cylindrical Iron Shell

In superconducting accelerator magnets, the coils are frequently placed inside a cylindrical iron yoke to (a) reduce the stray magnetic field outside the magnet and (b) as an added benefit to enhance the field in the aperture of the magnet. Due to the non-linear properties of the iron, the fraction of field generated by the iron at any current depends on how much the yoke is magnetized. This is too complex a problem to solve analytically. However, one can obtain simple expressions if one assumes that the permeability (μ) of the iron is constant everywhere in the yoke. Expressions for the vector potential and the field are given for the case in which a $COS(m\theta)$ current sheet at radius a is inside in an iron shell with inner radius of R_f and outer radius of R_a.

In this case, the method of matching the boundary conditions at the air and iron interfaces, as described in the last section, can be used to include the contribution from the iron. This is equivalent to the method of images when the effect of the iron is replaced by the equivalent image currents.

In the presence of a cylindrical iron yoke, the vector potential and the field components given in Eqs. (2.89) and Eqs. (2.92), for $r < a$, are modified to

$$A_z\,(r,\theta) = \frac{\mu_o I_o}{2m}\;cos\,(m\theta)\left(\frac{r}{a}\right)^m \;\times \left[1+\frac{\mu-1}{\mu+1}\left(\frac{a}{R_f}\right)^{2m}\frac{\left[1-\left(\frac{R_f}{R_a}\right)^{2m}\right]}{\left[1-\left(\frac{\mu-1}{\mu+1}\right)^2\left(\frac{R_f}{R_a}\right)^{2m}\right]}\right], \tag{2.111}$$

$$B_\theta\,(r,\theta) = -\frac{\mu_o I_o}{2a}\;cos\,(m\theta)\left(\frac{r}{a}\right)^{m-1} \;\times \left[1+\frac{\mu-1}{\mu+1}\left(\frac{a}{R_f}\right)^{2m}\frac{\left[1-\left(\frac{R_f}{R_a}\right)^{2m}\right]}{\left[1-\left(\frac{\mu-1}{\mu+1}\right)^2\left(\frac{R_f}{R_a}\right)^{2m}\right]}\right], \tag{2.112a}$$

$$B_r\,(r,\theta) = -\frac{\mu_o I_o}{2a}\;sin\,(m\theta)\left(\frac{r}{a}\right)^{m-1} \;\times \left[1+\frac{\mu-1}{\mu+1}\left(\frac{a}{R_f}\right)^{2m}\frac{\left[1-\left(\frac{R_f}{R_a}\right)^{2m}\right]}{\left[1-\left(\frac{\mu-1}{\mu+1}\right)^2\left(\frac{R_f}{R_a}\right)^{2m}\right]}\right]. \tag{2.112b}$$

The other components are obtained using Eqs. (2.46)

$$B_x(r,\theta) = -\frac{\mu_o I_o}{2a}\ sin\left((m-1)\theta\right)\left(\frac{r}{a}\right)^{m-1} \times \left[1+\frac{\mu-1}{\mu+1}\left(\frac{a}{R_f}\right)^{2m}\frac{\left[1-\left(\frac{R_f}{R_a}\right)^{2m}\right]}{\left[1-\left(\frac{\mu-1}{\mu+1}\right)^2\left(\frac{R_f}{R_a}\right)^{2m}\right]}\right], \tag{2.113a}$$

$$B_y(r,\theta) = -\frac{\mu_o I_o}{2a}\ cos\left((m-1)\theta\right)\left(\frac{r}{a}\right)^{m-1} \times \left[1+\frac{\mu-1}{\mu+1}\left(\frac{a}{R_f}\right)^{2m}\frac{\left[1-\left(\frac{R_f}{R_a}\right)^{2m}\right]}{\left[1-\left(\frac{\mu-1}{\mu+1}\right)^2\left(\frac{R_f}{R_a}\right)^{2m}\right]}\right], \tag{2.113b}$$

$$B_z(r,\theta) = 0. \tag{2.113c}$$

Similarly, the vector potential and field outside the current sheet but inside the iron, i.e. $a < r < R_f$, is given by :

Between Coil and Iron ($\mathbf{a < r < R_f}$)

$$A_z(r,\theta) = \frac{\mu_o I_o}{2m}\left(1+\frac{\mu-1}{\mu+1}\left(\frac{r}{R_f}\right)^{2m}\frac{\left[1-\left(\frac{R_f}{R_a}\right)^{2m}\right]}{\left[1-\left(\frac{\mu-1}{\mu+1}\right)^2\left(\frac{R_f}{R_a}\right)^{2m}\right]}\right) \times \left(\frac{a}{r}\right)^m cos\left(m\theta\right), \tag{2.114}$$

$$B_r = -\frac{\mu_o I_o}{2a}\left(1+\frac{\mu-1}{\mu+1}\left(\frac{r}{R_f}\right)^{2m}\frac{\left[1-\left(\frac{R_f}{R_a}\right)^{2m}\right]}{\left[1-\left(\frac{\mu-1}{\mu+1}\right)^2\left(\frac{R_f}{R_a}\right)^{2m}\right]}\right) \times \left(\frac{a}{r}\right)^{m+1} sin\left(m\theta\right), \tag{2.115a}$$

$$B_\theta = \frac{\mu_o I_o}{2a}\left(1-\frac{\mu-1}{\mu+1}\left(\frac{r}{R_f}\right)^{2m}\frac{\left[1-\left(\frac{R_f}{R_a}\right)^{2m}\right]}{\left[1-\left(\frac{\mu-1}{\mu+1}\right)^2\left(\frac{R_f}{R_a}\right)^{2m}\right]}\right) \times \left(\frac{a}{r}\right)^{m+1} cos\left(m\theta\right). \tag{2.115b}$$

Inside Iron ($\mathbf{R_f < r < R_a}$)

$$A_z(r,\theta) = \frac{\mu\mu_o I_o}{m\left(\mu+1\right)}\left(\frac{1-\frac{\mu-1}{\mu+1}\left(\frac{r}{R_a}\right)^{2m}}{1-\left(\frac{\mu-1}{\mu+1}\right)^2\left(\frac{R_f}{R_a}\right)^{2m}}\right) \times$$

$$\left(\frac{a}{r}\right)^{m} cos\left(m\theta\right), \tag{2.116}$$

$$B_r = -\frac{\mu\mu_o I_o}{a\left(\mu+1\right)} \left(\frac{1-\frac{\mu-1}{\mu+1}\left(\frac{r}{R_a}\right)^{2m}}{1-\left(\frac{\mu-1}{\mu+1}\right)^{2}\left(\frac{R_f}{R_a}\right)^{2m}}\right) \times \left(\frac{a}{r}\right)^{m+1} sin\left(m\theta\right), \tag{2.117a}$$

$$B_\theta = \frac{\mu\mu_o I_o}{a\left(\mu+1\right)} \left(\frac{1+\frac{\mu-1}{\mu+1}\left(\frac{r}{R_a}\right)^{2m}}{1-\left(\frac{\mu-1}{\mu+1}\right)^{2}\left(\frac{R_f}{R_a}\right)^{2m}}\right) \times \left(\frac{a}{r}\right)^{m+1} cos\left(m\theta\right). \tag{2.117b}$$

Outside Iron ($\mathbf{r > R_a}$)

$$A_z\left(r,\theta\right) = \frac{2\mu\mu_o I_o}{m\left(\mu+1\right)^2} \frac{1}{1-\left(\frac{\mu-1}{\mu+1}\right)^{2}\left(\frac{R_f}{R_a}\right)^{2m}} \left(\frac{a}{r}\right)^{m} cos\left(m\theta\right), \tag{2.118}$$

$$B_r = -\frac{2\mu\mu_o I_o}{a\left(\mu+1\right)^2} \frac{1}{1-\left(\frac{\mu-1}{\mu+1}\right)^{2}\left(\frac{R_f}{R_a}\right)^{2m}} \left(\frac{a}{r}\right)^{m+1} sin\left(m\theta\right), \tag{2.119a}$$

$$B_\theta = \frac{2\mu\mu_o I_o}{a\left(\mu+1\right)^2} \frac{1}{1-\left(\frac{\mu-1}{\mu+1}\right)^{2}\left(\frac{R_f}{R_a}\right)^{2m}} \left(\frac{a}{r}\right)^{m+1} cos\left(m\theta\right). \tag{2.119b}$$

2.3.8. Intersecting Circles with a Constant Current Density for Ideal Fields

It has been shown [137] that a pure dipole field can be created simply by two intersecting circles carrying constant current densities in opposite directions. To demonstrate this, the field is evaluated inside and outside a circular conductor with a radius a and carrying a constant current density J in the direction of the axis (perpendicular to the plane of paper). For a radius $R > a$ (outside the conductor), Ampere's law gives

$$2\pi R \cdot H = \pi a^2 \ J.$$

Therefore,

$$H = \frac{Ja^2}{2R}. \tag{2.120}$$

The direction of the magnetic field is azimuthal, with (x, y) components of the field at any point outside the conductor given by

$$\begin{aligned} H_x &= -\frac{Ja^2}{2R} sin\,(\theta) = -\frac{J}{2}\left(\frac{a}{R}\right)^2 y, \\ H_y &= \frac{Ja^2}{2R} cos\,(\theta) \quad = \frac{J}{2}\left(\frac{a}{R}\right)^2 x. \end{aligned}$$

The field inside the conductor $(R < a)$ can be obtained as

$$\begin{aligned} 2\pi R \cdot H &= \pi R^2 \ J, \\ i.e., \qquad H &= \frac{JR}{2}. \end{aligned} \tag{2.121}$$

with the components of the field being given by

$$\begin{aligned} H_x &= -\frac{J}{2} R \ sin\,(\theta) = -\frac{J}{2} y, \\ H_y &= \frac{J}{2} R \ cos\,(\theta) \quad = \frac{J}{2} x. \end{aligned}$$

Now expressions will be derived for the field produced by the conductors in two intersecting circles. The coordinate system is defined such that the x-axis passes through the centers of the two circles with the origin of the new coordinate system (x', y') being in the middle of the two. The distance between the centers of the two circles is s with circle 2 to the right such that $x' = x_1 - \frac{s}{2} = x_2 + \frac{s}{2}$ and $y_1 = y_2 = y'$. The direction of the current

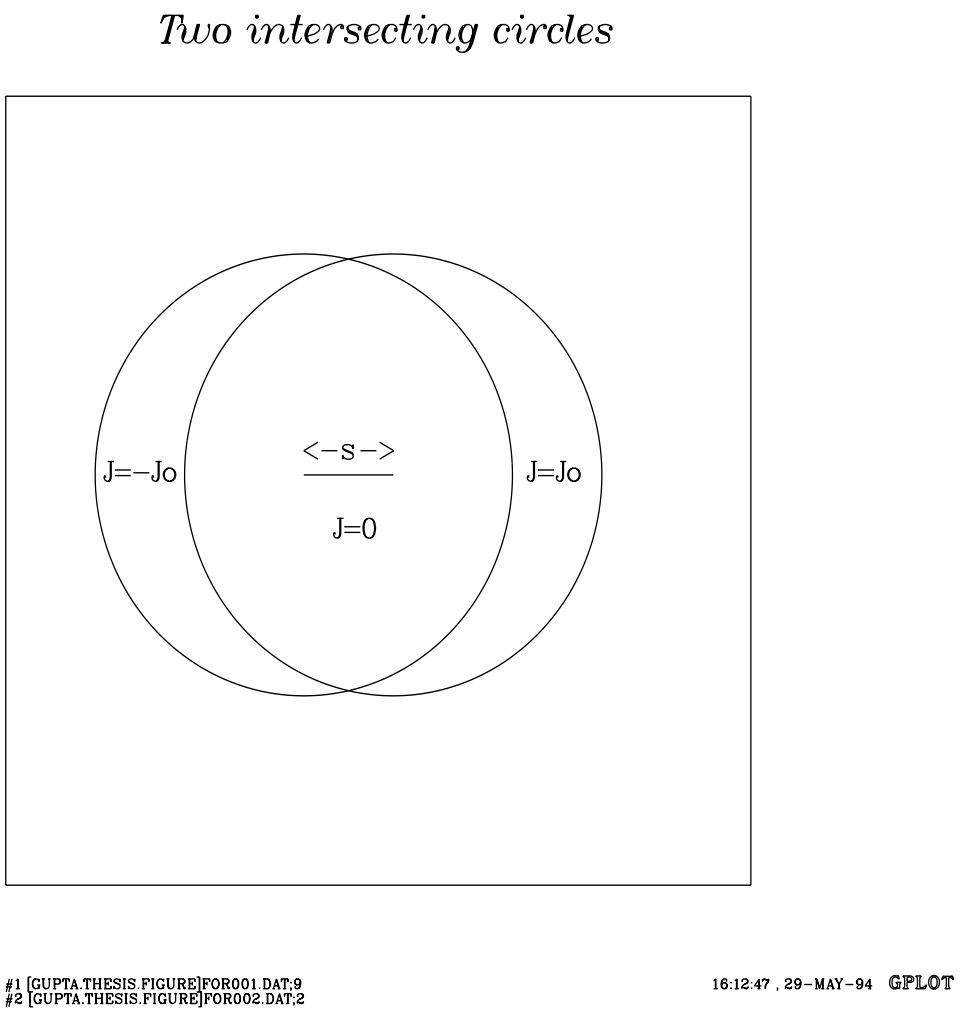

Figure 2.3: This figure shows the two intersecting circles of equal size with one carrying a current with a constant density $J = -J_o$ and the other $J = J_o$. The two circles are separated by a distance s. In the intersection region of the two circles, the net current density is zero and therefore it can be replaced by a current free region. It is demonstrated that this configuration produces a vertical dipole field given by $\frac{J_o}{2}s$.

is opposite in the two circles, with constant current densities J_1 and $-J_2$ respectively. The components of the field inside the region created by the two intersecting circles can be

computed by superimposing the field produced by the conductors in the two circles

$$H_x = \frac{y'}{2}(J_2 - J_1)\,,$$
$$H_y = \frac{x'}{2}(J_1 - J_2) + \frac{s}{4}(J_1 + J_2)\,.$$

A special case comes when the magnitude of the current densities in the two circles is J_o but the direction is opposite as shown in Fig. 2.3. This means that the intersection region is a current free region which can be used as an aperture for the particle beam and and the aperture has a constant vertical magnetic field given by $H_y = \frac{J_o}{2}s$.

It can be shown [14] that four intersecting circles create a quadrupole field and in general $2m$ intersecting circles create a $2m$-order multipole. The treatment has been also been extended to ellipses by a number of authors (see for example Beth [14]).

2.4. Complex Variable Method in 2-d Magnetic Field Calculations

The method of complex variable is found very useful in deriving many expressions in superconducting magnets. [12-18,81] These methods can be applied to 2-dimensional field computations, which is the case for the most part of long superconducting magnets. Mills and Morgan [115] have shown that the complex method can also be extended throughout the ends, however, to the field integral ($\int B.dz$). The complex variables have two parts (real and imaginary) and the following variables will be used :

$$z = x \ + \ i \ y, \tag{2.122a}$$

$$H\,(z) = H_y \ + \ i \ H_x, \tag{2.122b}$$

$$B\,(z) = B_y \ + \ i \ B_x, \tag{2.122c}$$

$$W\,(z) = -\,(A \ + \ i \ \phi) \ + \ constant. \tag{2.122d}$$

where W is the complex potential having ϕ and A (scalar and vector potentials) as the two components, and $i \ = \ \sqrt{-1}$. z^* is the complex conjugate of z with

$$z^* = x \ - \ i \ y.$$

In the 2-d case the following relations are valid :

$$B_x = \frac{\partial A}{\partial y} \tag{2.123a}$$

$$B_y = -\frac{\partial A}{\partial x}, \tag{2.123b}$$

$$with \quad B_x = \mu_0 \mu H_x,$$

$$and \quad B_y = \mu_0 \mu H_y.$$

Moreover, in air ($\mu = 1$),

$$H_x = -\frac{1}{\mu_0}\frac{\partial \phi}{\partial x} = \frac{1}{\mu_0}\frac{\partial A}{\partial y}, \tag{2.124a}$$

$$H_y = -\frac{1}{\mu_0}\frac{\partial \phi}{\partial y} = -\frac{1}{\mu_0}\frac{\partial A}{\partial x}. \tag{2.124b}$$

The Cauchy-Riemann equations are the necessary and sufficient conditions for a function to be analytic in Z-plane. For a function $F_w \ = \ u \ + \ i \ v$, these conditions are:

$$\frac{\partial u}{\partial x} \ = \ \frac{\partial v}{\partial y}, \tag{2.125a}$$

$$\frac{\partial u}{\partial y} \ = -\frac{\partial v}{\partial x}. \tag{2.126a}$$

In a medium free of magnetic material with $\mu = 1$, Eqs. (2.124) gives

$$\begin{aligned} \frac{\partial A}{\partial x} &= \frac{\partial \phi}{\partial y}, \\ \frac{\partial A}{\partial y} &= -\frac{\partial \phi}{\partial x}, \end{aligned}$$

which are the Cauchy-Riemann conditions for $W(z) = -(A + i\phi) + constant$ to be analytic. In the same way, B(z) (and similarly H(z)) is analytic if :

$$\begin{aligned} \frac{\partial B_y}{\partial x} &= \frac{\partial B_x}{\partial y}, \\ \frac{\partial B_y}{\partial y} &= -\frac{\partial B_x}{\partial x}, \end{aligned}$$

which are just Maxwell's equations in a current free region. It may be noted that the choice of variable $B(z)$ as $B(z) = B_y + iB_x$ is important since B_x and B_y do not the satisfy the Cauchy-Rieman conditions if the variable is $B_x + iB_y$.

Since $W(z)$ is analytic, the derivative of $W(z)$ gives the the complex field function :

$$\frac{dW}{dz} = -\frac{\partial A}{\partial x} - \; i \; \frac{\partial \phi}{\partial x} = i \; \frac{\partial A}{\partial y} - \frac{\partial \phi}{\partial y} = H_y + \; i \; H_x \; = \; H(z) .$$

To deal with a region with current, a new analytic function is defined as follows :

$$F(z) = B(z) - \frac{1}{2}\mu_o J z^* = (B_y - \tfrac{1}{2}\mu_o J x) \; + \; i \; (B_x + \tfrac{1}{2}\mu_o J y) , \tag{2.127}$$

where the current density J is constant throughout the region. The Cauchy-Riemann conditions become :

$$\begin{aligned} & \frac{\partial B_y}{\partial x} - \tfrac{1}{2}\mu_o J = \frac{\partial B_x}{\partial y} + \tfrac{1}{2}\mu_o J \\ \Longrightarrow \quad & \frac{\partial B_y}{\partial x} - \frac{\partial B_x}{\partial y} = \mu_o J \\ & and, \quad \frac{\partial B_y}{\partial y} = -\frac{\partial B_x}{\partial x} \\ \Longrightarrow \quad & \frac{\partial B_x}{\partial x} + \frac{\partial B_y}{\partial y} = 0 \end{aligned}$$

which are Maxwell's equations in the presence of current.

2.4.1. Field due to an array of Line Currents

The complex potential at a point z, due a current flowing in a direction perpendicular to the Z-plane at $z = z_o$, is given by :

$$W(z) \;=\; \frac{I}{2\pi}\; log\,(z - z_o) \;+\; constant\;,$$

and the magnetic field is given by :

$$H(z) \;=\; \frac{dW}{dz} \;=\; \frac{I}{2\pi\,(z - z_o)}. \tag{2.128}$$

The direction of the field is that of $(z - z_o)^*$, which is perpendicular to the vector $(z - z_o)$. The superposition principle can be used to obtain the field due to n filaments with the k^{th} filament carrying I_k amperes and located at $z = z_k$:

$$H(z) \;=\; \sum_{k=1}^{n} \frac{I_k}{2\pi\,(z - z_k)}. \tag{2.129}$$

Cauchy's Residue Theorem gives [29]

$$\oint_C f(z)\;\; dz \;=\; 2\pi i \sum_k Res\,(a_k), \tag{2.130}$$

where $Res(a_k)$ are the residues which are defined as the coefficients of $\frac{1}{z - z_k}$ inside the contour C over which the contour integral of the function $f(z)$ is taken. Applying this to Eq. (2.129) while taking the contour integral of the field around the wires in the Z-plane, one obtains

$$\oint H(z)\;\; dz \;=\; i\;\sum_{k=1}^{n} I_k. \tag{2.131}$$

which is basically Ampere's law.

The Cauchy integral formula [29] gives :

$$f(z_o) = \frac{1}{2\pi i} \oint_C \frac{f(z)}{(z - z_o)} dz, \tag{2.132}$$

where the function $f(z)$ is analytic everywhere within and on a closed contour C and $f(z_o)$ is the value of $f(z)$ at $z = z_o$.

2.4.2. Beth's Current Sheet Theorem

Beth's *"Current Sheet Theorem"* [12-18] can be derived from Eq. (2.131). As shown in Fig. 2.4 the current sheet is made up of a number of filaments carrying a total current ΔI perpendicular to the Z-plane along the curve from z to $z + \Delta z$. A contour integral on a closed path enclosing the current sheet will give

$$\oint H(z)\ dz \ = \ i\ \Delta I.$$

Now if the path is squeezed from the right and left sides (indicated by the subscripts R and L) on to the current sheet, then in the limiting case one obtains

$$H_R(z_o) \ - \ H_L(z_o) \ = \ i\ \frac{dI}{dz}, \tag{2.133}$$

where $H_R(z_o)$ and $H_L(z_o)$ are the limits of the analytic functions $H_R(z)$ and $H_L(z)$ when z approaches z_o from the right and left and $\frac{dI}{dz}$ is the limit of $\frac{\Delta I}{\Delta z}$ when Δz approaches 0 at any z.

The above equation Eqs. (2.133) is called Beth's current sheet theorem. To obtain another equation in potential form this equation is integrated to give

$$W_R(z_o) \ - \ W_L(z_o) \ = \ i\ I \ + \ Constant\ , \tag{2.134}$$

where $W_R(z_o)$ and $W_L(z_o)$ are the limits of the analytic functions $W_R(z)$ and $W_L(z)$ when z approaches z_o from the right and left.

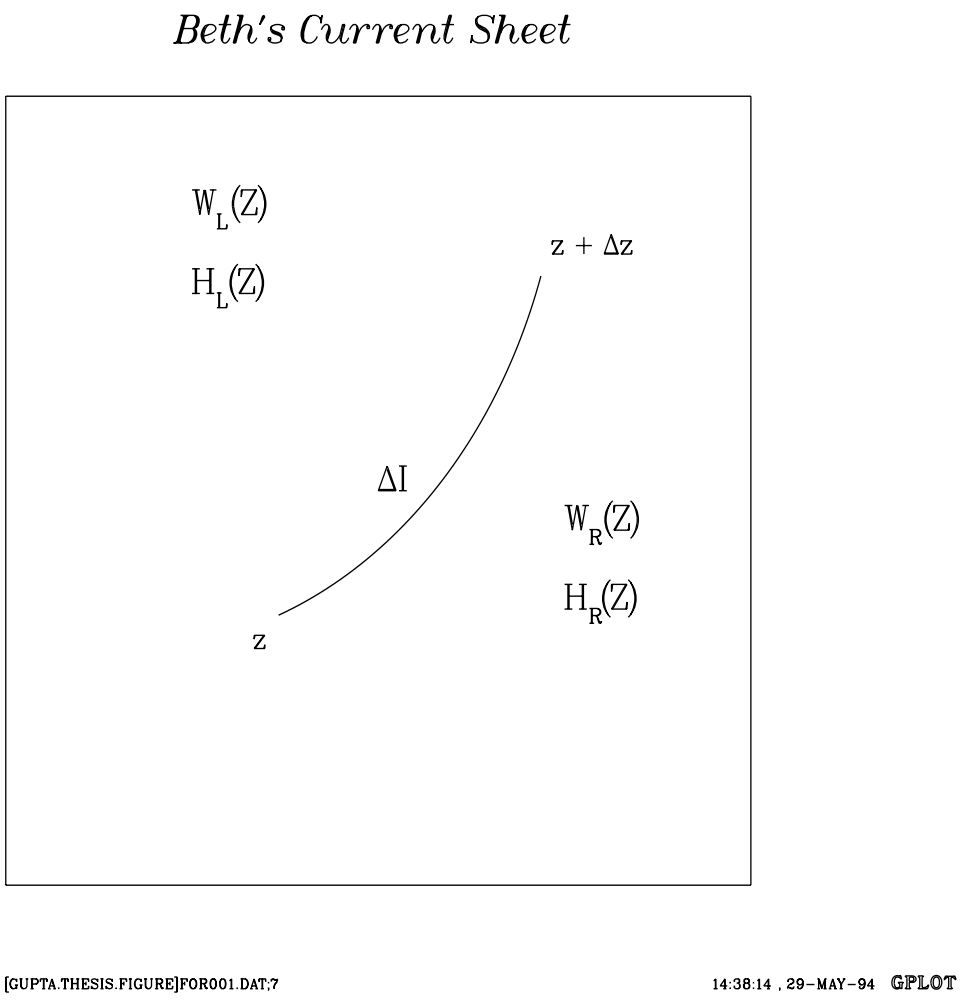

Figure 2.4: Beth's current sheet is shown here, which is made up of a number of filaments, carrying a total current ΔI perpendicular to the Z-plane along the curve from z to $z + \Delta z$. The sub-script "R" denotes the right side and "L" denotes the left side to the sheet.

2.4.3. Example – Cos(m θ) current distribution

As an example of use of the complex variable methods, expressions are derived here for the field due to a cylindrical current sheet at a radius $r = a$, as shown in Fig. 2.2. An angular current density distribution, mentioned earlier, is :

$$\frac{dI}{d\phi} = I_o \cos(m\phi).$$

In complex coordinates, the above current sheet is located at $z = a\ e^{i\phi}$. Then,

$$\frac{dI}{dz} = \left(\frac{dI}{d\phi}\right) / \left(\frac{dz}{d\phi}\right) = \frac{I_o \cos(m\phi)}{i\ a\ e^{i\phi}}.$$

Since H(z) is analytic both inside and outside the current sheet, a general expression for the field to remain finite inside the current sheet ($r < a$) is $H_{in} = \sum_n a_n z^n$ and for outside the current sheet ($r > a$) is $H_{out} = \sum_n b_n z^{-n}$. To obtain the coefficients a_n and b_n, the fields (H_{in}) and (H_{out}) are linked using Beth's current sheet theorem (Eqs. (2.133)) as follows :

$$\begin{aligned} H_{out} - H_{in} &= I_o \frac{\cos(m\phi)}{a\ e^{i\phi}} \\ &= \frac{I_o}{2\ a}\left[e^{-i(m+1)\phi} + e^{i(m-1)\phi}\right] \\ &= \frac{I_o}{2\ a}\left[\left(\frac{a}{z}\right)^{m+1} + \left(\frac{z}{a}\right)^{m-1}\right]. \end{aligned}$$

The right hand side of the above equation gives the field on the current sheet and it acts as a boundary condition which must match interior and exterior solutions. Hence a_n=0 for n≠m-1 and b_n=0 for n≠m+1, giving

$$\begin{aligned} H_{in} &= \frac{-I_o}{2\ a}\left(\frac{z}{a}\right)^{m-1} \qquad |z| < a, \\ H_{out} &= \frac{I_o}{2\ a}\left(\frac{a}{z}\right)^{m+1} \qquad |z| > a. \end{aligned}$$

3. SSC 50 mm Aperture Collider Dipole Magnet Cross-section

In this section the magnetic design of the two dimensional coil and iron cross section for the prototype 50 mm aperture main ring dipole magnet for the Superconducting Super Collider (SSC) is presented. Several prototype dipole magnets based on this design have been built at Brookhaven National Laboratory (BNL) and at Fermi National Accelerator Laboratory (FNAL). Except for a few minor differences (which will be discussed in more detail later), the magnetic design of the BNL and FNAL magnets is nearly the same. The computed values of the allowed field harmonics as a function of current, the quench performance predictions, the stored energy calculations, the effect of construction errors on the field harmonics and the Lorentz forces on the coil will be discussed. The yoke has been optimized to reduce the effects of iron saturation on the field harmonics. A summary of this design will also be presented.

3.1. Coil Design

The coil is made of two layers of superconducting cables. Some parameters of the cables used in the inner and outer layers are given in Table 3.1.

The coil is designed by placing the cables in such a way that they produce a field with a high degree of uniformity. This is done using the computer program PAR2DOPT [130] which uses analytic expressions for computing the field harmonics at the center of the magnet of coils in a circular $\infty\mu$ iron aperture. It also computes the peak field on the surface of the conductor.

A large number of configurations for the coil design were examined. The one selected has a total of 45 turns in each quadrant in two layers. The inner layer has 19 turns in four blocks (three wedges) and the outer has 26 turns in two blocks (one wedge). In the final selection of the optimized coil cross section, the peak field (the maximum magnitude of the magnetic field in the conductor) was also used as an important parameter in addition to the other magnetic and mechanical parameters. For the same transfer function, a coil design with a lower peak field will produce a magnet which will quench at a higher current. In a search for the optimum coil configuration, the number of wedges in the outer layer

Table 3.1: Properties of the cables used in the SSC 50 mm dipoles. J_c gives the value of the critical current density which was used in the design calculations for the superconducting part of the wires (strands) and cables.

Cable parameters	Inner layer	Outer Layer
Filament diameter, micron	6.0	6.0
Strand diameter, mm	0.808	0.648
Strand $J_c(5T, 4.2K)$, A/mm^2	2750	2750
No. of strands	30	36
No. of strands $\times$ Strand Area, mm^2 (area of metal)	15.382	11.872
Cable $J_c(5T, 4.2K)$, A/mm^2	2612.5	2612.5
Cable width, bare, mm	12.34	11.68
Cable width, insulated, mm	12.51	11.85
Cable mid-thickness, bare, mm	1.458	1.156
Cable mid-thickness, insulated, mm	1.626	1.331
Cable area, bare, mm^2	17.99	13.50
Cable area, insulated, mm^2	20.34	15.77
Keystone, (max-min) thickness, mm	0.262	0.206

was kept at one whereas for the inner layer, solutions with a variable number of wedges were examined. The designs with two wedges in the inner layer were, in general, found to have a higher peak field or excessive harmonic content. For this reason, the design chosen has three wedges in the inner layer. However, the present coil is optimized in such a way that the two wedges nearest to the pole in the inner layer are identical and symmetric. A symmetric wedge design has a lower chance of incorrect installation as compared to a non-symmetric wedge design. The final design with symmetric wedges has performance comparable to those that did not require the wedges to be symmetric. The wedge in the

outer layer is close to symmetric and in fact, in magnets built at FNAL this wedge was also made mechanically symmetric, without changing its effective size in the coil.

The cross section of the optimized coil placed in the stainless steel collar is shown in Fig. 3.1.

3.2. Low Field Harmonics

The iron aperture is not completely circular in this magnet. It has a pole notch and a small vertical straight face at the midplane. These features introduce small but noticeable values of the b_2 and b_4 harmonics. These harmonics should be cancelled in the coil design if the magnet is to produce zero low field harmonics. Therefore, to cancel the effects of the non-circular iron inner radius, -0.28 unit of b_2 and +0.01 of b_4 were desired in the optimized coil. In addition, a non-zero value of b_8 harmonic was desired for centering the coil during the field measurements. Since the given tolerance in b_8 was 0.05 unit at the time of design, a solution was sought which had a magnitude for this harmonic between 0.04 and 0.05. This requirement on b_8 eliminated many coil configurations from contention. However, the final design that satisfied all of the above requirements was equal in performance to those that did not. An alternate cross section with a zero b_8 harmonic was also designed which was mechanically very close to this cross section and, moreover, had all wedges perfectly symmetric. However, no magnet was ever built with this alternate cross section.

In Table 3.2 the desired and optimized values of field harmonics are presented. Harmonics higher than b_{12} had an optimized value of < 0.001, as desired. In the row labelled "Desired" the allowed systematic errors are also listed. In the row "BNL magnets", the harmonics include the effects of the pole notch and the flat face in the iron at the midplane. These would be the expected values of low field harmonics in this magnet, not including the contributions from persistent currents in the superconductor. The size of the cable used in the actual magnets was different (inner layer cable wider and outer layer cable thinner) by a small amount from that assumed in the original design. This produced noteworthy deviations in the three lowest allowed field harmonics. The last two rows of the table, "Revised BNL" and "Revised FNAL", refer to the values of field harmonics in the magnet after this change in the cable size.

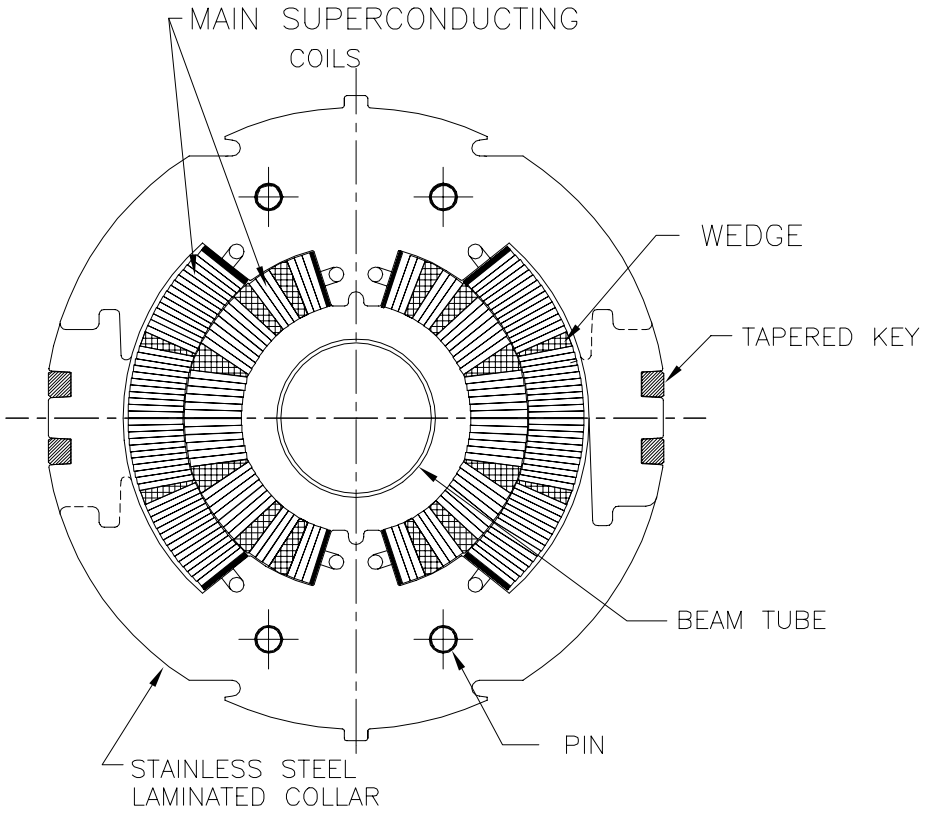

Figure 3.1: The cross section of the optimized coil for the prototype SSC 50 mm main collider dipole magnet. The coil is shown inside the stainless steel collar, which provides the compression on the coil.

Table 3.2: Desired and Optimized values of *low field* harmonics with a circular aperture. The harmonics in "BNL magnets" include the effects of the pole notch and a flat face in the iron at the midplane. These harmonics are in units of 10^{-4} at 10 mm reference radius. The last two rows include the effects of a change in cable size.

Values	b_2	b_4	b_6	b_8	b_{10}	b_{12}
Desired	-.28±.4	.01±.1	0±.05	±.045±.05	0±.05	0±.05
Optimized	-0.280	0.009	-0.004	0.044	0.014	-0.001
BNL magnets	0.000	-0.001	-0.004	0.044	0.014	-0.001
Revised BNL	1.566	0.070	-0.024	0.043	0.015	-0.001
Revised FNAL	0.165	0.073	-0.021	0.043	0.015	-0.001

A small difference in the "Revised BNL" and "Revised FNAL" harmonics is due to the fact that (a) the pole angle in the outer layer of the FNAL cross section is 10 mil (0.254 mm) smaller than in the BNL version (the wedge size was the same therefore the effective cable thickness in the coil was reduced) and (b) the notch in the aperture of the vertically split iron is at the midplane and in the horizontally split iron is at the pole. The normalization or reference radius (R_0) for the field harmonics is 10 mm and as usual the harmonics are given in units 10^{-4} of the central field.

3.3. Iron Yoke Design

In this section, the process used in designing the iron yoke is discussed. The iron contributes about 22% to the magnetic field at 6.7 tesla (somewhat higher at lower field). Since the magnetization of the iron is not a linear function of the current in the coil and varies throughout the cross section, the uniformity of the field becomes a function of the current in the coil. The yoke is optimized to produce a minimum change in the field harmonics due to iron saturation for the maximum achievable value of transfer function at 6.7 tesla. The results of field computations with the computer codes POISSON and MDP will be presented here. The computer model of the final design and the results of field calculations

with POISSON will be discussed in more detail. An iron packing factor of 97.5% has been used in these calculations.

If no special technique for controlling iron saturation were used, the change in the b_2 harmonic due to iron saturation would be over 1 unit. The following three options were considered for reducing the b_2 saturation swing. They all try to control the iron saturation at the iron aperture so that it saturates evenly.

- Reduced (shaved) iron o.d.
- Stainless Steel (non-magnetic) key at the midplane
- Shim at the iron inner surface

The first scheme, though most straight forward, produces a larger loss in transfer function at 6.7 tesla than the other two schemes. The third scheme, though actually increasing the transfer function at 6.7 tesla due to extra iron, requires more engineering development due to its non-circular aperture. The second scheme produces very little loss in transfer function (0.3% at 6.7 tesla compared to a keyless or magnetic key version) for a comparatively large reduction in b_2 due to saturation ($\frac{3}{4}$ unit). Moreover, it has the advantage of giving a way to control the b_2 due to saturation by changing the location and/or size of the key without affecting the other parts of the magnet design. It may be pointed out that besides the change due to iron saturation, b_2 and the other harmonics are also a function of current because of the coil deformation due to Lorentz forces. This has been observed in several SSC 40 mm aperture dipole magnets [64]. If the measured change in the b_2 harmonic is more than desired (either due to saturation or due to coil motion due to Lorentz forces), then this could be a useful and convenient method of correction.

The cross section of the cold mass (coil, collar and yoke) for the BNL-built SSC 50 mm prototype dipole is shown in Fig. 3.2. The POISSON model of this optimized cross section is given in a previous chapter as Fig. **@Fg.ssc-50mm-model@**. The cross section for the vertically split iron used by FNAL is shown in Fig. 3.3. The field lines at 6500 ampere are also shown in this figure. The iron i.d. is 135.6 mm; leaving a space of 17 mm for the collar, and the iron o.d. is 330.2 mm. The stainless steel key in the horizontally split yoke design is located at 91.4 mm and has a size of 12.7 mm $\times$ 12.7 mm. In the vertically split design for the FNAL-built magnet, a cutout at the horizontal midplane is incorporated to reduce

iron saturation. The size and location of this cutout is the same as in the BNL yoke. As mentioned earlier, the iron aperture is not completely circular. The BNL yoke has a pole notch of size 5.11 mm $\times$ 2.67 mm and a vertical straight face at the midplane which starts at $x = 67.13$ mm. The FNAL yoke has both the notch at the midplane and a vertical face at the midplane. The FNAL yoke has an additional pin located below the bus slot. This pin is made of non-magnetic steel and produces a noticeable effect on iron saturation. Other features in the two yokes are shown in the above mentioned figures.

The computed transfer function (T.F.) and b_2 as a function of current in the BNL and FNAL magnets are listed in Table 3.3. The b_2 harmonic has been adjusted so that it starts from zero; a non-zero value is artificial and is related to the way the computer model of a given coil and the iron geometry is set up in the two codes. The maximum computed b_2 due to saturation is about 0.3 unit. The calculations presented here, however, do not include the effects of the cryostat wall which modifies the current dependence of the harmonics at high current. POISSON uses a generalized finite difference method whereas MDP uses an integral method. Despite the fact that these two programs use two different methods for solving the problem, it is encouraging to see that both predict a small saturation shift. Similar calculations have been made by Kahn [64] with the computer code PE2D which uses the finite element method and good agreement has been found with the above calculations.

The maximum change in the b_2 and b_4 harmonics and the drop in transfer function, $\delta(TF)$, at 6.6 tesla (as compared to its value at low field) due to iron saturation as computed by these codes are listed in Table 3.4. All higher harmonics remain practically unchanged. In the case of the FNAL yoke, the computations have been done only with the code POISSON.

In Table 3.5 the results of POISSON calculations are presented for various values of current in the BNL design. In Fig. 3.4, the variation in field harmonics as a function of central field is plotted.

The coldmass (see Fig. 3.2) is placed in the cryostat. To provide the maximum space for the support posts which minimizes the heat leak, the cold mass is placed above the center of the cryostat, which breaks the top-bottom symmetry. At high field, when the field lines can not be contained in the iron yoke, the cryostat provides an extra return path for flux. A top-bottom asymmetry in the magnet structure is then seen in the magnetic field.

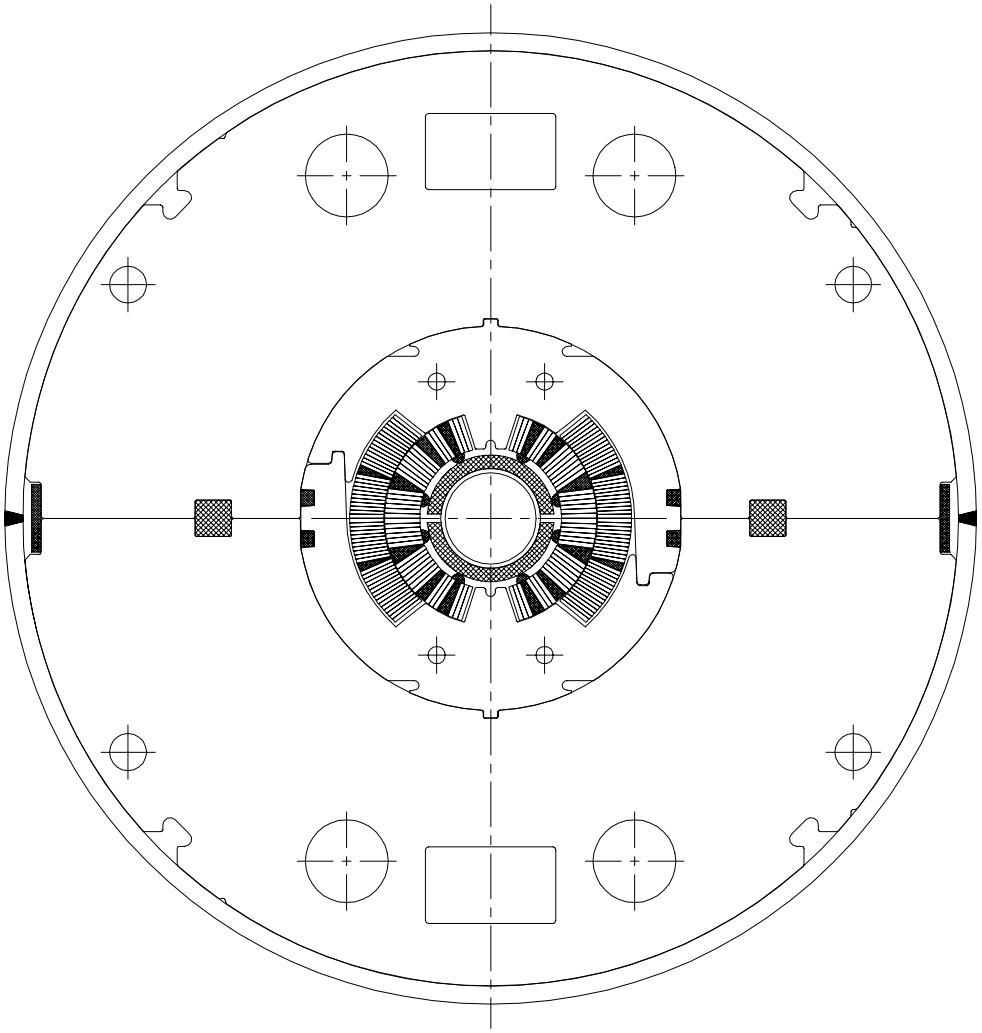

Figure 3.2: The cross section of the cold mass of 50 mm aperture horizontally split iron SSC arc dipoles. This cross section has been used in BNL built prototype magnets for SSC. The above cold mass is put inside a cryostat (not shown here).

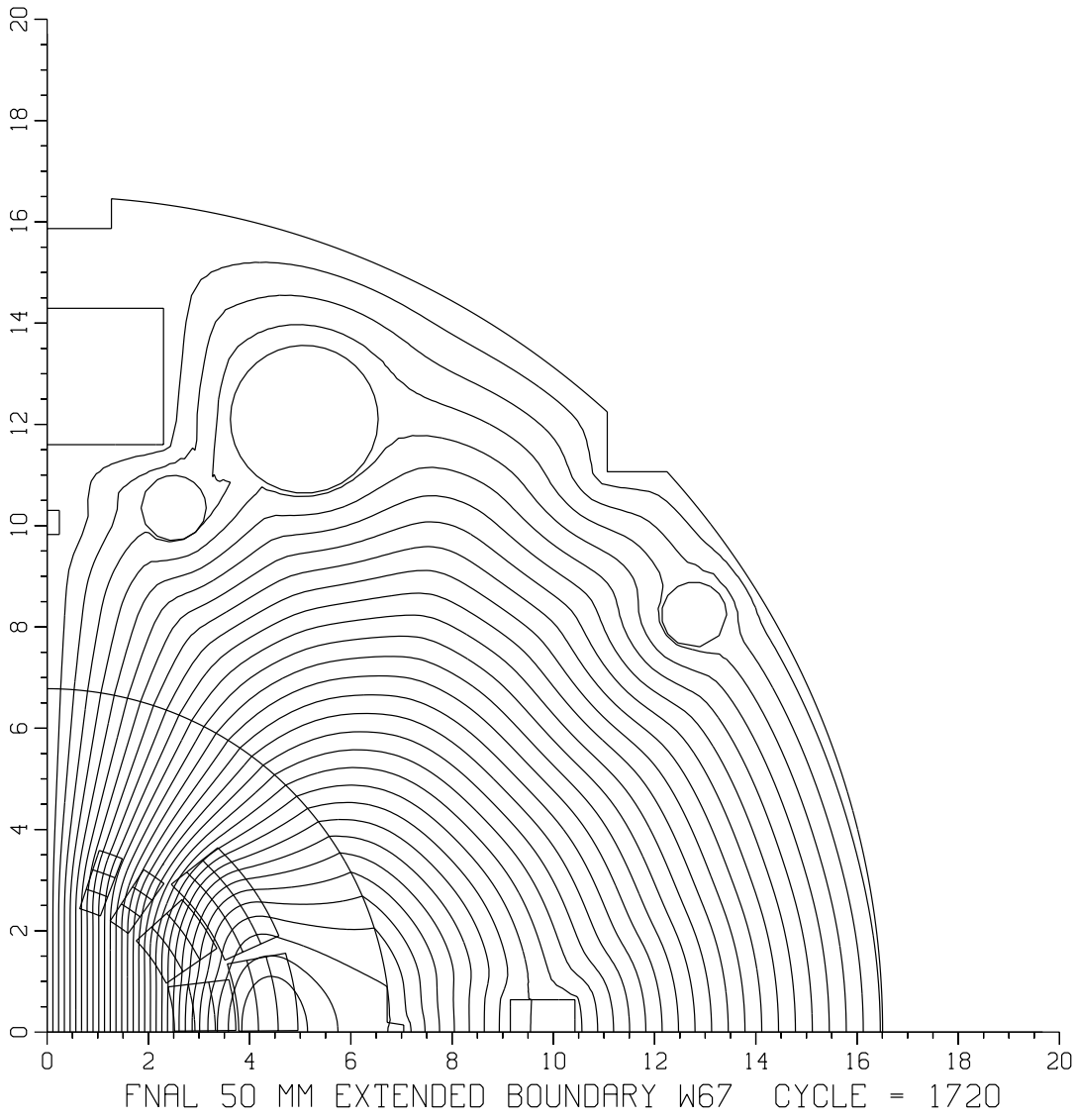

Figure 3.3: POISSON model and field lines at 6500 ampere for SSC 50 mm Dipole with vertically split iron laminations. This magnetic design was used in the prototype magnets built at FNAL.

Table 3.3: Transfer function and b_2 variation as function of current. In all cases b_2 is corrected to start from zero at 3.0 kA. FNAL yoke calculations were done only with the code POISSON.

I	T.F. (T/kA)			$b_2 \times 10^{-4}$		
kA	FNAL	BNL yoke		FNAL	BNL yoke	
	yoke	POISSON	MDP	yoke	POISSON	MDP
3.0	1.0450	1.0447	1.0430	0.00	0.00	0.00
4.0	1.0445	1.0441	1.0413	-0.02	0.08	0.05
5.0	1.0398	1.0397	1.0364	-0.04	0.22	0.16
5.5	1.0339	1.0340	1.0311	0.19	0.26	0.21
6.0	1.0257	1.0262	1.0236	0.36	0.14	0.17
6.25	1.0209	1.0219	1.0194	0.38	0.07	0.11
6.5	1.0159	1.0173	1.0148	0.35	-0.03	0.03
7.0	1.0053	1.0073	1.0051	0.17	-0.33	-0.19
7.6	0.9926	0.9955	0.9935	-0.15	-0.77	-0.60
8.0	0.9845	0.9877	0.9861	-0.38	-1.06	-0.85
8.6	0.9732	0.9766	0.9758	-0.70	-1.43	-1.20

The most prominent harmonic to reflect this asymmetry is the skew quadrupole (a_1) term. The presence of the skew quadrupole harmonic at high field and methods to minimize it have been discussed in a previous chapter.

Table 3.4: Drop in transfer function at 6.6 tesla and the maximum change in b_2 and b_4; higher harmonics remain practically unchanged.

Harmonic	POISSON FNAL yoke	POISSON BNL yoke	MDP BNL yoke
$\delta(TF)$, at 6.6T	2.84%	2.62%	2.70%
$\delta(b_2)_{max}$, 10^{-4}	0.36	0.28	0.22
$\delta(b_4)_{max}$, 10^{-4}	0.02	-0.03	-0.02

Table 3.5: Results of POISSON computations for the SSC 50 mm dipole with the horizontally split yoke design built at BNL.

I kA	B_o tesla	T.F. T/kA	b_2 10^{-4}	b_4 10^{-4}	b_6 10^{-4}	b_8 10^{-4}	b_{10} 10^{-4}	b_{12} 10^{-4}
$\infty\mu$	$\infty\mu$	1.04493	0.020	-0.046	0.000	0.047	0.015	-0.001
3.000	3.1341	1.04471	0.031	-0.046	0.001	0.047	0.015	-0.001
4.000	4.1762	1.04406	0.111	-0.050	0.001	0.047	0.015	-0.001
4.500	4.6921	1.04268	0.140	-0.055	0.001	0.047	0.015	-0.001
4.750	4.9464	1.04135	0.182	-0.060	0.001	0.047	0.015	-0.001
5.000	5.1985	1.03969	0.255	-0.063	0.001	0.047	0.015	-0.001
5.250	5.4454	1.03721	0.299	-0.066	0.001	0.047	0.015	-0.001
5.500	5.6871	1.03402	0.291	-0.069	0.001	0.048	0.015	-0.001
5.750	5.9240	1.03027	0.235	-0.071	0.001	0.048	0.015	-0.001
6.000	6.1573	1.02621	0.172	-0.073	0.000	0.048	0.015	-0.001
6.250	6.3868	1.02189	0.100	-0.073	0.000	0.048	0.015	-0.001
6.500	6.6121	1.01725	-0.003	-0.072	0.000	0.048	0.015	-0.001
7.000	7.0513	1.00733	-0.300	-0.072	0.000	0.049	0.015	-0.001
7.600	7.5654	0.99545	-0.738	-0.070	0.000	0.049	0.015	-0.001
8.000	7.9014	0.98767	-1.032	-0.068	0.000	0.050	0.015	-0.001
8.600	8.3984	0.97656	-1.403	-0.064	0.000	0.050	0.015	-0.001

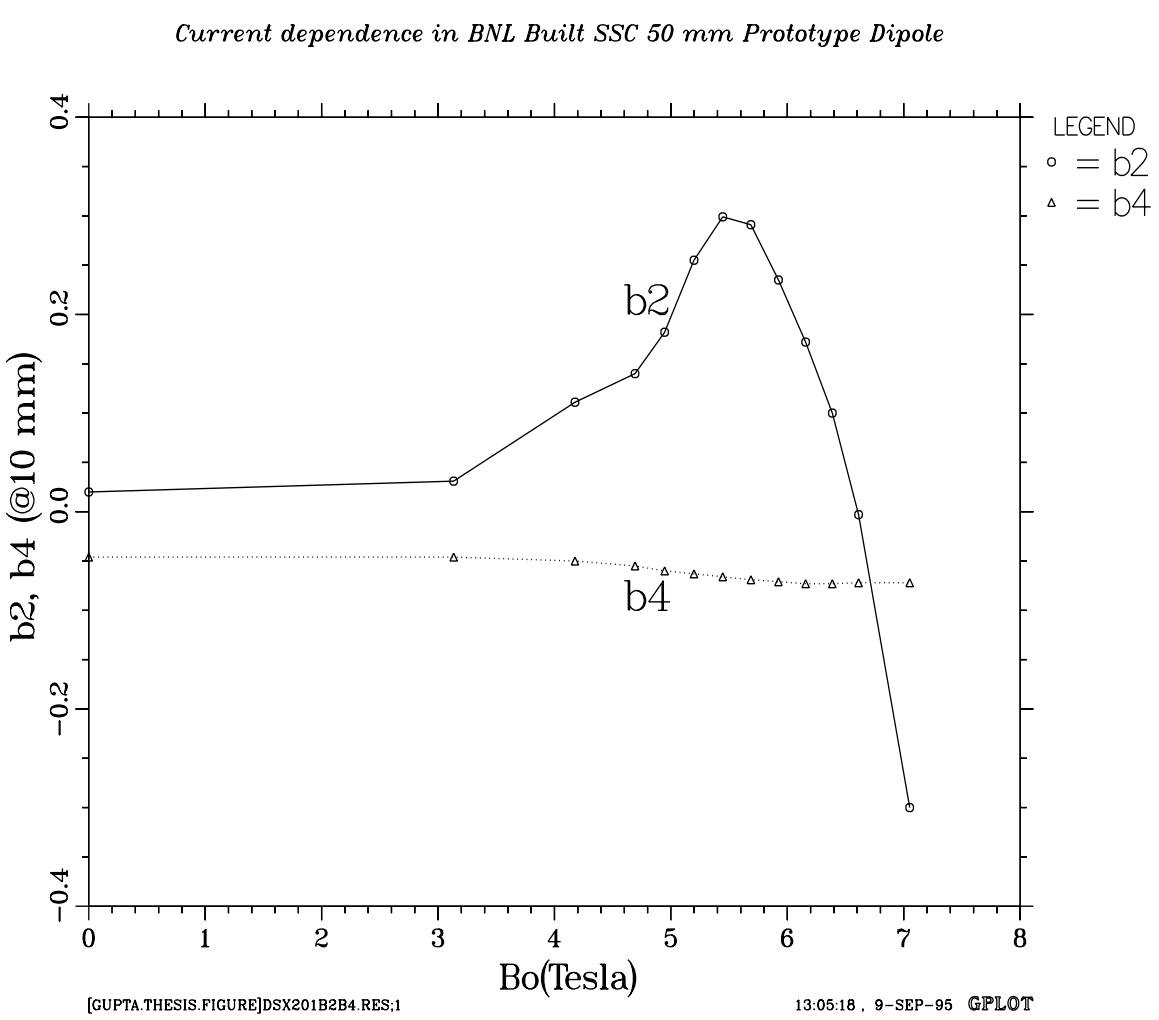

Figure 3.4: Variation in Field Harmonics as a function of Current in the SSC 50 mm BNL built prototype dipole magnet as computed by POISSON.

3.4. Expected Quench Performance

The central field at which a given cable looses its superconducting properties (B_{SS}, with "ss" standing for Short Sample) depends on the current in the cable which is a function of the maximum magnetic field at the conductor (the peak field) and the bath temperature. The superconducting cables for the inner and outer layers are optimized to provide a critical current (Ic) at a specified temperature and magnetic field. In a two layer coil design the magnetic design is optimized such that the computed short sample currents in the inner and outer layers are nearly the same. The peak field (B_{pk}) in the inner and outer layers of the SSC 50 mm dipole are listed in Table 3.6 for two values of central field (B_o). The ratio of B_{pk} to B_o, the *Enhancement Factor*, is given in the next column. In each layer, the peak field is found on the upper side of the top-most pole turn. The location of the peak field is listed in the next column. It is expressed as % of the cable width, measured from the upper-inner corner. The peak field calculations are done using the code MDP. MDP is based on the integral method and therefore is expected to give a more accurate field at the surface of the conductor as compared to codes based on the finite element method which require meshing the conductor.

Table 3.6: Peak fields in the SSC 50 mm dipole as computed using code MDP.

I	B_o	Inner			Outer		
kA	tesla	B_{pk},T	$\frac{B_{pk}}{B_o}$	Location	B_{pk},T	$\frac{B_{pk}}{B_o}$	Location
6.85	6.9058	7.2374	1.048	5%	6.0016	0.869	11%
7.20	7.2100	7.5595	1.048	5%	6.2660	0.869	11%

The calculations assume that the superconductor in the wire will have a critical current density $J_c(5T, 4.2K)$ of 2750 A/mm^2. The quality of the superconductor is degraded when the wires are made in to a cable and put in the magnet. The calculations presented in Table 3.7 have been done assuming 5% degradation (J_c=2612.5) and 4.35 K bath temperature.

Table 3.7: Expected quench performance of the SSC 50 mm dipole with 5% cable degradation ($J_c = 2612.5 A/mm^2$) and at 4.35 K temperature. S_{quench} is the computed current density in the copper at quench and $S_{6.7T}$ at the design field of 6.7 Tesla.

Layer ↓	Cu/Sc Ratio	B_{ss} tesla	I_c A	B_{margin} %over 6.7T	T_{margin} kelvin	S_{quench} A/cm^2	$S_{6.7T}$ A/cm^2
Inner	1.7	7.149	7126	6.7	0.519	736	681
	1.5	7.273	7273	8.6	0.625	788	715
	1.3	7.399	7411	10.4	0.730	853	759
Outer	2.0	7.268	7267	8.7	0.580	919	834
	1.8	7.445	7470	11.1	0.709	980	865

In Table 3.7, the field margin (B_{margin}) and the temperature margin (T_{margin}) are listed. The temperature margin is defined as the maximum possible computed rise in the operating temperature (over the design value of normal operation, which is 4.35 K) before the magnet will quench at the design central field (B_{design}=6.7 tesla). The field margin is defined as follows

$$B_{margin}\,(\%) = \frac{B_{ss} - B_{design}}{B_{design}} \times 100$$

The calculations are done for copper to superconductor ratios, CSR or Cu/Sc, of 2.0 and 1.8 in the outer layer and 1.7, 1.5 and 1.3 in the inner layer. The computed central field (B_{ss}) at the magnet quench point is listed together with the current in the cable at that point (I_c) and the current density (S_{quench}) in the copper available to carry that current after quench. A lower current density in the copper is expected to give better stability. The current density in the copper at 6.7 tesla ($S_{6.7T}$) is also listed. For stability purposes, $S_{6.7T}$ may be a more appropriate parameter to consider than S_{quench}.

The design values selected were a copper to superconductor ratio of 1.8 in the outer layer and of 1.5 in the inner layer. The quench field B_{ss} of 7.273 tesla in the inner layer gives a field margin of 8.6% over the design operating field B_{ss} of 6.7 tesla. The quench field of 7.445 tesla in the outer layer gives a field margin of 11.1%.

3.5. Effect of Manufacturing Errors on the Allowed Harmonics

For various reasons, the actual value of a parameter used in designing the coil may turn out to be somewhat different than desired. In particular, deviations in the locations of various turns in the coil are very important. This causes changes in the transfer function and the field harmonics. In this section the effect of these errors in various cases are estimated using a procedure developed by P.A. Thompson [130]. The basic four fold symmetry in the dipole coil geometry is retained in this analysis. Though this is not a realistic assumption, it is useful in estimating the size of some errors. In Table 3.8 these effects are listed for a nominal 0.05 mm variation in the given parameter.

First, the change in harmonics due to a change of +0.05 mm in the radius of every turn in each current block, one block at a time, is given. The counting of the blocks in the table starts at the inner layer and at the midplane of each layer. Next the effect of changing the wedge size by +0.05 mm is estimated. Pole angle is held constant in this calculation by reducing the conductor thickness by an appropriate amount. The counting scheme for the wedges is the same as it is for the current blocks. It is possible that during the molding, the thickness of the cable is not reduced uniformly within a layer. To estimate this effect, a linear increase in the cable thickness is assumed going from the midplane towards the pole, followed by a linear decrease, such that the middle turn is displaced azimuthally by 0.05 mm. The pole angle does not change during this perturbation. This effect is given for the inner and outer layers in the next two rows of the table. The effect of increasing the pole angle by 0.05 mm in the inner and in the outer layer is shown in the last two rows. In each group the Root Mean Square (RMS) change of these variations is also given.

Table 3.8: The effect of a 0.05 mm increase in the given parameter on the transfer function and the field harmonics.

Parameter changed	TF T/kA	b_2 10^{-4}	b_4 10^{-4}	b_6 10^{-4}
Radius of Block No. 1	0.31	-0.25	-0.10	-0.01
Radius of Block No. 2	-0.32	0.31	0.12	0.01
Radius of Block No. 3	-0.12	0.36	-0.02	-0.01
Radius of Block No. 4	-0.20	0.33	-0.08	0.01
Radius of Block No. 5	-0.11	-0.04	-0.01	0.00
Radius of Block No. 6	-0.78	0.22	0.03	0.00
RMS Blocks	0.38	0.27	0.07	0.01
Thickness of Wedge No. 1	-1.56	-0.48	0.02	0.01
Thickness of Wedge No. 2	0.83	0.59	0.05	-0.01
Thickness of Wedge No. 3	2.32	0.71	-0.04	0.00
Thickness of Wedge No. 4	-0.57	-0.11	0.00	0.00
RMS Wedges	1.48	0.52	0.03	0.01
Cable thickness inner	2.63	1.08	0.05	-0.01
Cable thickness outer	1.99	0.48	0.02	0.00
RMS Cable thickness	2.33	0.83	0.04	0.01
Pole angle inner	-4.01	-0.45	0.06	-0.01
Pole angle outer	-2.26	-0.42	0.00	0.00
RMS Pole angles	3.25	0.43	0.04	0.01

3.6. Stored Energy and Inductance Calculations

Stored energy calculations are done with the computer code POISSON [135]. POISSON uses the following formula to compute the stored energy per unit length (E_l) over the cross section area :

$$E_l = \tfrac{1}{2} \int_a J \ A_z \ da,$$

where A_z is the vector potential and J is the current density in the mesh triangle having an area da. The integration needs to be performed only over the regions containing current. At low fields when the field B is proportional to I (i.e. when yoke saturation is not significant), the stored energy is expected to be proportional to B^2 or I^2.

The stored energy and the inductance are related through the following formula :

$$Stored \ Energy = \tfrac{1}{2} Inductance \times (Current)^2.$$

The inductance decreases at high field as the iron yoke saturates.

The results of POISSON computations for the SSC 50 mm aperture dipole are given at 6.5 kA in Table 3.9 for the stored energy per unit length and the inductance per unit length. The total stored energy and the inductance for a 15 m long dipole are also given.

Table 3.9: Stored Energy and Inductance at 6.5 kA as computed with the code POISSON for the SSC 50 mm aperture dipole.

Stored Energy per unit length, kJ/m	105.0
Stored Energy for 15 m long Dipole, kJ	1575.6
Inductance per unit length, mH/m	4.972
Inductance for 15 m long Dipole, mH	74.585

3.7. Lorentz Force Calculations

The value of Lorentz force per unit of axial length on each turn is obtained from the components of the magnetic field (B_x, B_y). These components are calculated using program MDP. Since B_x and B_y are not uniform in a turn, an average value of these components is obtained from a grid of 10×2 across the width and thickness of the cable.

The variation in the magnitude of the radial and azimuthal components of the Lorentz forces, namely F_r and F_a (also referred to as F_θ), with turn number is shown in Fig. 3.5. The turn numbers are counted from the midplane. The Lorentz force acts on the coil such that the azimuthal component compresses the coil on the midplane and the radial component expands it outward. Though the radial Lorentz force on the turns in the outer layer is very small, the force on the turns in the inner layer must be transmitted through the outer layer to the structure of the magnet.

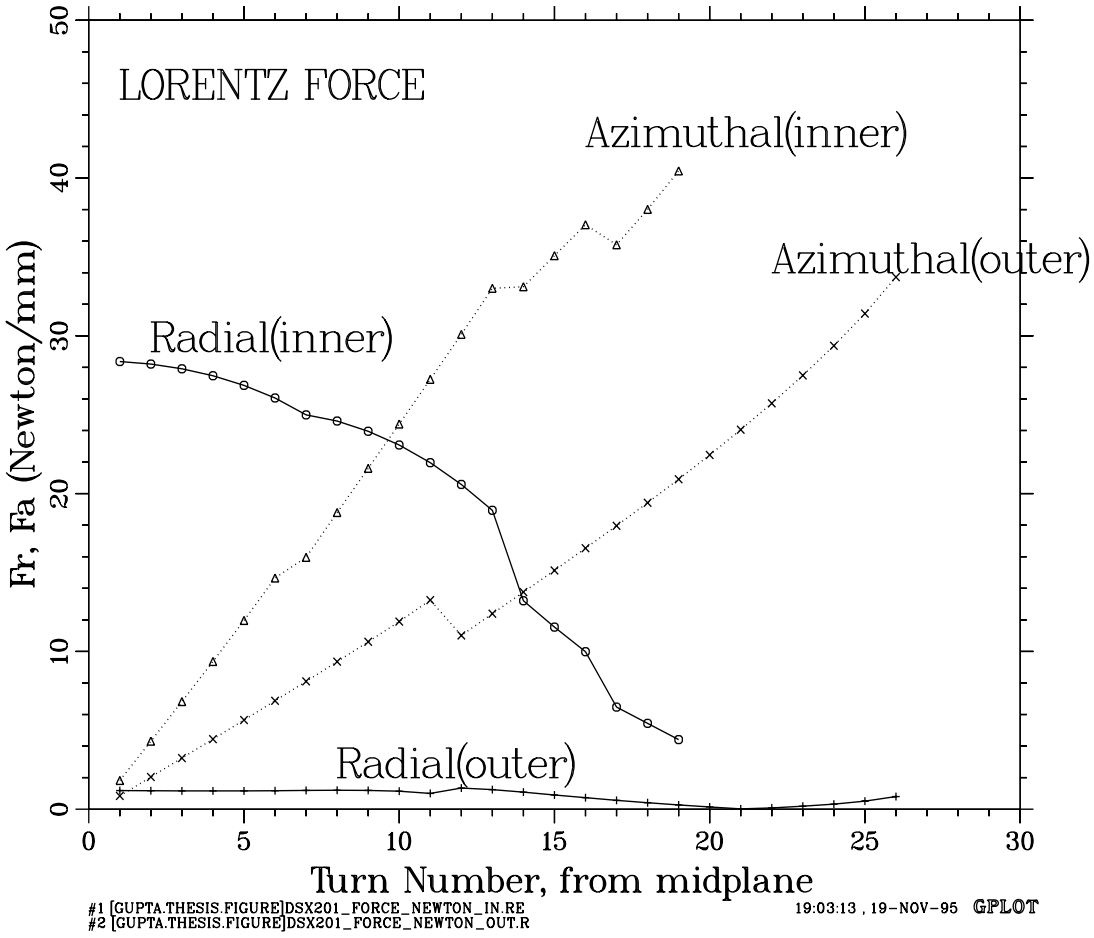

Figure 3.5: The magnitude of the components of the Lorentz force on the individual turns in a SSC 50 mm prototype magnet. The radial component of the force (F_r) pushes the coil outward and the azimuthal component (F_a) compresses the coil towards the midplane (horizontal plane). There are 19 turns in the inner layer and 26 turns in the outer layer of each quadrant.

3.8. Summary of the Design

A summary of the coil and iron cross-sections are given respectively in Table 3.10 and Table 3.11. The coil has two layers and the number of turns is the number of turns in the upper or lower half of a layer. The field margin in this cross section is limited by the inner layer. If the cable used in the inner layer had a copper to superconductor ratio of 1.3, the margin would be 10.4% (see Table 3.7).

Table 3.10: Summary of SSC 50 mm dipole coil cross section.

Layer →	Inner	Outer
No. of Turns	19	26
Strand Diameter, mm	0.808	0.648
Strands per turn	30	36
Coil i.d., mm	49.56	74.91
Coil o.d., mm	75.36	99.42
B_{peak}/B_o	1.048	0.869
Cu/SC	1.5	1.8
Margin over 6.7 T ...	8.6%	11.1%

Table 3.11: Summary of SSC 50 mm dipole iron cross section. $\delta(TF)$ is the change in transfer function, δb_2 in b_2 and and δb_4 in b_4 due to saturation.

Inner Diameter, mm	135.6
Outer Diameter, mm	330.2
$\delta(TF)$, at 6.7 T	2.6%
δb_2, prime unit	0.3
δb_4, prime unit	0.03

References

1. D. Abeshouse, H. Hahn, *Perturbation Method for Cosine theta Magnet with Nonlinear Iron Shields*, The Fourth International Conference on Magnet Technology, Brookhaven National Laboratory, NY, USA, MT-4, pp. 594-599 (1972).
2. J. Allinger, et al., *High Field Superconducting Magnets for Accelerators and Particle Beams*, 1974 Applied Superconductivity Conference; IEEE Transaction on Magnetics, Vol. MAG-11, No. 2, pp.467-470 (1974).
3. J. Allinger, et al., *ISABELLE Ring Magnets*, 1976 Applied Superconductivity Conference; IEEE Transaction on Magnetics, Volume MAG-13, No. 1, pp. 275-278 (1976).
4. M. Anerella, et al., *Construction and Test Results from 15 m-Long, 50 mm Aperture SSC Dipole Models*, Supercollider 4, Proceedings of the Fourth International Industrial Symposium on the Super Collider, March 4-6 1992, New Orleans, USA, pp. 535-549 (1992).
5. M. Anerella, et al., *Improved Cable Insulation for Superconducting Magnets*, Proceedings of the 1993 Particle Accelerator Conference, Washington, D.C., pp. 2790-2792 (1993).
6. M. Anerella, et al., *Industrial Production of RHIC Magnets*, Proceedings of the Fourteenth International Conference on Magnet Technology (MT-14), Tampere, Finland, June 11-16 (1995).
7. J. Swanson, *ANSYS Finite Element Code Revision 5.0*, Swanson, Analysis System, Inc. (1992).
8. AUTOCAD is a commercial software package available from Autodesk, Inc.; AUTOCAD is a registered Trademark of Autodesk, Inc. (1992).
9. D. Beavis, et al., *Letter of intent for a forward angle and midrapidity hadron spectrometer at RHIC*, RHIC-LOI-8, Brookhaven National Laboratory (1992).
10. D. Bein and J. Zbasnik, *Utilization of Gamma Ray Inspection System for Tomographic Imaging and Dimensional Analysis of Complete Model Magnet Cold Masses*

and Collared Coil Sections, Supercollider 4, Proceedings of the Fourth International Industrial Symposium on the Super Collider, New Orleans, USA, pp. 225-233 (1992).

11. G.F. Bertsch, *Searching for the Quark-Gluon Plasma*, Science, Vol. 265, pp. 480-481 (1994).

12. R.A. Beth, *Complex representation and computation of two-dimensional magnetic fields*, Journal of Applied Physics, Vol. 37, No. 7, p. 2568 (1966).

13. R.A. Beth, *An Integral Formula for Two-Dimensional Fields*, Journal of Applied Physics, Vol. 38, No. 12, pp. 4689-4692 (1967).

14. R.A. Beth, *Elliptical and Circular Current Sheets to Produce a Prescribed Internal Field*, 1967 National Accelerator Conference, IEEE Trans. of Nucl. Sci., No. 3, pp. 368-370 (1967).

15. R.A. Beth, *Analytic design of superconducting multipolar magnets*, Proc. 1968 Summer Study on Superconducting Devices and Accelerators, Brookhaven National Laboratory p. 843 (1968).

16. R.A. Beth, *Evaluation of Current-Produced Two-Dimensional Magnetic Fields*, Journal of Applied Physics, Vol. 40, No. 12, pp. 4782-4786 (1969).

17. R.A. Beth, *Currents and Coil Forces as Contour Integrals in Two-Dimensional Magnetic Field*, Journal of Applied Physics, Vol 40, No. 6, pp. 2445-2449, (1969).

18. R.A. Beth, *Induced EMFS in Two-Dimensional Fields*, The Fourth International Conference on Magnet Technology, MT-4, Brookhaven National Laboratory, NY, USA (1972).

19. K.J. Binns and P.J. Lawrenson, *Analysis and Computation of Electric and Magnetic Field Problems*, Published by Pergamon Press, Second edition (1973).

20. E.J. Bleser, et al., *Superconducting Magnets for the CBA Project*, Nuclear Instruments and Methods in Physics Research A235, pp. 435-463 (1985).

21. J.P. Blewett, *Iron Shielding for Air Core Magnets*, Proc. 1968 Summer Study on Superconducting Devices and Accelerators, Brookhaven National Laboratory, p. 1042 (1968).

22. H. Brechna, *Superconducting Magnet System*, Technische Physik in Einzeldarstellungen Band 18, Springer-Verlag, Berlin (1973).

23. H. Brechna, et al., *Workshop on Magnets: Superconducting Magnets for High Energy Accelerators*, The Seventh International Conference on Magnet Technology, MT-7, Karlsruhe Nuclear Research Center, Germany, pp. 2355-2365 (1981).

24. G. Brianti, *General Aspects and Present Limits in the Accelerator Technology*, The Ninth International Conference on Magnet Technology, MT-9, Zurich, Switzerland, pp. 53-61 (1985).

25. K.L. Brown and R.V. Servranckx, *First- and Second- Order Charged Particle Optics*, AIP Conference Proceedings No. 127, pp. 62-138 (1983).

26. CAD OVERLAY GS is a commercial software package available from Image System Technology; CAD Overlay GS is a registered Trademark of Image System Technology (1992).

27. S. Caspi, et al., *Incorporation of Boundary Condition into the POISSON Program*, The Ninth International Conference on Magnet Technology, MT-9, Zurich, Switzerland, pp. 1560-1566 (1985).

28. S. Caspi, et al., *The effects of filament magnetization in superconducting magnets as computed by Poisson*, 1986 Applied Superconductivity Conference, Baltimore, Maryland, USA, IEEE Transactions on Magnetics, March 1987, Volume MAG-23, No. 2 , pp. 510-513 (1986).

29. R.V. Churchill, *Complex Variables and Applications*, Published by McGraw-Hill Book Company, Inc (1950).

30. J.H. Coupland, *Dipole, quadrupole and higher order fields from simple coils*, Nuclear Instruments and Methods, 78, pp. 181-184 (1970).

31. J. Coupland, et al., *Very High Field Synchrotron Magnets with Iron Yokes*, Nuclear Instruments and Methods 106, p. 595 (1973).

32. E.D. Courant and H.S. Snyder, *Theory of the Alternating Gradient Synchrotron*, Annals of Physics, Vol 3, pp 1-48 (1958).

33. P. Dahl, et al., *Superconducting Magnet Models for ISABELLE*, 1973 Particle Accelerator Conference, San Francisco, USA, pp. 688-692 (1973).

34. P. Dahl, et al., *Performance of three 4.5 m Dipoles for SSC Reference Design D*, The Ninth International Conference on Magnet Technology, MT-9, Zurich, Switzerland, pp. 80-83 (1985).

35. P. Dahl, et al., *Construction of Cold Mass Assembly for Full-Length Dipoles for the SSC Accelerator*, 1986 Applied Superconductivity Conference, Baltimore, Maryland, USA, IEEE Transactions on Magnetics, Volume MAG-23, No. 2, pp. 1215-1218 (1987).

36. P. Dahl, et al., *Performance of Initial Full-length RHIC Dipoles*, The Tenth International Conference on Magnet Technology, MT-10, Boston, MA, USA, pp. 723-725 (1987).

37. P. Dahl, et al., *Test Results from 1.8-m SSC Model Dipoles*, The Tenth International Conference on Magnet Technology, MT-10, Boston, MA, USA, pp. 816-819 (1987).

38. P. Dahl, *Superconducting Magnet System*, 1989 US Particle Accelerator School, AIP Conference Proceedings 184, pp. 1327-1376 (1989).

39. G. Danby, *Ultraprecise Magnet Design and Shimming*, 1987 Particle Accelerator Conference, Washington DC, pp. 1517-1519 (1987).

40. C. Daum, *Three-dimensional computation of magnetic fields and Lorentz forces of an LHC dipole magnet*, NIKHEF-H/89-12, LHC Note No. 94 (1989).

41. D. Dell'Orco, S. Caspi, et al., *A 50 mm Bore Superconducting Dipole with a Unique Iron Yoke Structure*, Published in the proceedings of the 1992 Applied Superconductivity Conference, Chicago (1992).

42. H. Desportes, *Superconducting Magnets for Accelerators, Beam Lines, and Detectors*, The Seventh International Conference on Magnet Technology, MT-7, Karlsruhe Nuclear Research Center, Germany, pp. 1560-1566 (1981).

43. A. Devred, *Quench Origins*, The Physics of Particle Accelerators, AIP Conference Proceedings 249, pp. 1262-1308 (1990).

44. A. Devred, et al., *About the Mechanics of SSC Dipole Magnet Prototypes*, The Physics of Particle Accelerators, AIP Conference Proceedings 249, pp. 1309-1374 (1990).

45. A. Devred, et al., *Status of 4-cm Aperture, 17-m-long SSC Dipole Magnet R&D Dipole Magnet Program at BNL Part I: Magnet Assembly*, Supercollider 3, Proceedings of the Third International Industrial Symposium on the Super Collider, Atlanta, USA, pp. 549-573 (1991).

46. A. Devred, et al., *Review of SSC Dipole Magnet Mechanics and Quench Performance*, Supercollider 4, Proceedings of the Fourth International Industrial Symposium on the Super Collider, New Orleans, USA, pp. 113-136 (1992).

47. G.E. Fischer, *Iron Dominated Magnets*, 1985 SLAC Summer School, AIP Conference Proceedings 153, pp. 1120-1227 (1985).

48. H.E. Fisk, et al., *The Ironless Cos theta Magnet Option for the SSC*, 1985 Particle Accelerator Conference in Vancouver, Canada, pp. 3456-3461 (1985).

49. G. Ganetis, et al., *Field Measuring Probe for SSC Magnets*, 1987 Particle Accelerator Conference, Washington DC, pp. 1393-1395 (1987).

50. M. Green, *Control of the Fields due to Superconductor Magnetization in the SSC Magnets*, IEEE Transactions on Magnetics, Vol. MAG-23, No. 2, pp. 506-509 (1987).

51. A. Greene, et al., *The Magnet System of the Relativistic Heavy Ion Collider (RHIC)*, Fourteenth International Conference on Magnet Technology (MT-14), Tampere, Finland, June 11-16 (1995).

52. E. Gregory, *Conventional Wire and Cable Technology*, The Physics of Particle Accelerators, AIP Conference Proceedings 249, pp. 1198-1229 (1990).

53. R.C. Gupta, J.I.M. Botman, M.K. Craddock, *A High Transition Energy Lattice for a TRIUMF KAON Factory Synchrotron*, Western Region Nuclear Physics Conference, Lake Louise, Canada (1984).

54. R.C. Gupta, J.I.M. Botman, M.K. Craddock, *High Transition Energy Magnet Lattices*, Proceedings of the 1985 Particle Accelerator Conference, Vancouver, Canada; IEEE Transaction on Nuclear Science, Volume NS-32, Oct 1985, pp. 2308-2310 (1985).

55. R.C. Gupta, G.H. Morgan, *A Design for a High Field Combined Function Superferric Magnet*, Proceedings of the 1985 Particle Accelerator Conference, Vancouver, Canada; IEEE Transaction on Nuclear Science, Volume NS-32, Oct 1985, pp. 3687-88 (1985).

56. R.C. Gupta, *Modifications in the AUTOMESH and other POISSON Group Codes*, Proceedings of the Workshop in Electromagnetic Field Computations, Schnectady, NY, pp. H38-H42 (1986).

57. R.C. Gupta, *Improvements in the Mesh Generator of the POISSON Group Codes*, Proceedings of the 1987 Particle Accelerator Conference, Washington DC, pp. 1449-1451 (1987).

58. R.C. Gupta, G.H. Morgan, P.A. Thompson, *A Single Layer Coil Superconducting Magnet for SSC*, Proceedings of the 1987 Particle Accelerator Conference, Washington DC, pp. 1413-1415 (1987).

59. R.C. Gupta, G.H. Morgan, P.J. Wanderer, *A Comparison of Calculations and Measurements of the Iron Saturation Characteristic of the SSC Design D Dipole Magnet*, Proceedings of the 1987 Particle Accelerator Conference, Washington DC, pp. 1405-1407 (1987).

60. R.C. Gupta, S.Y. Lee, Y.Y. Lee, X.F. Zhao, *Beam Transfer Lines for the AGS Booster*, Proceedings of the 1987 Particle Accelerator Conference, Washington DC, pp. 1193-1195 (1987).

61. R.C. Gupta, G.H. Morgan, *Collarless, Close-in, Shaped Iron Aperture Designs for the SSC Dipole*, Proceedings of the 1989 Particle Accelerator Conference, Chicago, pp. 500-502 (1989).

62. R.C. Gupta, S.A. Kahn and G.H. Morgan, *Coil and Iron Design for SSC 50 mm Magnet*, Proceedings of the 1990 American Society of Mechanical Engineers (ASME) Winter Annual Meeting in Dallas (1990).

63. R.C. Gupta, *POISSON-BNL*, Computer Codes for Particle Accelerator Design and Analysis : A Compendium, Los Alamos Accelerator Code Group, Second Addition, LA-UR-90-1766 (1990).

64. R.C. Gupta, S.A. Kahn and G.H. Morgan, *A Comparison of Calculations and Measurements of the Field Harmonics as a Function of Current in the SSC Dipole Magnets*, Proceedings of the 1991 IEEE Particle Accelerator Conference, San Francisco, pp. 42-44 (1991).

65. R.C. Gupta, et al., *RHIC Insertion Magnets*, Proceedings of the 1991 IEEE Particle Accelerator Conference, San Francisco, pp. 2239-2241 (1991).

66. R.C. Gupta, S.A. Kahn and G.H. Morgan, *SSC 50 mm Dipole Cross section*, Proceedings of the 3^{rd} International Industrial Symposium on Super Collider (IISSC), Atlanta, pp. 587-600 (1991).

67. R.C. Gupta, *Correcting Field Harmonics after Design in Superconducting Magnets*, Proceedings of the 4^{th} International Industrial Symposium on Super Collider (IISSC), New Orleans, pp. 773-780 (1992).

68. R. Gupta, *Iron Shims to Correct the Measured Harmonics in 130 mm Aperture RHIC Insertion Quadrupoles*, Magnet Division Internal Note 480-16 (RHIC-MD-185), Dec. 10, 1992, Unpublished (1992).

69. R. Gupta, et al., *Large Aperture Quadrupoles for RHIC Interaction Regions*, Proceedings of the 1993 Particle Accelerator Conference, Washington, D.C., pp. 2745-2747 (1993).

70. R.C. Gupta, A.K. Jain, *Variation in a_1 saturation in SSC Collider Dipoles*, Proceedings of the 1993 Particle Accelerator Conference, Washington, D.C., pp. 2778-2780 (1993).

71. R. Gupta, et al., *Field Quality Improvements in Superconducting Magnets for RHIC*, Proceedings of the 1994 European Particle Accelerator Conference, London, UK, pp. 2928-2930 (1994).

72. R. Gupta, et al., *Field Quality Control Through the Production Phase of RHIC Arc Dipoles*, Proceedings of the 1995 International Particle Accelerator Conference, Dallas, Texas (1995).

73. R. Gupta, et al., *Tuning Shims for High Field Quality in Superconducting Magnets*, Proceedings of the Fourteenth International Conference on Magnet Technology (MT-14), Tampere, Finland, June 11-16 (1995).

74. R. Gupta, *Estimating and Adjusting Field Quality in Superconducting Accelerator Magnets*, Proceedings of the LHC Collective Effects Workshop, Montreux, 1995; Submitted to the Particle Accelerators (1995).

75. R. Gupta, *Field Quality in the Superconducting Magnets for Large Particle Accelerators*, Proceedings of the 1996 European Particle Accelerator Conference at Sitges, Spain (1996).

76. H. Gurol, General Dynamics, Private communication, (1993).

77. H. Hahn, et al., *Upgrade Coil Configuration for Isabelle Magnets*, The Seventh International Conference on Magnet Technology, MT-7, Karlsruhe Nuclear Research Center, Germany, pp. 1575-1578 (1981).

78. H. Hahn, *ISABELLE - A Progress Report*, IEEE Transaction on Magnetics, January 1981, Vol MAG-17, No. 1, 1981 Applied Superconductivity Conference, pp. 702-708 (1981).

79. K. Halbach, *A Program for Inversion of System Analysis and its Application to the Design of Magnets*, Proceedings of the second conference on Magnet Technology, Oxford, England (1967).

80. K. Halbach, *Application of Conformal Mapping to Evaluation and Design of Magnets Containing Iron with Nonlinear B(H) Characteristics*, Nuclear Instruments and Methods 64, pp. 278-284 (1968).

81. K. Halbach, *Fields and first order perturbation effects in two-dimensional conductor dominated magnets*, Nuclear Instruments and Methods, 78, p. 185 (1970).

82. K. Halbach, *Speciality Magnets*, 1985 SLAC Summer School, AIP Conference Proceedings 153, pp. 1277-1295 (1985).

83. R. Hannaford, et al., *Resolution to difficulties experienced in SSC cable Fabrication during the initial scale-up period*, 1990 Applied Superconductivity Conference, Snowmass, Co, USA; IEEE Transaction on Magnetics, March 1991, Vol 27, No. 2, pp. 2024-2026 (1990).

84. M.A. Harrison, *The RHIC Project*, Proceedings of the 1994 European Particle Accelerator Conference, London, UK, pp. 156-160 (1994).

85. M.A. Harrison, *RHIC Status and Plan*, Proceedings of the 1995 International Particle Accelerator Conference, Dallas, Texas (1995).

86. W.V. Hassenzahl, R.B. Meuser, C. Taylor, *Technology of Superconducting Accelerator Dipoles*, 1982 Summer School on High Energy Particle Accelerators, AIP Conference Proceedings 105, pp. 732-800 (1982).

87. J. Herrera, et al., *Random Errors in the Magnetic Field Coefficients of Superconducting Magnets*, pp. 3689-3691, 1985 Particle Accelerator Conference in Vancouver, Canada, May 13-16, 1985.

88. J. Herrera, et al., *Measurement of the Magnetic Field Coefficients of Particle Accelerator Magnets*, 1989 Particle Accelerator Conference in Chicago, USA, pp. 1774-1776 (1989).

89. H. Hillmann, *Large Scale Fabrication of Superconductors*, The Seventh International Conference on Magnet Technology, MT-7, Karlsruhe Nuclear Research Center, Germany, pp. 1614-1621 (1991).

90. R.F. Holsinger, original version of the *User's Guide to POISSON Group Codes*. This and a new version of the User's Guide and Reference Manual for POISSON Group Codes can be obtained from the Los Alamos Accelerator Code Group, Los Alamos National Laboratory Publication No. LA-UR-87-126, or latest version (1967).

91. "Paintbrush" is a commercial software package available from the Hewlett Packard Corporation; "HP Paintbrush" is a registered Trademark of Hewlett Packard Corporation. Scan Gallery version 5 has been used here. (1992).

92. "SCANJET Plus" is a package of commercial hardware and software which is available from the Hewlett Packard Corporation; "HP ScanJet Plus" is a Registered Trademark of Hewlett Packard Corp (1992).

93. B.B. Gamble, et al., *Prospects for HTS Applications*, Fourteenth International Conference on Magnet Technology (MT-14), Tampere, Finland, June 11-16 (1995).

94. F.R. Huson et al., *Superferric magnet option for the SSC*, 1985 Particle Accelerator Conference in Vancouver, Canada, pp. 3462-3465 (1985).

95. J.D. Jackson, *Classical Electrodynamics*, Second Edition, Published by John Wiley & Sons (1975).

96. J.D. Jackson, editor, *Conceptual Design of the Superconducting Super Collider*, SSC-SR-1020 (1986).

97. A. Jain, R. Gupta, et al., *Skew Quadrupole in RHIC Dipole Magnets at High Fields*, Fourteenth International Conference on Magnet Technology (MT-14), Tampere, Finland, June 11-16 (1995).

98. S. Kahn, et al., *Field Quality Aspects of CBA Superconducting Magnets*, 1983 Particle Accelerator Conference, Santa Fe, USA, pp. 3469-3471 (1983).

99. S. Kahn, R. Gupta, G. Morgan, P. Thompson, *Comparison of Magnetic Field Calculations to Measurements on a CBA 2-in-1 Magnet System*, Proceedings of the 1985 Particle Accelerator Conference, Vancouver; IEEE Transaction on Nuclear Science, Volume NS-32 (1985).

100. S.A. Kahn and G.H. Morgan, *Magnetic Properties of Iron Yoke Laminations for SSC Dipole Magnets*, 1991 IEEE Particle Accelerator Conference, San Francisco, pp. 2170-2172 (1991).

101. S. Kahn, Private communication (1992).

102. S.A. Kahn, R.C. Gupta, A.K. Jain, G.H. Morgan, P.A. Thompson, *Calculations of Magnetic Field for the End Design of the RHIC Arc Dipole*, Proceedings of the 1993 Particle Accelerator Conference, Washington, D.C., pp. 2754-2756 (1993).

103. J.F. Kallsen, et al., *SSC Type NbTi Superconductor Research Program at Teledyne SC*, 1990 Applied Superconductivity Conference, September 24-28, 1990, Snowmass,

Co, USA; IEEE Transaction on Magnetics, March 1991, Vol 27, No. 2, pp. 1799-1802 (1990).

104. "Kapton" is a registered trademark of E.I. Dupont de Nemours & Co.

105. T.K. Khoe, R.J. Lari, *FORGY, A Companion Computer Program of TRIM to Calculate Forces and Energy in Electromagnets*, The Fourth International Conference on Magnet Technology, MT-4, Brookhaven National Laboratory, NY, USA, pp. 585-593 (1972).

106. H. Kirk, et al., *Magnetic Field Properties of the Isabelle Project Superconducting Dipole Magnets*, 1981 Particle Accelerator Conference, Washington, D.C., pp. 3237-3239 (1981).

107. H.G. Kirk, et al., *End Fields of CBA Superconducting Magnets*, 1983 Particle Accelerator Conference, Santa Fe, USA, pp. 3375-3377 (1983).

108. Koska W., et al., *Test of Fermilab Built 40 mm Aperture Full Length SSC Dipole Magnets*, The Twelfth International Conference on Magnet Technology, MT-12, Leningrad, USSR, pp. 303-306 (1991).

109. J. Kuzminski, et al., *Test Results of BNL built 40-mm aperture, 17-m-long SSC Collider Dipole Magnets*, The Twelfth International Conference on Magnet Technology, MT-12, Leningrad, USSR, pp. 311-314 (1991).

110. D.C. Larbalestier, *Recent Advances in Practical Superconductors*, The Ninth International Conference on Magnet Technology, MT-9, Zurich, Switzerland, pp. 453-458 (1985).

111. Y.Y. Lee, et al., *The AGS Booster Lattice*, 1987 Particle Accelerator Conference, Washington DC (1987).

112. Ludlam T.W. and Stevens A.J., *A Brief Description of The Relativistic Heavy Ion Collider Facility*, Informal Report BNL-49177 (1993).

113. R. Meinke, *Superconducting Magnet System for HERA*, 1990 Applied Superconductivity Conference, September 24-28, 1990, Snowmass, Co, USA; IEEE Transaction on Magnetics, March 1991, Vol 27, No. 2, pp. 1728-1734 (1990).

114. R. Meinke, P. Schmuser and Y. Zhao, *Methods of Harmonics Measurements in the Superconducting HERA Magnets and Analysis of Systematic Errors*, DESY HERA 91-13 (1991).

115. F.E. Mills and G. Morgan, *A Flux Theorem for the Design of Magnet Coil Ends*, Particle Accelerators, Vol 5, pp. 227-235 (1973).

116. G.H. Morgan, *Two-dimensional, uniform current density, air-core coil configurations for the production of specified magnetic fields*, IEEE Trans. Nucl. Sci., NS-16, No. 3, Part 1, p. 843 (1969).

117. G.H. Morgan, *Stationary Coil for Measuring the Harmonics in Pulsed Transport Magnets*, The Fourth International Conference on Magnet Technology, MT-4, Brookhaven National Laboratory, NY, USA, pp. 787-790 (1972).

118. G. Morgan, *Use of an Elliptical Aperture to Control Saturation in Closely-Coupled, Cold Iron Superconducting Dipole Magnets*, 1985 Particle Accelerator Conference in Vancouver, Canada, IEEE Trans. on Nuclear Science, Vol. NS-32, No. 5, pp. 3695-3697 (1985).

119. G.H. Morgan, *Shaping of Magnetic Fields in Beam Transport Magnets*, The Physics of Particle Accelerators, AIP Conference Proceedings 249, pp. 1242-1261 (1990).

120. G.H. Morgan, et al., *Construction and results of the 50 mm short R&D dipole magnets*, Proceedings of the 1991 IEEE Particle Accelerator Conference, San Francisco (1991).

121. G.H. Morgan, *A Computer Program for the 2-D Magnetostatic Problem Based on Integral Equations for the Field of the Conductors and Boundary Elements*, The Twelfth International Conference on Magnet Technology, MT-12, Leningrad, USSR, pp. 912-915 (1991).

122. S. Mulhall Private communication, (1993).

123. J.F. Muratore, et al., *Construction and Test Results from 1.8 m-Long, 50 mm Aperture SSC Dipole Models*, Supercollider 4, Proceedings of the Fourth International Industrial Symposium on the Super Collider, March 4-6 1992, New Orleans, USA, pp. 559-573 (1992).

124. M.J. Newman, C.W. Trowbridge, L.R. Turner, *GFUN: An Interactive Program as an AID to Magnet Design*, The Fourth International Conference on Magnet Technology, MT-4, Brookhaven National Laboratory, NY, USA, pp. 617-626 (1972).

125. The RHIC Project and its scope have been endorsed by the DOE/NSF *Nuclear Science Advisory Committee* (NSAC) in its Dec., 1989 Long Range Plan for Nuclear Science (1989).

126. D. Orrell, Private Communication (1991).

127. R.B. Palmer, et al., *Status Report on Isabelle Magnets*, 1982 Applied Superconductivity Conference, Knoxville, TN, USA; IEEE Transaction on Magnetics, May 1983, Vol MAG-19, No. 3, pp. 189-194 (1992).

128. R. Palmer and A.V. Tollestrup, *Superconducting Magnet Technology for Accelerators*, Ann. Rev. Nucl. Part. Sci. 34, pp. 247-284 (1984).

129. W.K.H. Panofsky and M. Phillips, *Classical Electricity and Magnetism*, Second Edition, Published by Addison-Wesley (1962).

130. R. Fernow, G. Morgan, R. Palmer, P. Thompson, *PAR2DOPT is a coil design program used at the Brookhaven National Laboratory for superconducting magnets*; P. Thompson is responsible for its current form, unpublished (1995).

131. G. Parzen G. and K. Jellett, *Coil Configurations in Superconducting Dipoles and Quadrupoles*, The Fourth International Conference on Magnet Technology, MT-4, Brookhaven National Laboratory, NY, USA, pp. 642-649 (1972).

132. J. Peoples, *Status of the SSC superconducting magnet program*, IEEE Transaction on Magnetics, March 1989, Vol 25, No. 2, 1988 Applied Superconductivity Conference, pp. 1444-1450 (1988).

133. E.G. Pewitt, editor, *Requirements and Specifications for 50 mm Collider Dipole Magnet*, Fermilab Publication (1990).

134. PHENIX, *PHENIX Conceptual Design Report*, 29 January 1993. Contact PHENIX Collaboration Office at BNL or Research Library at BNL (1993).

135. Los Alamos Accelerator Code Group, *User's Guide and Reference Manual for POISSON Group Codes*, the standard version of POISSON Group Codes along with these

manuals can be obtained from the Los Alamos Accelerator Code Group, Los Alamos National Laboratory Publication No. LA-UR-87-126, or latest version (1987).

136. A number of Quark Matter Conferences have been held which are relevant to physics at RHIC. See for example, *The Proceedings of the Ninth International Conference on Ultra-Relativistic Nucleus-Nucleus Collisions (Quark Matter,'91)*, T. Awes et al., editors, Published by North Holland (1992).

137. I.I. Rabi, *A method of producing uniform magnetic fields*, Review of Scientific Instruments, 5, p. 78 (1934).

138. P. Radusewicz, et al., *Results from a Partial Lifetime Test of a 40-mm aperture, 17-m-Long SSC Model Dipole*, Supercollider 4, Proceedings of the Fourth International Industrial Symposium on the Super Collider, March 4-6 1992, New Orleans, USA, pp. 551-558 (1992).

139. P. Reardon, *Cold Iron Cos theta Magnet Option for the SSC*, 1985 Particle Accelerator Conference in Vancouver, Canada, pp. 3466-3470 (1985).

140. *Conceptual Design of the Relativistic Heavy Ion Collider RHIC*, Brookhaven National Laboratory Report No. BNL 52195 (1989).

141. S. Russenschuck, et al., *Tracing Back Magnetic Field Imperfection in LHC Magnets by Means of the Inverse Problem Approach*, Proceedings of the Thirteenth Magnet Technology Conference (MT-13), Victoria, Canada (1993).

142. W.B. Sampson, *New Superconducting Material for Magnet Applications*, The Fourth International Conference on Magnet Technology, MT-4, Brookhaven National Laboratory, NY, USA, pp. 487-492 (1972).

143. J.R. Sanford and D.M. Matthews, editors, *Site-Specific Conceptual Design of the Superconducting Super Collider*, SSCL-SR-1056 (1990).

144. P. Schmuser, *Superconducting Magnets for Particle Accelerators*, The Physics of Particle Accelerators, AIP Conference Proceedings 249, pp. 1099-1158 (1990).

145. E.V. Shuryak, *Quantum Chromodynamics and The Theory of Superdense Matter*, Physics Reports, Vol. 61, p. 71 (1980).

146. The STAR collaboration, *Conceptual Design Report for the Solenoidal Tracker at RHIC*, PUB-5347, LBL, June 15 (1992).

147. J. Starit, et al., *Full Length Prototype SSC Dipole Test Results*, 1986 Applied Superconductivity Conference, Baltimore, Maryland, USA, IEEE Transactions on Magnetics, March 1987, Volume MAG-23, No. 2, pp. 1208-1214 (1986).

148. J. Strait, et al., *Test of Prototype SSC Magnets*, 1987 Particle Accelerator Conference in Washington, D.C., pp. 1537-1539 (1987).

149. J. Strait, et al., *Tests of Prototype SSC Magnets*, The Tenth International Conference on Magnet Technology, MT-10, Boston, MA, USA, pp. 730-733 (1987).

150. A.S. Stratton, *Electromagnetic Theory*, Published by McGraw-Hill Book Company, Inc (1941).

151. B.P. Strauss, et al., *Results of Magnet Prototype Evaluation for the Fermilab Energy Doubler Project*, IEEE Transaction on Magnetics, 1974 Applied Superconductivity Conference, pp. 451-454, Volume MAG-11, No. 2 (1974).

152. M.J. Tannenbaum, et al., *Magnetic Properties of the Iron Laminations for CBA Magnets*, 1983 Particle Accelerator Conference, Santa Fe, USA, pp. 3472-3474 (1983).

153. T. Ludlam and A. Schwarzchild, *Task Force for Relativistic Heavy Ion Physics*, Nucl. Phys., Vol. A418, 657c (1984).

154. D.B. Thomas, M.N. Wilson, *Filamentary Superconductor for Pulsed Application*, The Fourth International Conference on Magnet Technology, MT-4, Brookhaven National Laboratory, NY, USA, pp. 493-497 (1972).

155. R. Thomas, *Performance of field measuring probes for SSC magnets*, Proc. 5^{th} International Industrial Symposium on the Super Collider, San Francisco, California, USA, May 6-8, 1993, in Supercollider 5, pp. 715-718 (1994).

156. P. Thompson, et al., *Superconducting Magnet System for RHIC*, 1985 Particle Accelerator Conference in Vancouver, Canada, pp. 3698-3670 (1985).

157. P.A. Thompson, R.C. Gupta, et al., *Iron Saturation Control in RHIC Dipole Magnets*, Proceedings of the 1991 IEEE Particle Accelerator Conference, San Francisco (1991).

158. P.A. Thompson, R.C. Gupta, et al., *Revised Cross section for RHIC Dipole Magnets*, Proceedings of the 1991 IEEE Particle Accelerator Conference, San Francisco (1991).

159. P. Thompson, Private communication, (1992).

160. P. Thompson, et al., *B Series RHIC Arc Quadrupoles*, Proceedings of the 1993 Particle Accelerator Conference, Washington, D.C., pp. 2766-2768 (1993).

161. A.V. Tollestrup, *Superconducting Magnets*, 1981 Summer School on High Energy Particle Accelerators, AIP Conference Proceedings 87, pp. 699-804 (1981).

162. C.W. Trowbridge, *Progress in Magnet Design by Computer*, The Fourth International Conference on Magnet Technology, MT-4, Brookhaven National Laboratory, NY, USA, pp. 555-565 (1972).

163. C.W. Trowbridge, *Status of Electromagnetic Field Computation*, The Ninth International Conference on Magnet Technology, MT-9, Zurich, Switzerland, pp. 707-713 (1985).

164. P. Wanderer, et al., *Study of Factors which Affect Training in Isabelle R&D Magnets*, 1981 Particle Accelerator Conference, Washington, D.C., pp. 3208-3210 (1981).

165. P. Wanderer, *Performance of SSC R&D Dipoles*, The Physics of Particle Accelerators, AIP Conference Proceedings 249, pp. 1374-1388 (1990).

166. P. Wanderer, et al., *Experiments with all-Kapton insulation and axial prestress in 1.8 m-long SSC R&D magnets*, 1991 IEEE Particle Accelerator Conference, San Francisco, pp. 2164-2166 (1991).

167. P. Wanderer, et al., *Results of Magnetic Measurements of 40 mm Aperture 17-m Long SSC Model Collider Dipole Magnets*, The Twelfth International Conference on Magnet Technology, MT-12, Leningrad, USSR, pp. 307-310 (1991).

168. P. Wanderer, et al., *Effect of Prestress on Performance of A 1.8 m SSC R&D Dipole*, Supercollider 3, Proceedings of the Third International Industrial Symposium on the Super Collider, Atlanta, USA, pp. 325-333 (1991).

169. P. Wanderer, et al., *A Summary of SSC Dipole Magnet Field Quality Measurements*, Supercollider 4, Proceedings of the Fourth International Industrial Symposium on the Super Collider, New Orleans, USA, pp. 137-149 (1992).

170. P. Wanderer, et al., *Construction and Testing of Arc Dipoles and Quadrupoles for the Relativistic Heavy Ion Collider (RHIC) at BNL*, Proceedings of the 1995 International Particle Accelerator Conference, Dallas, Texas (1995).

171. J. Wei, R. Gupta, S. Peggs, *Magnetic Correction for RHIC Triplets*, Proceedings of the 1993 Particle Accelerator Conference, Washington, D.C., pp. 258-260 (1993).

172. J. Wei, R. Gupta, et al., *Field Quality Evaluation of the Superconducting Magnets of the Relativistic Heavy Ion Collider*, Proceedings of the 1995 International Particle Accelerator Conference, Dallas, Texas (1995).

173. F. Wilczek, *10^{12} Degree in the Shade*, The Sciences, Jan./Feb. 1994 pp. 22-30 (1994).

174. E. Willen, et al., *Magnetic Properties of Isabelle Superconducting Quadrupoles*, Proceedings of the 1981 Particle Accelerator Conference, Washington, D.C., pp. 3300-3302 (1981).

175. E. Willen, P. Dahl, J. Herrera, *Superconducting Magnets*, 1985 SLAC Summer School, AIP Conference Proceedings 153, pp. 1228-1276 (1985).

176. M.N. Wilson, Rutherford Lab. Report RHEL/M/A26.

177. M.N. Wilson, *Superconducting Magnets*, Oxford Science Publication, Clarendon Press, Oxford (1983).

178. A.M. Winslow, *Numerical Solution of Quasilinear POISSON Equation in a Nonuniform Triangular Mesh*, Journal of Comp. Physics, 2, pp. 149-172 (1967).

179. S. Wolff, *Superconducting Accelerator Magnet Design*, The Physics of Particle Accelerators, AIP Conference Proceedings 249, pp. 1159-1197 (1990).

180. S. Wolff, *Review of Accelerator Magnet Design in the World*, The Physics of Particle Accelerators, AIP Conference Proceedings 249, pp. 1389-1401 (1990).